Mathematical Modelling and Numerical Analysis Will be set by the publisher
Modélisation Mathématique et Analyse Numérique

A POSTERIORI ERROR ANALYSIS OF A VIRTUAL ELEMENT METHOD FOR STRESS-ASSISTED DIFFUSION PROBLEMS *

Franco Dassi[1], Rekha Khot[2], Andrés E. Rubiano[3] and Ricardo Ruiz-Baier[4]

Abstract. We develop and analyse residual-based a posteriori error estimates for the virtual element discretisation of a nonlinear stress-assisted diffusion problem. The model problem involves a two-way coupling between elasticity and diffusion equations in perturbed saddle-point form. A robust global inf-sup condition under a small data assumption and a Helmholtz decomposition for $\mathbf{H}(\mathrm{div},\Omega)$ lead to a reliable and efficient error estimator based on appropriately weighted norms. The complete analysis is carried out in two dimensions and we provide the required ingredients for the extension to the three dimensional case. The analysis relies on novel quasi-interpolation operators for Stokes and edge virtual element spaces. Since these interpolation operators and the corresponding error estimates are non-trivial in the three-dimensional case and are of independent interest, we provide the detailed proofs, while several remaining arguments follow analogously to the two-dimensional case. Finally, we present numerical experiments in both 2D and 3D to demonstrate the optimal performance of the proposed error estimator.

2020 Mathematics Subject Classification. 65N30, 65N12, 65N15, 74F25.

Updated: July 21, 2026.

1. Introduction

The physical interaction between solute diffusion, driven by chemical reactions, in a deformable medium was first formally addressed in [50, 52] known as the stress-assisted diffusion model. This phenomenon appears in a variety of scientific, medical, and engineering applications such as the lithiation of ion batteries [49], cardiac tissue electromechanics [38], semiconductor fabrication [47], biomechanics of brain tissue [45], among others. The multiscale nature of these applications demands robust modelling frameworks.

The mathematical analysis and discretisation of this model have been conducted using mixed-primal and mixed-mixed finite element methods (FEM) in Hilbert spaces [31], pseudo-stress-based formulations using Banach spaces [33], and well-posedness results for a primal formulation [37, 39]. More recently, a posteriori error analysis for the stress-assisted diffusion model is also developed in [32]. Adaptive schemes driven by a posteriori error estimators play a central role in recovering optimal convergence rates in challenging regimes, such as problems with singular solutions, low-regularity data, or geometrical singularities (e.g., non-convex domains and re-entrant corners).

However, standard finite element methods may face difficulties when dealing with complex geometries or highly distorted elements. Moreover, the adaptive mesh refinement generally leads to hanging nodes that are not allowed and require further mesh refinement to maintain the mesh conformity in FEM. In this context, the Virtual Element Method (VEM) (introduced in [5]), offers an attractive alternative. By extending classical finite element ideas to general polygonal and polyhedral meshes, VEM avoids the explicit construction of basis functions inside each element and instead relies on degrees of freedom together with computable polynomial projections. This

Keywords and phrases: A posteriori error analysis, virtual element method, stress-assisted diffusion, perturbed saddle-point problems, interpolation operators.

* *AER and RRB were partially supported by the Australian Research Council through the Future Fellowship grant FT220100496. FD was partially supported by the European Research Council through project NEMESIS – grant No. 101115663.*

[1] Dipartimento di Matematica e Applicazioni, Università degli Studi di Milano Bicocca, Via Roberto Cozzi 55, 20125 Milano, Italy. e-mail: `Franco.Dassi@unimib.it`

[2] Department of Mathematics, Indian Institute of Technology Palakkad, Kanjikode 678623, Kerala, India.
e-mail: `RekhaKhot@iitpkd.ac.in`

[3] Corresponding author. School of Mathematics, Monash University, 9 Rainforest Walk, 3800 Clayton VIC, Australia.
e-mail: `Andres.RubianoMartinez@monash.edu`

[4] School of Mathematics, Monash University, 9 Rainforest Walk, 3800 Clayton VIC, Australia; and Universidad Adventista de Chile, Casilla 7-D, Chillán, Chile. e-mail: `Ricardo.RuizBaier@monash.edu`

allows the method to retain consistency and stability while naturally handling irregular and non-convex meshes. While there is an extensive body of work on the VEM, we highlight a selection of key references [7,9,10,16,22,40] that are particularly relevant to the stress-assisted diffusion model.

These features make VEM particularly suitable for adaptive mesh refinement, where local mesh modifications frequently generate hanging nodes or general polytopal elements. A posteriori error estimates for VEM were first introduced in [18] for the Poisson problem, and the extension to displacement-based deformation models and reaction-diffusion equations can be found in [43, 51]. Despite these advantages, several challenges still remain open, including the development of efficient and widely available open-source implementations for conforming mesh refinement on general polytopal meshes [3].

The stress-assisted diffusion model within the VEM framework was first studied in [35, 46], where a robust mixed–mixed formulation was introduced. These works employ parameter-weighted norms to ensure the uniform well-posedness of two decoupled sub-problems across a wide range of parameter regimes. For the nonlinear fully coupled system, the well-posedness and the corresponding a priori error estimates are established via a fixed-point argument under a small data assumption. The main goal of the present work is to develop a reliable and efficient a posteriori error estimator for the stress-assisted diffusion model in the parameter-robust setting.

Main contributions. The following are the key contributions of the paper:

- **Global inf-sup condition.** We prove the global inf-sup condition within the Brezzi-Braess framework (Theorem 2.2), which provides (under small data assumption) an explicit upper bound for the total error in terms of residual operators.
- **Reliable a posteriori error estimator in 2D.** Recall that the stress assisted diffusion model involves a two-way nonlinear coupling between the elasticity and diffusion-reaction problems. Classical VEM techniques based on polynomial consistency errors and a quasi-interpolation operator for Stokes-like VEM space yield control of the residual operators associated with the elasticity problem (Lemma 4.11). The reaction–diffusion problem, however, is more delicate. Its analysis relies on the Helmholtz decomposition for $\mathbf{H}(\mathrm{div}, \Omega)$ functions, together with the Fortin and quasi-interpolation operators for mixed and C^0-VEM spaces (Lemma 4.12). The combination of these results establishes reliability (Theorem 4.13).
- **Efficient a posteriori error estimator in 2D.** We show that the proposed error estimator is efficient up to data oscillation, stabilisation, and higher-order terms. The derivation relies on standard bubble function techniques and the Lipschitz continuity of the nonlinear coupling terms (Theorem 4.16).
- **Quasi-interpolation operators in 3D.** While the 2D analysis employs existing interpolation operators, we develop Fortin and quasi-interpolation operators for Stokes-like and edge 3D VEM spaces (Propositions 5.1 and 5.4). Due to the inherent complexity of 3D spaces, deriving these interpolation error estimates is non-trivial and fills a gap in the literature. As the subsequent reliability and efficiency mirror the 2D setting, their proofs are omitted for conciseness.
- **Numerical validation in both 2D and 3D.** We develop an extensible open-source implementation of the proposed a posteriori error estimators in the library `VEM++` [21].

Plan of the paper. The contents of this paper have been organised as follows. The remainder of this section contains preliminary notational conventions and useful functional spaces. Section 2 presents the coupled stress-assisted diffusion model, weak formulation consisting of two coupled perturbed saddle-point problems, unique solvability result, and robust global inf-sup result. The mesh assumptions and VE spaces for the coupled problem along with their properties are provided in Section 3 for the 2D case. Section 4 is devoted to deriving a reliable and efficient error estimator. Next, we extend the VE spaces to the 3D case in Section 5, and construct two novel quasi-interpolation operators for Stokes and edge spaces. Finally, our theoretical results are illustrated via numerical examples in Section 6.

Recurrent notation. Let D be a domain of $\mathbb{R}^d$ $(d = 2, 3)$, with boundary ∂D. Given a tensor function $\boldsymbol{\sigma} : D \to \mathbb{R}^{d\times d}$, a vector field $\boldsymbol{u} : D \to \mathbb{R}^d$ and a scalar field $p : D \to \mathbb{R}$ we set the tensor divergence $\mathbf{div}\,\boldsymbol{\sigma} : D \to \mathbb{R}^d$, the vector gradient $\boldsymbol{\nabla}\boldsymbol{u} : D \to \mathbb{R}^{d\times d}$, the symmetric gradient $\boldsymbol{\varepsilon}(\boldsymbol{u}) : D \to \mathbb{R}^{d\times d}$, the vector divergence $\mathrm{div}\,\boldsymbol{u} : D \to \mathbb{R}$, the 3D vector rotational $\mathbf{curl}\,\boldsymbol{u} : D \to \mathbb{R}^3$, the 2D scalar rotational $\mathrm{rot}\,\boldsymbol{u} : D \to \mathbb{R}$, and the 2D vector rotational $\mathbf{rot}\,p : D \to \mathbb{R}^2$, as $(\mathbf{div}\,\boldsymbol{\sigma})_i := \sum_j \partial_j \boldsymbol{\sigma}_{ij}$, $(\boldsymbol{\nabla}\boldsymbol{u})_{ij} := \partial_j \boldsymbol{u}_i$, $\boldsymbol{\varepsilon}(\boldsymbol{u}) := \frac{1}{2}\left[\boldsymbol{\nabla}\boldsymbol{u} + (\boldsymbol{\nabla}\boldsymbol{u})^{\mathtt{t}}\right]$, $\mathrm{div}\,\boldsymbol{u} := \sum_i \partial_i \boldsymbol{u}_i$, $\mathbf{curl}\,\boldsymbol{u} := (\partial_2\boldsymbol{u}_3 - \partial_3\boldsymbol{u}_2, \partial_3\boldsymbol{u}_1 - \partial_1\boldsymbol{u}_3, \partial_1\boldsymbol{u}_2 - \partial_2\boldsymbol{u}_1)$, $\mathrm{rot}\,\boldsymbol{u} := \partial_1\boldsymbol{u}_2 - \partial_2\boldsymbol{u}_1$, and $\mathbf{rot}\,p := (\partial_2 p, -\partial_1 p)^{\mathtt{t}}$, respectively.

The component-wise inner product for vectors $\boldsymbol{u}, \boldsymbol{v} \in \mathbb{R}^d$ and matrices $\boldsymbol{\sigma}, \boldsymbol{\tau} \in \mathbb{R}^{d\times d}$ are defined by $\boldsymbol{u} : \boldsymbol{v} := \sum_i \boldsymbol{u}_i \boldsymbol{v}_i$, and $\boldsymbol{\sigma} : \boldsymbol{\tau} := \sum_{i,j} \boldsymbol{\sigma}_{ij}\boldsymbol{\tau}_{ij}$. For $s \geq 0$, we denote the Sobolev space of scalar functions with domain D as $\mathrm{H}^s(D)$, and their vector and tensor counterparts as $\mathbf{H}^s(D)$ and $\mathbb{H}^s(D)$, respectively. The norm in $\mathrm{H}^s(D)$ is denoted $\|\cdot\|_{s,D}$ and the corresponding semi-norm $|\cdot|_{s,D}$. We also use the convention $\mathrm{H}^0(D) := \mathrm{L}^2(D)$ and let $(\cdot,\cdot)_{\mathrm{D}}$ be the inner product for in $\mathrm{L}^2(D)$ (similarly for the vector and tensor counterparts). The space $\mathrm{H}^{\frac{1}{2}}(\partial D)$ contains traces of functions of $\mathrm{H}^1(D)$, $\mathrm{H}^{-\frac{1}{2}}(\partial D)$ denotes its dual, and $\langle\cdot,\cdot\rangle_{\partial D}$ stands for the duality pairing between them. The Hilbert space $\mathbf{H}(\mathrm{div}, D)$ of vectors in $\mathbf{L}^2(D)$ with divergence in $\mathrm{L}^2(D)$ equipped with the norm $\|\cdot\|^2_{\mathrm{div},D} := \|\cdot\|^2_{0,D} + \|\mathrm{div}\,\cdot\|^2_{0,D}$. Similarly, the Hilbert spaces $\mathbf{H}(\mathrm{rot}, D)$ and $\mathbf{H}(\mathbf{curl}, D)$ are equipped with the norms $\|\cdot\|_{\mathrm{rot},D}^2 := \|\cdot\|_{0,D}^2 + \|\mathrm{rot}\,\cdot\|_{0,D}^2$ and $\|\cdot\|_{\mathbf{curl},D}^2 := \|\cdot\|_{0,D}^2 + \|\mathbf{curl}\,\cdot\|_{0,D}^2$. The outward unit normal vector and unit tangential vector to ∂D are denoted respectively by $\boldsymbol{n}$ and $\boldsymbol{t}$.

Throughout this paper, we shall use the letter C to denote a generic positive constant independent of the mesh size h and physical constants, which might stand for different values at its different occurrences. Moreover, given any positive expressions X and Y, the notation $X \lesssim Y$ means that $X \le CY$ (and similarly for $X \gtrsim Y$).

2. The stress-assisted diffusion problem

This section recalls from [35] the weak formulation and its well-posedness analysis based on the Babuška–Brezzi–Braess theory and a fixed-point argument.

Model problem. Let Ω be a polytopal (polygonal in 2D and polyhedral in 3D) bounded domain with boundary $\Gamma = \Gamma_{\mathrm{D}} \cup \Gamma_{\mathrm{N}}$, such that $\Gamma_{\mathrm{D}} \cap \Gamma_{\mathrm{N}} = \emptyset$, and consider the following coupled PDE with mixed boundary conditions

$$-\mathbf{div}(2\mu\boldsymbol{\varepsilon}(\boldsymbol{u}) - p\mathbb{I}) = \boldsymbol{f}, \quad \text{in } \Omega, \quad \boldsymbol{u} = \mathbf{0}, \quad \text{on } \Gamma_{\mathrm{D}}, \tag{2.1a}$$

$$p = -\lambda \,\mathrm{div}\, \boldsymbol{u} + \ell(\varphi), \quad \text{in } \Omega, \quad (2\mu\boldsymbol{\varepsilon}(\boldsymbol{u}) - p\mathbb{I})\boldsymbol{n} = \mathbf{0}, \quad \text{on } \Gamma_{\mathrm{N}}, \tag{2.1b}$$

$$\boldsymbol{\zeta} = \mathbb{M}(\boldsymbol{\varepsilon}(\boldsymbol{u}), p)\nabla\varphi, \quad \text{in } \Omega, \quad \varphi = \varphi_{\mathrm{D}}, \quad \text{on } \Gamma_{\mathrm{D}}, \tag{2.1c}$$

$$\theta\varphi - \mathrm{div}(\boldsymbol{\zeta}) = g, \quad \text{in } \Omega, \quad \boldsymbol{\zeta}\cdot\boldsymbol{n} = 0, \quad \text{on } \Gamma_{\mathrm{N}}. \tag{2.1d}$$

The coupling uses an active stress approach defining the total Cauchy stress as $\boldsymbol{\sigma} = 2\mu\boldsymbol{\varepsilon}(\boldsymbol{u}) - p\mathbb{I}$, where $\boldsymbol{u}$ is the displacement vector, $\boldsymbol{\varepsilon}(\boldsymbol{u})$ is the tensor of infinitesimal strains, p denotes a Herrmann-type pressure, $\mathbb{I}$ denotes the identity tensor in $\mathbb{R}^{d\times d}$, φ is the solute's concentration, μ and λ are the Lamé parameters of the solid, $\boldsymbol{f}$ is a vector of external body loads, ℓ modulates the (isotropic) active stress. On the other hand, $\boldsymbol{\zeta}$ is the diffusive flux $\mathbb{M}(\boldsymbol{\varepsilon}(\boldsymbol{u}), p)$ is the stress-assisted diffusion coefficient (assumed uniformly bounded away from zero), θ is a model parameter that lies in $[0,1]$, and g is a given net volumetric source of solute.

Assumptions on the nonlinear terms. We suppose that $\ell : \mathrm{L}^2(\Omega) \to \mathrm{L}^2(\Omega)$ satisfies $\|\ell(\vartheta)\|_{0,\Omega} \lesssim \|\vartheta\|_{0,\Omega}$ for all $\vartheta \in \mathrm{L}^2(\Omega)$. We also assume that $\mathbb{M}(\cdot,\cdot)$ is invertible, symmetric, positive semi-definite and uniformly bounded in $\mathbb{L}^\infty(\Omega)$ (likewise for $\mathbb{M}^{-1}(\cdot,\cdot)$). In addition, for all $\boldsymbol{w} \in \mathbf{H}^1(\Omega), r \in \mathrm{L}^2(\Omega)$ and $\boldsymbol{x}, \boldsymbol{y} \in \mathbb{R}^d$, there exists $M \ge 1$ such that

$$M^{-1}\boldsymbol{x}\cdot\boldsymbol{y} \le \boldsymbol{x}\cdot[\mathbb{M}^{-1}(\boldsymbol{\varepsilon}(\boldsymbol{w}), r)\boldsymbol{y}] \quad \text{and} \quad \boldsymbol{y}\cdot[\mathbb{M}^{-1}(\boldsymbol{\varepsilon}(\boldsymbol{w}), r)\boldsymbol{x}] \le M\boldsymbol{x}\cdot\boldsymbol{y}. \tag{2.2}$$

Finally, we assume that $\mathbb{M}^{-1}(\cdot,\cdot)$ and $\ell(\cdot)$ are Lipschitz continuous with Lipschitz constants $L_{\mathbb{M}}$ and L_ℓ. Examples of these terms can be found in [20] for the stress-assisted diffusion and [44, 49] for the active stress.

2.1. Weak formulation

In view of the boundary conditions, we define the Hilbert spaces

$$\mathbf{H}^1_{\mathrm{D}}(\Omega) := \{\boldsymbol{v} \in \mathbf{H}^1(\Omega) : \boldsymbol{v} = \mathbf{0} \quad \text{on } \Gamma_{\mathrm{D}}\}, \quad \mathbf{H}_{\mathrm{N}}(\mathrm{div},\Omega) := \{\boldsymbol{\xi} \in \mathbf{H}(\mathrm{div},\Omega) : \boldsymbol{\xi}\cdot\boldsymbol{n} = 0 \quad \text{on } \Gamma_{\mathrm{N}}\}.$$

With them, the weak form consists in, given $\boldsymbol{f} \in \mathbf{L}^2(\Omega)$, $g \in \mathrm{L}^2(\Omega)$, and $\varphi_{\mathrm{D}} \in \mathrm{H}^{\frac12}(\Gamma_{\mathrm{D}})$, finding $(\boldsymbol{u}, p, \boldsymbol{\zeta}, \varphi) \in \mathbf{H}^1_{\mathrm{D}}(\Omega) \times \mathrm{L}^2(\Omega) \times \mathbf{H}_{\mathrm{N}}(\mathrm{div},\Omega) \times \mathrm{L}^2(\Omega)$ such that

$$a_1(\boldsymbol{u},\boldsymbol{v}) + b_1(\boldsymbol{v}, p) = F_1(\boldsymbol{v}), \qquad \forall \boldsymbol{v} \in \mathbf{H}^1_{\mathrm{D}}(\Omega), \tag{2.3a}$$

$$b_1(\boldsymbol{u}, q) - \frac{1}{\lambda}c_1(p,q) = G_1^\varphi(q), \qquad \forall q \in \mathrm{L}^2(\Omega), \tag{2.3b}$$

$$a_2^{\boldsymbol{u},p}(\boldsymbol{\zeta},\boldsymbol{\xi}) + b_2(\boldsymbol{\xi},\varphi) = F_2(\boldsymbol{\xi}), \qquad \forall \boldsymbol{\xi} \in \mathbf{H}_{\mathrm{N}}(\mathrm{div},\Omega), \tag{2.3c}$$

$$b_2(\boldsymbol{\zeta},\psi) - \theta c_2(\varphi,\psi) = G_2(\psi), \qquad \forall \psi \in \mathrm{L}^2(\Omega). \tag{2.3d}$$

The bilinear forms $a_1 : \mathbf{H}^1_{\mathrm{D}}(\Omega) \times \mathbf{H}^1_{\mathrm{D}}(\Omega) \to \mathbb{R}$, $b_1 : \mathbf{H}^1_{\mathrm{D}}(\Omega) \times \mathrm{L}^2(\Omega) \to \mathbb{R}$, $c_1 : \mathrm{L}^2(\Omega) \times \mathrm{L}^2(\Omega) \to \mathbb{R}$, $a_2^{\boldsymbol{u},p} : \mathbf{H}_{\mathrm{N}}(\mathrm{div},\Omega) \times \mathbf{H}_{\mathrm{N}}(\mathrm{div},\Omega) \to \mathbb{R}$, $b_2 : \mathbf{H}_{\mathrm{N}}(\mathrm{div},\Omega) \times \mathrm{L}^2(\Omega) \to \mathbb{R}$, $c_2 : \mathrm{L}^2(\Omega) \times \mathrm{L}^2(\Omega) \to \mathbb{R}$, and linear functionals $F_1 : \mathbf{H}^1_{\mathrm{D}}(\Omega) \to \mathbb{R}$, $G_1^\varphi : \mathrm{L}^2(\Omega) \to \mathbb{R}$, $F_2 : \mathbf{H}_{\mathrm{N}}(\mathrm{div},\Omega) \to \mathbb{R}$, $G_2 : \mathrm{L}^2(\Omega) \to \mathbb{R}$, are

$$a_1(\boldsymbol{u},\boldsymbol{v}) := 2\mu\int_\Omega \boldsymbol{\varepsilon}(\boldsymbol{u}) : \boldsymbol{\varepsilon}(\boldsymbol{v}), \quad b_1(\boldsymbol{v}, q) := -\int_\Omega q\,\mathrm{div}\,\boldsymbol{v}, \quad c_1(p,q) := \int_\Omega pq,$$

$$F_1(\boldsymbol{v}) := \int_\Omega \boldsymbol{f}\cdot\boldsymbol{v}, \quad G_1^\varphi(q) := -\frac{1}{\lambda}\int_\Omega \ell(\varphi)q,$$

$$a_2^{\boldsymbol{u},p}(\boldsymbol{\zeta},\boldsymbol{\xi}) := \int_\Omega \mathbb{M}^{-1}(\boldsymbol{\varepsilon}(\boldsymbol{u}), p)\boldsymbol{\zeta}\cdot\boldsymbol{\xi}, \quad b_2(\boldsymbol{\xi},\psi) := \int_\Omega \psi\,\mathrm{div}\,\boldsymbol{\xi}, \quad c_2(\varphi,\psi) := \int_\Omega \varphi\psi,$$

$$F_2(\boldsymbol{\xi}) := \langle \varphi_{\mathrm{D}}, \boldsymbol{\xi}\cdot\boldsymbol{n}\rangle_{\Gamma_{\mathrm{D}}}, \quad G_2(\psi) := -\int_\Omega g\psi.$$

2.2. **Parameter-dependent norms and robust solvability**

Given $K \subseteq \Omega$, let $\mathbf{V}_1(K) := \mathbf{H}^1(K)$, $\mathrm{Q}_1(K) := \mathrm{L}^2(K)$, $\mathbf{V}_2(K) := \mathbf{H}(\mathrm{div}, K)$ and $\mathrm{Q}_2 := \mathrm{L}^2(K)$ be the displacement, Herrmann pressure, flux, and concentration spaces on K, respectively, equipped with the following weighted norms and semi-norms

$$\|(\boldsymbol{u}, p)\|^2_{\mathbf{V}_1(K)\times \mathrm{Q}_1(K)} := \|\boldsymbol{u}\|^2_{\mathbf{V}_1(K)} + \|p\|^2_{\mathrm{Q}_1(K)},\ \|\boldsymbol{u}\|^2_{\mathbf{V}_1(K)} := 2\mu\|\boldsymbol{\varepsilon}(\boldsymbol{u})\|^2_{0,K},$$
$$\|p\|^2_{\mathrm{Q}_1(K)} := \left(\frac{1}{2\mu} + \frac{1}{\lambda}\right)\|p\|^2_{0,K},$$
$$|\boldsymbol{u}|^2_{\mathbf{V}_1(K)} := 2\mu|\boldsymbol{u}|^2_{1,K},\ |p|^2_{\mathrm{Q}_1(K)} := \frac{1}{2\mu}\|p\|^2_{0,K},$$
$$\|(\boldsymbol{\zeta}, \varphi)\|^2_{\mathbf{V}_2(K)\times \mathrm{Q}_2(K)} := \|\boldsymbol{\zeta}\|^2_{\mathbf{V}_2(K)} + \|\varphi\|^2_{\mathrm{Q}_2(K)},\ \|\boldsymbol{\zeta}\|^2_{\mathbf{V}_2(K)} := \|\boldsymbol{\zeta}\|^2_{\mathbb{M},K} + M\|\mathrm{div}\,\boldsymbol{\zeta}\|^2_{0,K},$$
$$\|\boldsymbol{\zeta}\|^2_{\mathbb{M},K} := \int_K \mathbb{M}^{-1}(\boldsymbol{\varepsilon}(\boldsymbol{u}), p)\boldsymbol{\zeta}\cdot\boldsymbol{\zeta},\ \|\varphi\|^2_{\mathrm{Q}_2(K)} := \left(\frac{1}{M} + \theta\right)\|\varphi\|^2_{0,K},$$
$$|\boldsymbol{\zeta}|^2_{\mathbf{V}_2(K)} := M|\boldsymbol{\zeta}|^2_{1,K},\ |\varphi|^2_{\mathrm{Q}_2(K)} := \frac{1}{M}\|\varphi\|^2_{0,K}.$$

Note that the definition of $|\boldsymbol{\zeta}|^2_{\mathbf{V}_2(K)}$ requires $\boldsymbol{\zeta} \in \mathbf{V}_2(K)\cap \mathbf{H}^1(K)$. For simplicity, we denote the global spaces (i.e., $K = \Omega$) as $\mathbf{V}_1 := \mathbf{H}^1_{\mathrm{D}}(\Omega), \mathrm{Q}_1 = \mathrm{Q}_2 := \mathrm{L}^2(\Omega), \mathbf{V}_2 := \mathbf{H}_{\mathrm{N}}(\mathrm{div}, \Omega)$ while imposing the boundary conditions.

Theorem 2.1 below establishes the well-posedness of the fully coupled system (2.3) under the small data assumption

$$C_1 L_\ell \max\left\{\frac{1}{\sqrt{2\mu}}, \sqrt{2\mu}\right\} M^2 C_2^2 L_{\mathbb{M}} \left(\|\varphi_{\mathrm{D}}\|_{\frac{1}{2},\Gamma_{\mathrm{D}}} + \|g\|_{0,\Omega}\right) < 1. \tag{2.4}$$

We recall that this condition arises only from the fixed-point treatment of the nonlinearity; the method's robustness is guaranteed by the weighted norm spaces (see [14]) and the mixed formulation introduced before, for a detailed proof we refer to [35]. In addition, Theorem 2.2 provides a robust global inf-sup condition. The proof follows from the Brezzi–Braess conditions in [13, Theorem 2.1].

Theorem 2.1. *Suppose that $1 \le \lambda$, $0 < \mu$, $\theta \le \frac{1}{M}$, and that the small data assumption (2.4) holds. Then, there exists an unique solution $(\boldsymbol{u}, p, \boldsymbol{\zeta}, \varphi) \in \mathbf{V}_1 \times \mathrm{Q}_1 \times \mathbf{V}_2 \times \mathrm{Q}_2$ to (2.3) such that*

$$\|(\boldsymbol{u}, p)\|_{\mathbf{V}_1\times\mathrm{Q}_1} \le C_1\left(\|F_1\|_{\mathbf{V}_1'} + \|G_1^\varphi\|_{Q_1'}\right),$$
$$\|(\boldsymbol{\zeta}, \varphi)\|_{\mathbf{V}_2\times\mathrm{Q}_2} \le C_2\left(\|F_2\|_{\mathbf{V}_2'} + \|G_2\|_{Q_2'}\right),$$

where the corresponding constants C_1 and C_2 do not depend on the physical parameters.

Theorem 2.2. *Let $(V, \|\cdot\|_V)$ and $(Q_b, \|\cdot\|_{Q_b})$ be Hilbert spaces, let Q be a dense (with respect to $\|\cdot\|_{Q_b}$) linear subspace of Q_b and three bilinear forms $a(\cdot,\cdot)$ on $V\times V$ (continuous, symmetric and positive semi-definite), $b(\cdot,\cdot)$ on $V \times Q_b$ (continuous), and $c(\cdot,\cdot)$ on $Q\times Q$ (symmetric and positive semi-definite); defining the linear operators $A : V \to V'$, $B : V \to Q_b'$ and $C : Q \to Q'$, respectively. For $t \in [0, 1]$, consider the t-dependent energy norm*

$$\|(v, q)\|^2_{V\times Q} := \|v\|^2_V + \|q\|^2_Q = \|v\|^2_V + \|q\|^2_{Q_b} + t^2|q|^2_c.$$

Assume that Q is complete with respect to the norm $\|\cdot\|^2_Q := \|\cdot\|^2_{Q_b} + t^2|\cdot|^2_c$, where $|\cdot|^2_c := c(\cdot,\cdot)$ is a semi-norm in Q. Suppose further that there exist positive constants α, β, γ (independent of the model parameters) such that

$$\alpha\|\hat v\|^2_V \le a(\hat v, \hat v), \qquad \forall \hat v \in \mathrm{Ker}(B), \tag{2.5a}$$
$$\beta\|q\|_{Q_b} \le \sup_{v\in V}\frac{b(v, q)}{\|v\|_V}, \qquad \forall q \in Q_b, \tag{2.5b}$$
$$\gamma\|u\|_V \le \sup_{(v,q)\in V\times Q}\frac{a(u, v) + b(u, q)}{\|(v, q)\|_{V\times Q}}, \qquad \forall u \in V. \tag{2.5c}$$

Then, the multilinear form $\mathcal{A}(u, p; v, q) := a(u, v) + b(v, p) + b(u, q) - t^2c(p, q)$ satisfies the following condition

$$\|(u, p)\|_{V\times Q} \le \left(1 + \frac{4 + 4\|a\|}{\gamma} + \frac{2}{\beta} + \left(\frac{1 + \|a\|}{\gamma}\right)^2\right) \sup_{(v,q)\in V\times Q}\frac{\mathcal{A}(u, p; v, q)}{\|(v, q)\|_{V\times Q}}, \quad \forall (u, p) \in V \times Q.$$

Proof. The triangle inequality and the second Brezzi condition (2.5b) lead to

$$\|(u, p)\|_{V\times Q} \le \|u\|_V + \frac{1}{\beta}\sup_{v\in V}\frac{\mathcal{A}(u, p; v, 0) - a(u, v)}{\|v\|_V} + t|p|_c.$$

Note that $t|p|_c \le \big(a(u,u) + t^2 c(p,p)\big)^{\frac{1}{2}} = (\mathcal{A}(u,p;u,-p))^{\frac{1}{2}}$, which together with the continuity of $a(\cdot,\cdot)$ yields

$$\|(u,p)\|_{V\times Q} \le (1+\|a\|)\,\|u\|_V + \frac{1}{\beta} \sup_{(v,q)\in V\times Q} \frac{\mathcal{A}(u,p;v,q)}{\|(v,q)\|_{V\times Q}} + (A(u,p;u,-p))^{\frac{1}{2}} .$$

The Braess condition (2.5c) implies that

$$\|(u,p)\|_{V\times Q} \le \left(\frac{1+\|a\|}{\gamma}\right) \sup_{(v,q)\in V\times Q} \frac{a(u,v)+b(u,q)}{\|(v,q)\|_{V\times Q}} + \frac{1}{\beta} \sup_{(v,q)\in V\times Q} \frac{\mathcal{A}(u,p;v,q)}{\|(v,q)\|_{V\times Q}} + (\mathcal{A}(u,p;u,-p))^{\frac{1}{2}} .$$

Since $a(u,v) + b(u,q) = \mathcal{A}(u,p;v,q) - b(v,p) + t^2 c(p,q)$, we readily see that

$$\|(u,p)\|_{V\times Q} \le \left(\frac{1+\|a\|}{\gamma} + \frac{1}{\beta}\right) \sup_{(v,q)\in V\times Q} \frac{A(u,p;v,q)}{\|(v,q)\|_{V\times Q}} + \left(1 + \frac{1+\|a\|}{\gamma}\right) (\mathcal{A}(u,p;u,-p))^{\frac{1}{2}} .$$

Given that for all $0 < x, y, z$ the inequality $x \le y + z$ implies that $x \le 2y + \frac{z^2}{x}$, we have

$$\|(u,p)\|_{V\times Q} \le 2\left(\frac{1+\|a\|}{\gamma} + \frac{1}{\beta}\right) \sup_{(v,q)\in V\times Q} \frac{\mathcal{A}(u,p;v,q)}{\|(v,q)\|_{V\times Q}} + \left(1 + \frac{1+\|a\|}{\gamma}\right)^2 \frac{\mathcal{A}(u,p;u,-p)}{\|(u,p)\|_{V\times Q}}.$$

The proof concludes by taking the supremum for all $(v,q) \in V \times Q$. □

Remark 1. *The unique solvability of the separate Herrmann elasticity and mixed diffusion problems follows from Braess' theory for perturbed saddle-point problems [14]. The general result yields estimates that are parameter-robust, meaning that the stability bounds do not depend on parameters that can be delicate in applications of stress-assisted diffusion, such as very large Lamé coefficients or a very small diffusion coefficient. Robustness due to Braess' theory requires the perturbation (in our case, reaction and pressure terms) to be sufficiently small. This regime is indeed challenging in general, and the mixed formulations tackled with this approach successfully maintain parameter robustness.*

Note, however, that the abstract theory we use for the analysis of the coupled problem is a fixed-point contraction mapping argument. Inevitably, it requires small-data assumptions (in our case, small loads and concentration sources weighted with model parameters). This somewhat diminishes the robustness of the formulated coupled system, as solvability and stability now exhibit a parameter dependence. We do stress that even in this case, the admissible regime still contains not only the typical ranges for stress-assisted diffusion but also many other cases of applicative interest.

3. Virtual element discretisation

This section introduces the 2D VEM from [35], based on [5,7,10] with the estimates involving suitable polynomial projections adapted to the parameter-robust setting. Finally, we refer to [35, Section 4] for further details on the well-posedness of the discrete problem.

Mesh assumptions. Let $\mathcal{T}^h$ be a decomposition of Ω into polygonal elements E with diameter h_E, let $\mathcal{E}^h$ be the set of edges e of $\mathcal{T}^h$ with length h_e. We assume that there exists a universal constant $\rho > 0$ such that

(M1) Every polygonal element E of diameter h_E is star-shaped with respect to a disk of radius $\ge \rho h_E$,
(M2) Every edge e of E has length $\ge \rho h_E$.

We split the set of edges as $\mathcal{E}^h = \mathcal{E}^h_\Omega \cup \mathcal{E}^h_{\mathrm{D}} \cup \mathcal{E}^h_{\mathrm{N}}$, where $\mathcal{E}^h_\Omega = \{e \in \mathcal{E}^h : e \subset \Omega\}$, $\mathcal{E}^h_{\mathrm{D}} = \{e \in \mathcal{E}^h : e \subset \Gamma_{\mathrm{D}}\}$ and $\mathcal{E}^h_{\mathrm{N}} = \{e \in \mathcal{E}^h : e \subset \Gamma_{\mathrm{N}}\}$. The set of edges of $E \in \mathcal{T}^h$ is denoted as $\mathcal{E}^h(E)$, the edges of E which are not in the boundary $\partial\Omega$ are denoted by $\mathcal{E}^h_\Omega(E)$ and the ones lying on the Dirichlet portion of the boundary (resp. Neumann) are denoted by $\mathcal{E}^h_{\mathrm{D}}(E)$ (resp. $\mathcal{E}^h_{\mathrm{N}}(E)$), the set of elements E that share e as an edge is denoted by $\mathcal{T}^h_e$. The normal and tangential jump operators are defined as $[\![\boldsymbol{u}\cdot\boldsymbol{n}_e]\!] := (\boldsymbol{u}|_E - \boldsymbol{u}|_{E'})|_e \cdot \boldsymbol{n}_e$ and $[\![\boldsymbol{\zeta}\cdot\boldsymbol{t}_e]\!] := (\boldsymbol{\zeta}|_E - \boldsymbol{\zeta}|_{E'})|_e \cdot \boldsymbol{t}_e$, where $E, E' \in \mathcal{T}^h_e$, and $\boldsymbol{n}_e$ and $\boldsymbol{t}_e$ are the outward normal and tangential counterclockwise vectors of e with respect to ∂E. The space $D(E)$ denotes the union of elements in $\mathcal{T}^h$ intersecting E.

Polynomial spaces. Given an integer $k \ge 0$ the space of polynomials of degree $\le k$ on E is denoted by $\mathcal{P}_k(E)$ (resp. for edges e). The space of the gradients of polynomials of grade $\le k+1$ on E is denoted as $\boldsymbol{\mathcal{G}}_k(E) := \nabla(\mathcal{P}_{k+1}(E))$ with standard notation $\mathcal{P}_{-1}(E) = \{0\}$ for $k = -1$. The space $\boldsymbol{\mathcal{G}}^\oplus_k(E)$ denotes the complement of the space $\boldsymbol{\mathcal{G}}_k(E)$ in the vector polynomial space $\boldsymbol{\mathcal{P}}_k(E)$, that is, $\boldsymbol{\mathcal{P}}_k(E) = \boldsymbol{\mathcal{G}}_k(E) \oplus \boldsymbol{\mathcal{G}}^\oplus_k(E)$. In particular, following [12], we set $\boldsymbol{\mathcal{G}}^\oplus_k(E) = \boldsymbol{x}^\perp \mathcal{P}_{k-1}(E)$ where $\boldsymbol{x}^\perp = (x_2, -x_1)^{\mathtt{t}}$. Likewise, the space that defines the rotational of polynomials with degree $\le k+1$ is denoted as $\boldsymbol{\mathcal{R}}_k(E) := \mathbf{rot}(\mathcal{P}_{k+1}(E))$ where the associated complement space $\boldsymbol{\mathcal{R}}^\oplus_k(E)$ fulfills the property $\boldsymbol{\mathcal{P}}_k(E) = \boldsymbol{\mathcal{R}}_k(E) \oplus \boldsymbol{\mathcal{R}}^\oplus_k(E)$ with $\boldsymbol{\mathcal{R}}^\oplus_k(E) = \boldsymbol{x}\mathcal{P}_{k-1}(E)$.

Let $\boldsymbol{x}_E = (x_{1,E}, x_{2,E})^{\mathtt{t}}$ denote the barycentre of E and let $\mathcal{M}_k(E)$ be the set of scaled monomials

$$\mathcal{M}_k(E) := \left\{ \left(\frac{\boldsymbol{x} - \boldsymbol{x}_E}{h_E} \right)^{\boldsymbol{\alpha}}, 0 \le |\boldsymbol{\alpha}| \le k \right\},$$

where $\boldsymbol{\alpha} = (\alpha_1, \alpha_2)^{\mathtt{t}}$ is a non-negative multi-index with $|\boldsymbol{\alpha}| = \alpha_1 + \alpha_2$ and $\boldsymbol{x}^{\boldsymbol{\alpha}} = x_1^{\alpha_1} x_2^{\alpha_2}$ for $\boldsymbol{x} = (x_1, x_2)^{\mathtt{t}}$. In particular, we can take the basis of $\boldsymbol{\mathcal{G}}_k(E)$ and $\boldsymbol{\mathcal{G}}_k^{\oplus}(E)$ as $\boldsymbol{\mathcal{M}}_k^{\nabla}(E) := \nabla \mathcal{M}_{k+1}(E) \setminus \{\mathbf{0}\}$ and $\boldsymbol{\mathcal{M}}_k^{\oplus}(E) := \mathbf{m}^{\perp} \mathcal{M}_{k-1}(E)$, with $\mathbf{m}^{\perp} := (\frac{x_2 - x_{2,E}}{h_E}, \frac{x_{1,E} - x_1}{h_E})^{\mathtt{t}}$, $\mathbf{m} := \frac{\boldsymbol{x} - \boldsymbol{x}_E}{h_E}$, respectively.

The spaces introduced below are constructed to address the variational forms of (2.1a)–(2.1b) and (2.1c)–(2.1d), respectively. Their unisolvency in terms of *Degrees of Freedom* (DoFs) and other properties, are detailed in [7,10].

3.1. Discrete spaces

For $k_1 \ge 2$, the discrete displacement space locally solves a Stokes problem:

$$\begin{aligned} \mathbf{V}_1^{h,k_1}(E) := \{ \boldsymbol{v} \in \mathbf{H}^1(E) \colon \boldsymbol{v}|_{\partial E} \in \boldsymbol{\mathcal{B}}^{k_1}(\partial E),\ \operatorname{div} \boldsymbol{v} \in \mathcal{P}_{k_1 - 1}(E), \\ - 2\mu \, \mathbf{div}\, \boldsymbol{\varepsilon}(\boldsymbol{v}) - \nabla s \in \boldsymbol{\mathcal{G}}_{k_1 - 2}^{\oplus}(E),\ \text{for some } s \in \mathrm{L}_0^2(E) \}, \end{aligned}$$

where $\mathcal{B}^k(\partial E)$ is the continuous space of polynomials along the boundary ∂E of E defined as

$$\mathcal{B}^k(\partial E) := \left\{ v \in C^0(\partial E) \colon v|_e \in \mathcal{P}_k(e),\ \forall e \subset \partial E \right\}.$$

Observe that $\boldsymbol{\mathcal{P}}_{k_1}(E) \subseteq \mathbf{V}_1^{h,k_1}(E)$. Then, the global discrete spaces are defined as

$$\mathbf{V}_1^{h,k_1} := \{ \boldsymbol{v} \in \mathbf{V}_1 \colon \boldsymbol{v}|_E \in \mathbf{V}_1^{h,k_1}(E),\ \forall E \in \mathcal{T}^h \}, \quad \mathrm{Q}_1^{h,k_1} := \{ q \in \mathrm{Q}_1 \colon q|_E \in \mathcal{P}_{k_1 - 1}(E),\ \forall E \in \mathcal{T}^h \}.$$

The set of DoFs for $\boldsymbol{v}_h \in \mathbf{V}_1^{h,k_1}(E)$ and $q_h \in \mathrm{Q}_1^{h,k_1}(E)$ are selected as

- The values of $\boldsymbol{v}_h$ at the vertices of E,
- The values of $\boldsymbol{v}_h$ at the $k_1 - 1$ internal Gauss-Lobatto quadrature points on each edge of E,
- $\displaystyle\int_E (\operatorname{div} \boldsymbol{v}_h) m_{k_1 - 1}, \quad \forall m_{k_1 - 1} \in \mathcal{M}_{k_1 - 1}(E) \setminus \left\{ \frac{1}{h_E} \right\},$
- $\displaystyle\int_E \boldsymbol{v}_h \cdot \mathbf{m}_{k_1 - 2}^{\oplus}, \quad \forall \mathbf{m}_{k_1 - 2}^{\oplus} \in \boldsymbol{\mathcal{M}}_{k_1 - 2}^{\oplus}(E),$
- $\displaystyle\int_E q_h m_{k_1 - 1}, \quad \forall m_{k_1 - 1} \in \mathcal{M}_{k_1 - 1}(E).$

For the reaction-diffusion equation and for $k_2 \ge 0$, the discrete flux space locally solves a div-rot problem:

$$\mathbf{V}_2^{h,k_2}(E) := \{ \boldsymbol{\xi} \in \mathbf{H}(\operatorname{div}, E) \cap \mathbf{H}(\operatorname{rot}, E) \colon \boldsymbol{\xi} \cdot \boldsymbol{n}|_e \in \mathcal{P}_{k_2}(e),\ \forall e \subset \partial E,\ \operatorname{div} \boldsymbol{\xi} \in \mathcal{P}_{k_2}(E),\ \operatorname{rot} \boldsymbol{\xi} \in \mathcal{P}_{k_2 - 1}(E) \}.$$

Note that $\boldsymbol{\mathcal{P}}_{k_2}(E) \subseteq \mathbf{V}_2^{h,k_2}(E)$. In turn, the global discrete spaces are defined as follows

$$\mathbf{V}_2^{h,k_2} := \{ \boldsymbol{\xi} \in \mathbf{V}_2 \colon \boldsymbol{\xi}|_E \in \mathbf{V}_2^{h,k_2}(E),\ \forall E \in \mathcal{T}^h \}, \quad \mathrm{Q}_2^{h,k_2} := \{ \psi \in \mathrm{Q}_2 \colon \psi|_E \in \mathcal{P}_{k_2}(E),\ \forall E \in \mathcal{T}^h \}.$$

The set of DoFs for $\boldsymbol{\xi}_h \in \mathbf{V}_2^{h,k_2}(E)$ and $\psi_h \in \mathrm{Q}_2^{h,k_2}(E)$ can be taken as

- The values of $\boldsymbol{\xi}_h \cdot \boldsymbol{n}$ at the $k_2 + 1$ Gauss–Lobatto quadrature points of each edge of E,
- $\displaystyle\int_E \boldsymbol{\xi}_h \cdot \mathbf{m}_{k_2 - 1}^{\nabla}, \quad \forall \mathbf{m}_{k_2 - 1}^{\nabla} \in \boldsymbol{\mathcal{M}}_{k_2 - 1}^{\nabla}(E),$
- $\displaystyle\int_E \boldsymbol{\xi}_h \cdot \mathbf{m}_{k_2}^{\oplus}, \quad \forall \mathbf{m}_{k_2}^{\oplus} \in \boldsymbol{\mathcal{M}}_{k_2}^{\oplus}(E),$
- $\displaystyle\int_E \psi_h m_{k_2}, \quad \forall m_{k_2} \in \mathcal{M}_{k_2}(E).$

Although k_1 and k_2 are in general arbitrary and independent, we select $k_1 = k_2 + 1$ with $k_2 \ge 1$ to achieve optimal convergence. This choice is justified later by Theorem 3.4.

3.2. **Projection and interpolation operators**

The operators below are required for the discrete formulation and the subsequent error analysis. We follow [10] for the elasticity problem and [7] for the reaction-diffusion problem. Given $E \in \mathcal{T}^h$, the energy projection operator $\mathbf{\Pi}_1^{\boldsymbol{\varepsilon},k_1} : \mathbf{H}^1(E) \to \boldsymbol{\mathcal{P}}_{k_1}(E)$ is defined, for all $\boldsymbol{v} \in \mathbf{H}^1(E)$, by

$$\int_E \boldsymbol{\varepsilon}(\boldsymbol{v} - \mathbf{\Pi}_1^{\boldsymbol{\varepsilon},k_1}\boldsymbol{v}) : \boldsymbol{\varepsilon}(\mathbf{m}_{k_1}) = 0, \quad \forall \mathbf{m}_{k_1} \in \boldsymbol{\mathcal{M}}_{k_1}(E),$$
$$\int_{\partial E} (\boldsymbol{v} - \mathbf{\Pi}_1^{\boldsymbol{\varepsilon},k_1}\boldsymbol{v}) \cdot \mathbf{m}_{\mathbf{RBM}} = 0, \quad \forall \mathbf{m}_{\mathbf{RBM}} \in \mathbf{RBM}(E) := \left\{ \begin{pmatrix} \frac{1}{h_E} \\ 0 \end{pmatrix}, \begin{pmatrix} 0 \\ \frac{1}{h_E} \end{pmatrix}, \begin{pmatrix} \frac{x_{2,E}-x_2}{h_E} \\ \frac{x_1 - x_{1,E}}{h_E} \end{pmatrix} \right\},$$

where $\mathbf{RBM}(E)$ is the set of scaled rigid body motions. We also define the $\mathbf{L}^2$-projection $\mathbf{\Pi}_j^{0,k} : \mathbf{L}^2(E) \to \boldsymbol{\mathcal{P}}_{\boldsymbol{k}}(E)$ by

$$\int_E (\boldsymbol{\zeta} - \mathbf{\Pi}_j^{0,k}\boldsymbol{\zeta}) \cdot \mathbf{m}_k = 0, \quad \forall \mathbf{m}_k \in \boldsymbol{\mathcal{M}}_k(E), \forall \boldsymbol{\zeta} \in \mathbf{L}^2(E),$$

and analogously for scalar functions. For clarity, $\mathbf{\Pi}_1^{0,k_1}$ is the projection associated with the elasticity problem, with polynomial degree k_1 (resp. $\mathbf{\Pi}_2^{0,k_2}$ for the reaction-diffusion problem). Regarding computability of $\mathbf{\Pi}_1^{\boldsymbol{\varepsilon},k_1}, \mathbf{\Pi}_1^{0,k_1-2}$ on $\mathbf{V}_1^{h,k_1}$ and $\mathbf{\Pi}_2^{0,k_2}$ on $\mathbf{V}_2^{h,k_2}$ in terms of the respective DoFs, we refer to [10, Section 3.2] and [6, Theorem 3.2]. Next, we present a scaled version of classical polynomial approximation estimates [15].

Lemma 3.1. *For $E \in \mathcal{T}^h$, let $\boldsymbol{v} \in \mathbf{H}^1(E)$, $q \in \mathrm{L}^2(E)$, $\boldsymbol{\xi} \in \mathbf{H}^1(E)$, and $\psi \in \mathrm{L}^2(E)$. Then the following estimates hold:*

$$\|\boldsymbol{v} - \mathbf{\Pi}_1^{\boldsymbol{\varepsilon},k_1}\boldsymbol{v}\|_{\mathbf{V}_1(E)} \lesssim |\boldsymbol{v}|_{\mathbf{V}_1(E)}, \qquad \|q - \Pi_1^{0,k_1}q\|_{\mathrm{Q}_1(E)} \lesssim |q|_{\mathrm{Q}_1(E)},$$
$$\|\boldsymbol{\xi} - \mathbf{\Pi}_2^{0,k_2}\boldsymbol{\xi}\|_{\mathbb{M},E} \lesssim h_E|\boldsymbol{\xi}|_{\mathbf{V}_2(E)}, \quad \|\psi - \Pi_2^{0,k_2}\psi\|_{\mathrm{Q}_2(E)} \lesssim |\psi|_{\mathrm{Q}_2(E)}.$$

Finally, we can define a quasi–interpolation operator $\mathbf{I}_1^{Q,k_1} : \mathbf{H}^1(E) \to \mathbf{V}_1^{h,k_1}(E)$ and a Fortin operator $\mathbf{I}_2^{F,k_2} : \mathbf{H}^1(E) \to \mathbf{V}_2^{h,k_2}(E)$ satisfying the estimates in the next lemma.

Lemma 3.2. *Let $E \in \mathcal{T}^h$, and $e \in \mathcal{E}^h(E)$, and let $\boldsymbol{v} \in \mathbf{H}^1(E)$ and $\boldsymbol{\xi} \in \mathbf{H}^1(E)$. Then the following estimates hold:*

$$h_e^{-\frac{1}{2}} 2\mu \|\boldsymbol{v} - \mathbf{I}_1^{Q,k_1}\boldsymbol{v}\|_{0,e} + \|\boldsymbol{v} - \mathbf{I}_1^{Q,k_1}\boldsymbol{v}\|_{\mathbf{V}_1(E)} \lesssim |\boldsymbol{v}|_{\mathbf{V}_1(D(E))}, \tag{3.1a}$$
$$h_e^{\frac{1}{2}} M \|(\boldsymbol{\xi} - \mathbf{I}_2^{F,k_2}\boldsymbol{\xi}) \cdot \boldsymbol{n}_e\|_{0,e} + \|\boldsymbol{\xi} - \mathbf{I}_2^{F,k_2}\boldsymbol{\xi}\|_{\mathbb{M},E} \lesssim h_E|\boldsymbol{\xi}|_{\mathbf{V}_2(E)}. \tag{3.1b}$$

The 2D construction of $\mathbf{I}_1^{Q,k_1}$ is in [9, Proposition 4.2]. It does not require extra regularity [40], and (3.1b) follows from trace inequality. On the other hand, $\mathbf{I}_2^{F,k_2}$ can be defined directly through the DoFs for $\mathbf{H}^1(\Omega)$ functions. Moreover, the commutative property $\operatorname{div} \mathbf{I}_2^{F,k_2}(\cdot) = \Pi_2^{0,k_2} \operatorname{div}(\cdot)$ holds, leading to the discrete stability of the reaction-diffusion system (see [7, Section 3.2]). We refer to [43, Lemma 5.2] for a proof of (3.1a).

3.3. **The virtual element formulation for the stress-assisted diffusion problem**

The discrete formulation for the fully-coupled problem reads as follows: Given $\boldsymbol{f} \in \mathbf{L}^2(\Omega)$, $g \in \mathrm{L}^2(\Omega)$, and $\varphi_{\mathrm{D}} \in \mathrm{H}^{\frac{1}{2}}(\Gamma_{\mathrm{D}})$, find $(\boldsymbol{u}_h, p_h, \boldsymbol{\zeta}_h, \varphi_h) \in \mathbf{V}_1^{h,k_1} \times \mathrm{Q}_1^{h,k_1} \times \mathbf{V}_2^{h,k_2} \times \mathrm{Q}_2^{h,k_2}$ such that

$$a_1^h(\boldsymbol{u}_h, \boldsymbol{v}_h) + b_1(\boldsymbol{v}_h, p_h) = F_1^h(\boldsymbol{v}_h), \qquad \forall \boldsymbol{v}_h \in \mathbf{V}_1^{h,k_1}, \tag{3.2a}$$
$$b_1(\boldsymbol{u}_h, q_h) - \frac{1}{\lambda} c_1(p_h, q_h) = G_1^{\varphi_h}(q_h), \qquad \forall p_h \in \mathrm{Q}_1^{h,k_1}, \tag{3.2b}$$
$$a_2^{\overline{\boldsymbol{u}}_h, p_h, h}(\boldsymbol{\zeta}_h, \boldsymbol{\xi}_h) + b_2(\boldsymbol{\xi}_h, \varphi_h) = F_2(\boldsymbol{\xi}_h), \qquad \forall \boldsymbol{\xi}_h \in \mathbf{V}_2^{h,k_2}, \tag{3.2c}$$
$$b_2(\boldsymbol{\zeta}_h, \psi_h) - \theta c_2(\varphi_h, \psi_h) = G_2(\psi_h), \qquad \forall \psi_h \in \mathrm{Q}_2^{h,k_2}, \tag{3.2d}$$

where $\overline{\boldsymbol{u}}_h := \mathbf{\Pi}_1^{\boldsymbol{\varepsilon},k_1}\boldsymbol{u}_h$. The discrete bilinear and linear forms are defined by adding the local contributions, as

$$a_1^h(\boldsymbol{u}_h, \boldsymbol{v}_h) := \sum_{E \in \mathcal{T}^h} a_1^{h,E}(\boldsymbol{u}_h, \boldsymbol{v}_h) := \sum_{E \in \mathcal{T}^h} a_1^E(\mathbf{\Pi}_1^{\boldsymbol{\varepsilon},k_1}\boldsymbol{u}_h, \mathbf{\Pi}_1^{\boldsymbol{\varepsilon},k_1}\boldsymbol{v}_h) + \sum_{E \in \mathcal{T}^h} S_1^E(\boldsymbol{u}_h - \mathbf{\Pi}_1^{\boldsymbol{\varepsilon},k_1}\boldsymbol{u}_h, \boldsymbol{v}_h - \mathbf{\Pi}_1^{\boldsymbol{\varepsilon},k_1}\boldsymbol{v}_h),$$
$$a_2^{\overline{\boldsymbol{u}}_h, p_h, h}(\boldsymbol{\zeta}_h, \boldsymbol{\xi}_h) := \sum_{E \in \mathcal{T}^h} a_2^{\overline{\boldsymbol{u}}_h, p_h, h, E}(\boldsymbol{\zeta}_h, \boldsymbol{\xi}_h)$$

$$:= \sum_{E\in\mathcal{T}^h} a_2^{\overline{\boldsymbol{u}}_h,p_h,E}(\boldsymbol{\Pi}_2^{0,k_2}\boldsymbol{\zeta}_h,\boldsymbol{\Pi}_2^{0,k_2}\boldsymbol{\xi}_h) + \sum_{E\in\mathcal{T}^h} S_2^{\overline{\boldsymbol{u}}_h,p_h,E}(\boldsymbol{\zeta}_h - \boldsymbol{\Pi}_2^{0,k_2}\boldsymbol{\zeta}_h, \boldsymbol{\xi}_h - \boldsymbol{\Pi}_2^{0,k_2}\boldsymbol{\xi}_h),$$

$$F_1^h(\boldsymbol{v}_h) := \sum_{E\in\mathcal{T}^h} F_1^{h,E}(\boldsymbol{v}_h) := \sum_{E\in\mathcal{T}^h}\int_E \boldsymbol{f}\cdot\boldsymbol{\Pi}_1^{0,k_1-2}\boldsymbol{v}_h = \sum_{E\in\mathcal{T}^h}\int_E \boldsymbol{\Pi}_1^{0,k_1-2}\boldsymbol{f}\cdot\boldsymbol{v}_h.$$

The stabilisation $S_1^E(\cdot,\cdot)$ and $S_2^{\overline{\boldsymbol{u}}_h,p_h,E}(\cdot,\cdot)$ are symmetric and positive definite bilinear forms such that

$$a_1^E(\boldsymbol{v}_h,\boldsymbol{v}_h) \lesssim S_1^E(\boldsymbol{v}_h,\boldsymbol{v}_h) \lesssim a_1^E(\boldsymbol{v}_h,\boldsymbol{v}_h), \qquad \forall \boldsymbol{v}_h \in \ker(\boldsymbol{\Pi}_1^{\boldsymbol{\varepsilon},k_1}), \tag{3.3a}$$

$$a_2^{\overline{\boldsymbol{u}}_h,p_h,E}(\boldsymbol{\xi}_h,\boldsymbol{\xi}_h) \lesssim S_2^{\overline{\boldsymbol{u}}_h,p_h,E}(\boldsymbol{\xi}_h,\boldsymbol{\xi}_h) \lesssim a_2^{\overline{\boldsymbol{u}}_h,p_h,E}(\boldsymbol{\xi}_h,\boldsymbol{\xi}_h), \quad \forall \boldsymbol{\xi}_h \in \ker(\boldsymbol{\Pi}_2^{0,k_2}). \tag{3.3b}$$

We conclude by establishing the continuous dependence on data for (3.2) and the convergence result of the total error $\overline{\mathrm{e}}_h := \|(\boldsymbol{u}-\boldsymbol{u}_h, p-p_h, \boldsymbol{\zeta}-\boldsymbol{\zeta}_h, \varphi-\varphi_h)\|_{\mathbf{V}_1\times Q_1\times\mathbf{V}_2\times Q_2}$ (see [35, Sections 4-5] for a proof). Note that the convergence rate shown in Theorem 3.4 is optimal when $k_1 = k_2+1$ and $k_2 \geq 1$. For sake of simplicity, we introduce the constant $\overline{C}_3 := \max\left\{\frac{1}{\sqrt{2\mu}}, \sqrt{2\mu}\right\}\sqrt{M}L_{\mathbb{M}}\overline{C}_2(\|\varphi_{\mathrm{D}}\|_{\frac12,\Gamma_{\mathrm{D}}} + \|g\|_{0,E})$. Similar to the continuous case (see Section 2.2), we assume that the following small data assumptions are given

$$\overline{C}_1 L_\ell \overline{C}_3 \overline{C}_2 \sqrt{M^3} < 1, \tag{3.4a}$$

$$\overline{C}_1\sqrt{M}L_\ell + \overline{C}_3\overline{C}_2 M < \frac{1}{2}. \tag{3.4b}$$

Theorem 3.3. *Suppose that $1 \leq \lambda$, $0 < \mu$, $\theta \leq \frac{1}{M}$, and that the small data assumption (3.4a) holds. Then, there exists a unique solution $(\boldsymbol{u}_h, p_h, \boldsymbol{\zeta}_h, \varphi_h) \in \mathbf{V}_1^{h,k_1}\times \mathrm{Q}_1^{h,k_1}\times\mathbf{V}_2^{h,k_2}\times\mathrm{Q}_2^{h,k_2}$ to (3.2) such that*

$$\|(\boldsymbol{u}_h,p_h)\|_{\mathbf{V}_1\times\mathrm{Q}_1} \leq \overline{C}_1\left(\|F_1^h\|_{\mathbf{V}_1'} + \|G_1^{\varphi_h}\|_{Q_1'}\right), \tag{3.5a}$$

$$\|(\boldsymbol{\zeta}_h,\varphi_h)\|_{\mathbf{V}_2\times\mathrm{Q}_2} \leq \overline{C}_2\left(\|F_2\|_{\mathbf{V}_2'} + \|G_2\|_{Q_2'}\right), \tag{3.5b}$$

where the constants $\overline{C}_1$ and $\overline{C}_2$ do not depend on the physical parameters.

Theorem 3.4. *Adopt the assumptions of Theorem 2.1 and 3.3, along with the small data condition (3.4b). Let $(\boldsymbol{u},p,\boldsymbol{\zeta},\varphi) \in (\mathbf{H}^{s_1+1}(\Omega)\cap\mathbf{V}_1, |\cdot|_{s_1+1,\mathbf{V}_1})\times(\mathrm{H}^{s_1}(\Omega)\cap Q_{b_1}, |\cdot|_{s_1,Q_{b_1}})\times(\mathbf{H}^{s_2+1}(\Omega)\cap\mathbf{V}_2, |\cdot|_{s_2+1,\mathbf{V}_2})\times(\mathrm{H}^{s_2+1}(\Omega)\cap Q_{b_2}, |\cdot|_{s_2+1,Q_{b_2}})$, and $(\boldsymbol{u}_h,p_h,\boldsymbol{\zeta}_h,\varphi_h)\in\mathbf{V}_1^{h,k_1}\times\mathrm{Q}_1^{h,k_1}\times\mathbf{V}_2^{h,k_2}\times\mathrm{Q}_2^{h,k_2}$ solve respectively the continuous and discrete problems, with the data $\boldsymbol{f}\in(\mathbf{H}^{s_1-1}\cap\mathbf{Q}_{b_1}, |\cdot|_{s_1-1,\mathbf{Q}_{b_1}})$ and $g\in(\mathrm{H}^{s_2+1}(\Omega)\cap Q_{b_2}, |\cdot|_{s_2+1,Q_{b_2}})$ where $0\leq s_1\leq k_1$ and $0\leq s_2\leq k_2$. Then, the total error $\overline{\mathrm{e}}_h$ decays with the following rate*

$$\overline{\mathrm{e}}_h \lesssim h^{\min\{s_1,s_2+1\}}(|\boldsymbol{f}|_{s_1-1,\mathbf{Q}_{b_1}} + |\boldsymbol{u}|_{s_1+1,\mathbf{V}_1} + |p|_{s_1,Q_{b_1}} + |g|_{s_2+1,Q_{b_2}} + |\boldsymbol{\zeta}|_{s_2+1,\mathbf{V}_2} + |\varphi|_{s_2+1,Q_{b_2}}).$$

4. A posteriori error analysis

This section aims at deriving reliable and efficient residual-based a posteriori error estimators for the VEM of Section 3. The reliability is a consequence of the global inf-sup provided in Theorem 2.2, together with the tools given in Subsection 4.1. The efficiency is proven using bubble functions.

4.1. Preliminary toolkit

This subsection presents the necessary local estimates, Helmholtz decomposition, and bubble function results required for the a posteriori error analysis. First, an estimate involving the projection of the load term $\boldsymbol{f}$ is presented (see [10, Lemma 3.7]).

Lemma 4.1. *Let $\boldsymbol{f}\in L^2(E)$. Then, for all $\boldsymbol{v}\in\mathbf{H}^1(E)$, we have*

$$\left|\left[F_1 - F_1^h\right](\boldsymbol{v})\right| \lesssim h_E\|\boldsymbol{f}-\boldsymbol{\Pi}_1^{0,k_1-2}\boldsymbol{f}\|_{0,E}|\boldsymbol{v}|_{1,E}.$$

Next, we provide an estimate for the local virtual approximation of the bilinear form $a_1^E(\cdot,\cdot)$.

Lemma 4.2. *For all $\boldsymbol{u}_h,\boldsymbol{v}_h\in\mathbf{V}_1^{h,k_1}(E)$, the following estimate holds:*

$$\left|\left[a_1^{h,E}-a_1^E\right](\boldsymbol{u}_h,\boldsymbol{v}_h)\right| \lesssim \left(S_1^E(\boldsymbol{u}_h-\boldsymbol{\Pi}_1^{\boldsymbol{\varepsilon},k_1}\boldsymbol{u}_h, \boldsymbol{u}_h-\boldsymbol{\Pi}_1^{\boldsymbol{\varepsilon},k_1}\boldsymbol{u}_h)\right)^{\frac12}\|\boldsymbol{v}_h\|_{\mathbf{V}_1(E)}.$$

Proof. The definition of the polynomial projection $\boldsymbol{\Pi}_1^{\boldsymbol{\varepsilon},k_1}$ leads to

$$\left[a_1^{h,E}-a_1^E\right](\boldsymbol{u}_h,\boldsymbol{v}_h) = 2\mu\int_E \boldsymbol{\varepsilon}(\boldsymbol{\Pi}_1^{\boldsymbol{\varepsilon},k_1}\boldsymbol{u}_h):\boldsymbol{\varepsilon}(\boldsymbol{\Pi}_1^{\boldsymbol{\varepsilon},k_1}\boldsymbol{v}_h) + S_1^E(\boldsymbol{u}_h-\boldsymbol{\Pi}_1^{\boldsymbol{\varepsilon},k_1}\boldsymbol{u}_h, \boldsymbol{v}_h-\boldsymbol{\Pi}_1^{\boldsymbol{\varepsilon},k_1}\boldsymbol{v}_h) - 2\mu\int_E\boldsymbol{\varepsilon}(\boldsymbol{u}_h):\boldsymbol{\varepsilon}(\boldsymbol{v}_h)$$

$$= -2\mu \int_E \boldsymbol{\varepsilon}(\boldsymbol{u}_h - \boldsymbol{\Pi}_1^{\boldsymbol{\varepsilon},k_1}\boldsymbol{u}_h) : \boldsymbol{\varepsilon}(\boldsymbol{v}_h - \boldsymbol{\Pi}_1^{\boldsymbol{\varepsilon},k_1}\boldsymbol{v}_h) + S_1^E(\boldsymbol{u}_h - \boldsymbol{\Pi}_1^{\boldsymbol{\varepsilon},k_1}\boldsymbol{u}_h, \boldsymbol{v}_h - \boldsymbol{\Pi}_1^{\boldsymbol{\varepsilon},k_1}\boldsymbol{v}_h).$$

The proof is completed after using a Cauchy–Schwarz inequality, (3.3a), and Lemma 3.1. □

Two additional local estimates are required for the bilinear form $a_2^{\overline{\boldsymbol{u}}_h,p_h,h,E}(\cdot,\cdot)$ and the nonlinear term $\mathbb{M}^{-1}(\boldsymbol{\varepsilon}(\overline{\boldsymbol{u}}),p)\boldsymbol{\zeta}$. They are adapted from [43, Lemma 4.3] to the robust case.

Lemma 4.3. *Given $\overline{\boldsymbol{u}}_h \in \mathbf{V}_1^{h,k_1}(E)$, $p_h \in \mathrm{Q}_1^{h,k_1}(E)$ and $\boldsymbol{\zeta}_h, \boldsymbol{\xi}_h \in \mathbf{V}_2^{h,k_2}(E)$, the following estimate holds:*

$$\left|\left[a_2^{\overline{\boldsymbol{u}}_h,p_h,h,E} - a_2^{\overline{\boldsymbol{u}}_h,p_h,E}\right](\boldsymbol{\zeta}_h,\boldsymbol{\xi}_h)\right| \lesssim \Bigg(\left(S_2^{\overline{\boldsymbol{u}}_h,p_h,E}(\boldsymbol{\zeta}_h - \boldsymbol{\Pi}_2^{0,k_2}\boldsymbol{\zeta}_h, \boldsymbol{\zeta}_h - \boldsymbol{\Pi}_2^{0,k_2}\boldsymbol{\zeta}_h)\right)^{\frac{1}{2}}$$
$$+ \sqrt{M}\|\mathbb{M}^{-1}(\boldsymbol{\varepsilon}(\overline{\boldsymbol{u}}_h),p_h)\boldsymbol{\Pi}_2^{0,k_2}\boldsymbol{\zeta}_h - \boldsymbol{\Pi}_2^{0,k_2}(\mathbb{M}^{-1}(\boldsymbol{\varepsilon}(\overline{\boldsymbol{u}}_h),p_h)\boldsymbol{\Pi}_2^{0,k_2}\boldsymbol{\zeta}_h)\|_{0,E}\Bigg)\|\boldsymbol{\xi}_h\|_{\mathbf{V}_2(E)}.$$

Proof. The $\mathbf{L}^2$-orthogonality of $\boldsymbol{\Pi}_2^{0,k_1}$ shows that

$$\left[a_2^{\overline{\boldsymbol{u}}_h,p_h,h,E} - a_2^{\overline{\boldsymbol{u}}_h,p_h,E}\right](\boldsymbol{\zeta}_h,\boldsymbol{\xi}_h) = a_2^{\overline{\boldsymbol{u}}_h,p_h,E}(\boldsymbol{\Pi}_2^{0,k_2}\boldsymbol{\zeta}_h, \boldsymbol{\Pi}_2^{0,k_2}\boldsymbol{\xi}_h) - a_2^{\overline{\boldsymbol{u}}_h,p_h,E}(\boldsymbol{\zeta}_h,\boldsymbol{\xi}_h)$$
$$+ S_2^{\overline{\boldsymbol{u}}_h,p_h,E}(\boldsymbol{\zeta}_h - \boldsymbol{\Pi}_2^{0,k_2}\boldsymbol{\zeta}_h, \boldsymbol{\xi}_h - \boldsymbol{\Pi}_2^{0,k_2}\boldsymbol{\xi}_h)$$
$$= -\int_E \left[\mathbb{M}^{-1}(\boldsymbol{\varepsilon}(\overline{\boldsymbol{u}}_h),p_h)\boldsymbol{\Pi}_2^{0,k_2}\boldsymbol{\zeta}_h - \boldsymbol{\Pi}_2^{0,k_2}(\mathbb{M}^{-1}(\boldsymbol{\varepsilon}(\overline{\boldsymbol{u}}_h),p_h)\boldsymbol{\Pi}_2^{0,k_2}\boldsymbol{\zeta}_h)\right]\cdot(\boldsymbol{\xi}_h - \boldsymbol{\Pi}_2^{0,k_2}\boldsymbol{\xi}_h)$$
$$- \int_E \mathbb{M}^{-1}(\boldsymbol{\varepsilon}(\overline{\boldsymbol{u}}_h),p_h)(\boldsymbol{\zeta}_h - \boldsymbol{\Pi}_2^{0,k_2}\boldsymbol{\zeta}_h)\cdot\boldsymbol{\xi}_h + S_2^E(\boldsymbol{\zeta}_h - \boldsymbol{\Pi}_2^{0,k_2}\boldsymbol{\zeta}_h, \boldsymbol{\xi}_h - \boldsymbol{\Pi}_2^{0,k_2}\boldsymbol{\xi}_h).$$

Then, the Cauchy–Schwarz inequality, (3.3b), the continuity of $\boldsymbol{\Pi}_2^{0,k_2}$ and a proper scaling finish the proof. □

Lemma 4.4. *Let $(\boldsymbol{u},p,\boldsymbol{\zeta},\varphi) \in \mathbf{V}_1 \times \mathrm{Q}_1 \times \mathbf{V}_2 \times \mathrm{Q}_2$ and $(\boldsymbol{u}_h,p_h,\boldsymbol{\zeta}_h,\varphi_h) \in \mathbf{V}_1^{h,k_1} \times \mathrm{Q}_1^{h,k_1} \times \mathbf{V}_2^{h,k_2} \times \mathrm{Q}_2^{h,k_2}$ be the unique solutions to (2.3) and (3.2). For all $E \in \mathcal{T}^h$, the following estimate holds:*

$$\|\mathbb{M}^{-1}(\boldsymbol{\varepsilon}(\boldsymbol{u}),p)\boldsymbol{\zeta} - \boldsymbol{\Pi}_2^{0,k_2}(\mathbb{M}^{-1}(\boldsymbol{\varepsilon}(\overline{\boldsymbol{u}}_h),p_h)\boldsymbol{\Pi}_2^{0,k_2}\boldsymbol{\zeta}_h)\|_{0,E} \lesssim \overline{C}_3\Big(\|\boldsymbol{u}-\boldsymbol{u}_h\|_{\mathbf{V}_1(E)} + \|p-p_h\|_{\mathrm{Q}_1(E)}$$
$$+ S_1^E(\boldsymbol{u}_h - \boldsymbol{\Pi}_1^{\boldsymbol{\varepsilon},k_1}\boldsymbol{u}_h, \boldsymbol{u}_h - \boldsymbol{\Pi}_1^{\boldsymbol{\varepsilon},k_1}\boldsymbol{u}_h)^{\frac{1}{2}}\Big) + S_2^{\overline{\boldsymbol{u}}_h,p_h,E}(\boldsymbol{\zeta}_h - \boldsymbol{\Pi}_2^{0,k_2}\boldsymbol{\zeta}_h, \boldsymbol{\zeta}_h - \boldsymbol{\Pi}_2^{0,k_2}\boldsymbol{\zeta}_h)^{\frac{1}{2}}$$
$$+ \sqrt{M}\|\boldsymbol{\zeta}-\boldsymbol{\zeta}_h\|_{\mathbb{M},E} + \|\mathbb{M}^{-1}(\boldsymbol{\varepsilon}(\overline{\boldsymbol{u}}_h),p_h)\boldsymbol{\Pi}_2^{0,k_2}\boldsymbol{\zeta}_h - \boldsymbol{\Pi}_2^{0,k_2}(\mathbb{M}^{-1}(\boldsymbol{\varepsilon}(\overline{\boldsymbol{u}}_h),p_h)\boldsymbol{\Pi}_2^{0,k_2}\boldsymbol{\zeta}_h)\|_{0,E}.$$

Proof. The triangle inequality leads to

$$\|\mathbb{M}^{-1}(\boldsymbol{\varepsilon}(\boldsymbol{u}),p)\boldsymbol{\zeta} - \boldsymbol{\Pi}_2^{0,k_2}(\mathbb{M}^{-1}(\boldsymbol{\varepsilon}(\overline{\boldsymbol{u}}_h),p_h)\boldsymbol{\Pi}_2^{0,k_2}\boldsymbol{\zeta}_h)\|_{0,E} \le \|\mathbb{M}^{-1}(\boldsymbol{\varepsilon}(\overline{\boldsymbol{u}}_h),p_h)(\boldsymbol{\zeta}_h - \boldsymbol{\Pi}_2^{0,k_2}\boldsymbol{\zeta}_h)\|_{0,E}$$
$$+ \|\left[\mathbb{M}^{-1}(\boldsymbol{\varepsilon}(\boldsymbol{u}),p) - \mathbb{M}^{-1}(\boldsymbol{\varepsilon}(\overline{\boldsymbol{u}}_h),p_h)\right]\boldsymbol{\zeta}_h\|_{0,E} + \|\mathbb{M}^{-1}(\boldsymbol{\varepsilon}(\boldsymbol{u}),p)(\boldsymbol{\zeta}-\boldsymbol{\zeta}_h)\|_{0,E}$$
$$+ \|\mathbb{M}^{-1}(\boldsymbol{\varepsilon}(\overline{\boldsymbol{u}}_h),p_h)\boldsymbol{\Pi}_2^{0,k_2}\boldsymbol{\zeta}_h - \boldsymbol{\Pi}_2^{0,k_2}(\mathbb{M}^{-1}(\boldsymbol{\varepsilon}(\overline{\boldsymbol{u}}_h),p_h)\boldsymbol{\Pi}_2^{0,k_2}\boldsymbol{\zeta}_h)\|_{0,E}.$$

For the first term, the stability estimate (3.3b) implies that

$$\|\mathbb{M}^{-1}(\boldsymbol{\varepsilon}(\overline{\boldsymbol{u}}_h),p_h)(\boldsymbol{\zeta}_h - \boldsymbol{\Pi}_2^{0,k_2}\boldsymbol{\zeta}_h)\|_{0,E} \lesssim S_2^{\overline{\boldsymbol{u}}_h,p_h,E}(\boldsymbol{\zeta}_h - \boldsymbol{\Pi}_2^{0,k_2}\boldsymbol{\zeta}_h, \boldsymbol{\zeta}_h - \boldsymbol{\Pi}_2^{0,k_2}\boldsymbol{\zeta}_h)^{\frac{1}{2}}.$$

For the second term, the Cauchy–Schwarz inequality, the Lipschitz continuity of $\mathbb{M}^{-1}$, and the triangle inequality result in

$$\|\left[\mathbb{M}^{-1}(\boldsymbol{\varepsilon}(\overline{\boldsymbol{u}}_h),p_h) - \mathbb{M}^{-1}(\boldsymbol{\varepsilon}(\boldsymbol{u}),p)\right]\boldsymbol{\zeta}_h\|_{0,E} \lesssim \max\left\{\frac{1}{\sqrt{2\mu}},\sqrt{2\mu}\right\}\sqrt{M}L_{\mathbb{M}}\|(\overline{\boldsymbol{u}}_h - \boldsymbol{u}, p_h - p)\|_{\mathbf{V}_1(E)\times\mathrm{Q}_1(E)}\|\boldsymbol{\zeta}_h\|_{\mathbf{V}_2(E)}$$
$$\lesssim \max\left\{\frac{1}{\sqrt{2\mu}},\sqrt{2\mu}\right\}\sqrt{M}L_{\mathbb{M}}\Big(\|\boldsymbol{u}-\boldsymbol{u}_h\|_{\mathbf{V}_1(E)} + \|p-p_h\|_{\mathrm{Q}_1(E)} + \|\boldsymbol{u}_h - \overline{\boldsymbol{u}}_h\|_{\mathbf{V}_1(E)}\Big)\|\boldsymbol{\zeta}_h\|_{\mathbf{V}_2(E)}$$
$$\lesssim \overline{C}_3\Big(\|\boldsymbol{u}-\boldsymbol{u}_h\|_{\mathbf{V}_1(E)} + \|p-p_h\|_{\mathrm{Q}_1(E)} + S_1^E(\boldsymbol{u}_h - \boldsymbol{\Pi}_1^{\boldsymbol{\varepsilon},k_1}\boldsymbol{u}_h, \boldsymbol{u}_h - \boldsymbol{\Pi}_1^{\boldsymbol{\varepsilon},k_1}\boldsymbol{u}_h)^{\frac{1}{2}}\Big),$$

where we have used the stability estimate (3.3a) and the continuous data dependence (3.5b) in the last step. For the third term, the property (2.2) of the nonlinear term $\mathbb{M}^{-1}$ implies that

$$\|\mathbb{M}^{-1}(\boldsymbol{\varepsilon}(\boldsymbol{u}),p)(\boldsymbol{\zeta}-\boldsymbol{\zeta}_h)\|_{0,E}^2 \le M\int_E \mathbb{M}^{-1}(\boldsymbol{\varepsilon}(\boldsymbol{u}),p)(\boldsymbol{\zeta}-\boldsymbol{\zeta}_h)\cdot(\boldsymbol{\zeta}-\boldsymbol{\zeta}_h) = M\|\boldsymbol{\zeta}-\boldsymbol{\zeta}_h\|_{\mathbb{M},E}^2.$$

The combination of the previous estimates concludes the proof. □

To apply the Helmholtz decomposition in the forthcoming analysis (see [43]), we require the scalar space $\mathrm{V}_3 = \mathrm{H}^1_{\mathrm{N}}(\Omega) := \{\chi \in \mathrm{H}^1(\Omega) : \chi = 0 \text{ on } \Gamma_{\mathrm{N}}\}$ and its local discrete virtual space

$$\mathrm{V}_3^{h,k_2+1}(E) := \{\chi \in \mathrm{H}^1_{\mathrm{N}}(E) : \chi|_{\partial E} \in \mathcal{B}^{k_2+1}(\partial E) \text{ and } \Delta\chi \in \mathcal{P}_{k_2-1}(E)\}.$$

It is shown in [43, Lemma 5.1] that $\mathbf{rot}\,\chi_h \in \mathbf{V}_2^{h,k_2}$ for $\chi_h \in \mathrm{V}_3^{h,k_2+1}$, where the global space is given by

$$\mathrm{V}_3^{h,k_2+1} := \{\chi \in \mathrm{V}_3 \colon \chi|_E \in \mathrm{V}_3^{h,k_2+1}(E),\, \forall E \in \mathcal{T}^h\}.$$

This relation plays an important role in the argument used in Lemma 4.12.

Next, we introduce the quasi-interpolation error operator for functions in the auxiliary space V_3 defined as $\mathrm{I}_3^{Q,k_2+1} : \mathrm{H}^1(E) \to \mathrm{V}_3^{h,k_2+1}(E)$ (see [41, Proposition 4.2] for details). The interpolation error involving the $\|\cdot\|_{0,e}$ norm and functions in $\mathrm{H}^1(E)$ can be proven directly from [27, Theorem 3.10] and [29, Section 1.3.2].

Lemma 4.5. *Let $E \in \mathcal{T}^h$, and $e \in \mathcal{E}^h(E)$. For $\chi \in \mathrm{H}^1(E)$, the following estimate holds:*

$$h_e^{\frac{1}{2}}\|\chi - \mathrm{I}_3^{Q,k_2+1}\chi\|_{0,e} + \|\chi - \mathrm{I}_3^{Q,k_2+1}\chi\|_{0,E} \lesssim h_E|\chi|_{1,E}.$$

As a consequence of the mesh assumptions from Section 3, a shape-regular triangulation $\widetilde{\mathcal{T}}^h$ of Ω can be constructed via a sub-triangulation of each polygon into triangles (see [2] for the construction of bubble functions in triangles). Let us recall the following results from [18] regarding element and edge bubble functions supported in polygonal elements and edges (union of triangles sharing an edge), respectively.

Lemma 4.6. *Let $E \in \mathcal{T}^h$ and Ψ_E be an element bubble function. For all $\mathbf{q}_E \in \boldsymbol{\mathcal{P}}_k(E)$, the following bounds hold*

$$\|\mathbf{q}_E\|^2_{0,E} \lesssim \|\sqrt{\Psi_E}\mathbf{q}_E\|^2_{0,E} \lesssim \|\mathbf{q}_E\|^2_{0,E}, \quad \|\mathbf{q}_E\|_{0,E} \lesssim \|\Psi_E\mathbf{q}_E\|_{0,E} + h_E|\Psi_E\mathbf{q}_E|_{1,E} \lesssim \|\mathbf{q}_E\|_{0,E}. \tag{4.1}$$

Lemma 4.7. *For $E \in \mathcal{T}^h$, let $e \subset \partial E$ and Ψ_e be the corresponding edge bubble function. For all $\mathbf{q}_e \in \boldsymbol{\mathcal{P}}_k(e)$, we have*

$$\|\mathbf{q}_e\|^2_{0,e} \lesssim \|\sqrt{\Psi_e}\mathbf{q}_e\|^2_{0,e} \lesssim \|\mathbf{q}_e\|^2_{0,e}, \quad \frac{1}{\sqrt{h_E}}\|\Psi_e\mathbf{q}_e\|_{0,E} + \sqrt{h_E}|\Psi_e\mathbf{q}_e|_{1,E} \lesssim \|\mathbf{q}_e\|_{0,e}, \tag{4.2}$$

where $\mathbf{q}_e$ is also used to denote the constant prolongation of $\mathbf{q}_e$ in the direction normal to e.

4.2. **Error estimators**

We now define residual-based a posteriori error estimators for the VE formulation from Section 3. We require a stronger assumption on the boundary data, namely that $\varphi_{\mathrm{D}} \in \mathrm{H}^r(\Gamma_{\mathrm{D}})$ for $r > 3/2$. First, we define the local error estimator $\Theta_E^2 := \Theta_{1,E}^2 + \Theta_{2,E}^2$ for $E \in \mathcal{T}^h$ conformed by the elasticity contribution and the reaction-diffusion one. These are given explicitly by

$$\Theta_{1,E}^2 := \frac{1}{2\mu}\Xi_{1,E}^2 + \frac{1}{2\mu}\eta_{1,E}^2 + 2\mu\Lambda_{1,E}^2 + S_{1,E}^2, \quad \Theta_{2,E}^2 := M\Xi_{2,E}^2 + M\eta_{2,E}^2 + M\Lambda_{2,E}^2 + S_{2,E}^2, \tag{4.3}$$

where $\Xi_{j,E}$ represents the local residual estimator, which encapsulates boundary and volume terms as

$$\begin{aligned}
\Xi_{1,E}^2 &:= \sum_{e\in\mathcal{E}^h_{\mathrm{N}}(E)} h_e\|(2\mu\varepsilon(\boldsymbol{\Pi}_1^{\boldsymbol{\varepsilon},k_1}\boldsymbol{u}_h) - p_h\mathbb{I})\boldsymbol{n}_e\|^2_{0,e} + \sum_{e\in\mathcal{E}^h_{\Omega}(E)} h_e\|[\![(2\mu\varepsilon(\boldsymbol{\Pi}_1^{\boldsymbol{\varepsilon},k_1}\boldsymbol{u}_h) - p_h\mathbb{I})\boldsymbol{n}_e]\!]\|^2_{0,e}\\
&\quad + h_E^2\|\boldsymbol{\Pi}_1^{0,k_1-2}\boldsymbol{f} + 2\mu\,\mathbf{div}(\varepsilon(\boldsymbol{\Pi}_1^{\boldsymbol{\varepsilon},k_1}\boldsymbol{u}_h)) - \nabla p_h\|^2_{0,E},\\
\Xi_{2,E}^2 &:= \sum_{e\in\mathcal{E}^h_{\mathrm{D}}(E)} h_e\|\varphi_{\mathrm{D}} - \varphi_h\|^2_{0,e} + \sum_{e\in\mathcal{E}^h_{\mathrm{D}}(E)} h_e\|(\nabla\varphi_{\mathrm{D}} - \boldsymbol{\Pi}_2^{0,k_2}(\mathbb{M}^{-1}(\boldsymbol{\varepsilon}(\overline{\boldsymbol{u}}_h), p_h)\boldsymbol{\Pi}_2^{0,k_2}\boldsymbol{\zeta}_h))\cdot\boldsymbol{t}_e\|^2_{0,e}\\
&\quad + h_E^2\|\boldsymbol{\Pi}_2^{0,k_2}(\mathbb{M}^{-1}(\boldsymbol{\varepsilon}(\overline{\boldsymbol{u}}_h), p_h)\boldsymbol{\Pi}_2^{0,k_2}\boldsymbol{\zeta}_h) - \nabla\varphi_h\|^2_{0,E} + h_E^2\|\mathrm{rot}(\boldsymbol{\Pi}_2^{0,k_2}(\mathbb{M}^{-1}(\boldsymbol{\varepsilon}(\overline{\boldsymbol{u}}_h), p_h)\boldsymbol{\Pi}_2^{0,k_2}\boldsymbol{\zeta}_h))\|^2_{0,E}.
\end{aligned}$$

The local data oscillation, mixed, and stabilisation estimators, are respectively given by

$$\begin{gathered}
\eta_{1,E}^2 := h_E^2\|\boldsymbol{f} - \boldsymbol{\Pi}_1^{0,k_1-2}\boldsymbol{f}\|^2_{0,E}, \quad \eta_{2,E}^2 := \|\mathbb{M}^{-1}(\boldsymbol{\varepsilon}(\overline{\boldsymbol{u}}_h), p_h)\boldsymbol{\Pi}_2^{0,k_2}\boldsymbol{\zeta}_h - \boldsymbol{\Pi}_2^{0,k_2}(\mathbb{M}^{-1}(\boldsymbol{\varepsilon}(\overline{\boldsymbol{u}}_h), p_h)\boldsymbol{\Pi}_2^{0,k_2}\boldsymbol{\zeta}_h)\|^2_{0,E},\\
\Lambda_{1,E}^2 := \|\frac{1}{\lambda}\ell(\varphi_h) - \mathrm{div}\,\boldsymbol{u}_h + \frac{1}{\lambda}p_h\|^2_{0,E}, \quad \Lambda_{2,E}^2 := \|-g - \mathrm{div}\,\boldsymbol{\zeta}_h + \theta\varphi_h\|^2_{0,E},\\
S_{1,E}^2 := S_1^E(\boldsymbol{u}_h - \boldsymbol{\Pi}_1^{\boldsymbol{\varepsilon},k_1}\boldsymbol{u}_h, \boldsymbol{u}_h - \boldsymbol{\Pi}_1^{\boldsymbol{\varepsilon},k_1}\boldsymbol{u}_h), \quad S_{2,E}^2 := S_2^{\overline{\boldsymbol{u}}_h,p_h,E}(\boldsymbol{\zeta}_h - \boldsymbol{\Pi}_2^{0,k_2}\boldsymbol{\zeta}_h, \boldsymbol{\zeta}_h - \boldsymbol{\Pi}_2^{0,k_2}\boldsymbol{\zeta}_h).
\end{gathered}$$

The global error, global residual, global mixed, global data oscillation, and global stabilisation estimators are defined as

$$\Theta^2 := \sum_{E\in\mathcal{T}^h} \Theta_E^2, \quad \Xi^2 := \sum_{E\in\mathcal{T}^h} \left(\frac{1}{2\mu}\Xi_{1,E}^2 + M\Xi_{2,E}^2\right), \quad \Lambda^2 := \sum_{E\in\mathcal{T}^h} \left(2\mu\Lambda_{1,E}^2 + M\Lambda_{2,E}^2\right),$$
$$\eta^2 := \sum_{E\in\mathcal{T}^h} \left(\frac{1}{2\mu}\eta_{1,E}^2 + M\eta_{2,E}^2\right), \quad S^2 := \sum_{E\in\mathcal{T}^h} \left(S_{1,E}^2 + S_{2,E}^2\right).$$

Similar estimators can be found for the uncoupled divergence-free Stokes problem in [51] and for the uncoupled mixed Poisson problem in [43].

4.3. **Reliability**

This subsection establishes an upper bound for the total error in terms of the error estimator. We begin by deriving estimates for the elasticity and reaction-diffusion partial errors in terms of a residual operator, pointing out that the non-linear terms satisfy the assumptions in Section 2.

For the remainder of the paper, assume that $(\boldsymbol{u}, p, \boldsymbol{\zeta}, \varphi) \in \mathbf{V}_1 \times \mathrm{Q}_1 \times \mathbf{V}_2 \times \mathrm{Q}_2$ and $(\boldsymbol{u}_h, p_h, \boldsymbol{\zeta}_h, \varphi_h) \in \mathbf{V}_1^{h,k_1} \times \mathrm{Q}_1^{h,k_1} \times \mathbf{V}_2^{h,k_2} \times \mathrm{Q}_2^{h,k_2}$ are the unique solutions to (2.3) and (3.2), respectively (i.e. the small data assumptions of Theorem 2.1 and 3.3 hold). Given the fixed functions $\vartheta_h \in \mathrm{Q}_2^{h,k_2}$ and $(\boldsymbol{w}_h, r_h) \in \mathbf{V}_1^{h,k_1} \times \mathrm{Q}_1^{h,k_1}$, we introduce the linear operators

$$\begin{aligned}
R_{F_1}(\boldsymbol{v}) &:= F_1(\boldsymbol{v}) - a_1(\boldsymbol{u}_h, \boldsymbol{v}) - b_1(\boldsymbol{v}, p_h), && \forall \boldsymbol{v} \in \mathbf{V}_1,\\
R_{G_1^{\vartheta_h}}(q) &:= G_1^{\vartheta_h}(q) - b_1(\boldsymbol{u}_h, q) + \frac{1}{\lambda}c_1(p_h, q), && \forall q \in \mathrm{Q}_1,\\
R_{F_2}(\boldsymbol{\xi}) &:= F_2(\boldsymbol{\xi}) - a_2^{\overline{\boldsymbol{w}}_h, r_h}(\boldsymbol{\zeta}_h, \boldsymbol{\xi}) - b_2(\boldsymbol{\xi}, \varphi_h), && \forall \boldsymbol{\xi} \in \mathbf{V}_2,\\
R_{G_2}(\psi) &:= G_2(\psi) - b_2(\boldsymbol{\zeta}_h, \psi) + \theta c_2(\varphi_h, \psi), && \forall \psi \in \mathrm{Q}_2.
\end{aligned}$$

The results below allow us to bound the error of each decoupled problem in terms of the associated residuals.

Lemma 4.8. *Given $\vartheta \in \mathrm{Q}_2$ and $\vartheta_h \in \mathrm{Q}_2^{h,k_2}$, assume that $1 \le \lambda$ and $0 < \mu$. Then, the following estimate holds:*

$$\|(\boldsymbol{u} - \boldsymbol{u}_h, p - p_h)\|_{\mathbf{V}_1\times\mathrm{Q}_1} \le C_1 \left\{ \|R_{F_1}\|_{\mathbf{V}_1'} + \|R_{G_1^{\vartheta_h}}\|_{Q_1'} + \sqrt{M} L_\ell \|\vartheta - \vartheta_h\|_{\mathrm{Q}_2} \right\}.$$

Proof. The global inf-sup from Theorem 2.2 applied to $(\boldsymbol{u} - \boldsymbol{u}_h, p - p_h) \in \mathbf{V}_1 \times \mathrm{Q}_1$, the Lipschitz continuity of $\ell(\cdot)$, and a proper use of the term $G_1^{\vartheta_h}(q)$ lead to

$$\begin{aligned}
\|(\boldsymbol{u} - \boldsymbol{u}_h, p - p_h)\|_{\mathbf{V}_1\times\mathrm{Q}_1} &\le C_1 \sup_{(\boldsymbol{v},q)\in\mathbf{V}_1\times\mathrm{Q}_1} \frac{\left|F_1(\boldsymbol{v}) + G_1^{\vartheta}(q) - a_1(\boldsymbol{u}_h, \boldsymbol{v}) - b_1(\boldsymbol{v}, p_h) - b_1(\boldsymbol{u}_h, q) + \frac{1}{\lambda}c_1(p_h, q)\right|}{\|(\boldsymbol{v}, q)\|_{\mathbf{V}_1\times\mathrm{Q}_1}}\\
&= C_1 \sup_{(\boldsymbol{v},q)\in\mathbf{V}_1\times\mathrm{Q}_1} \frac{\left|R_{F_1}(\boldsymbol{v}) + R_{G_1^{\vartheta_h}}(q) + \left[G_1^{\vartheta} - G_1^{\vartheta_h}\right](q)\right|}{\|(\boldsymbol{v}, q)\|_{\mathbf{V}_1\times\mathrm{Q}_1}}\\
&\le C_1 \left\{ \|R_{F_1}\|_{\mathbf{V}_1'} + \|R_{G_1^{\vartheta_h}}\|_{Q_1'} + \sqrt{M} L_\ell \|\vartheta - \vartheta_h\|_{\mathrm{Q}_2} \right\}.
\end{aligned}$$

□

Lemma 4.9. *For the fixed pairs $(\boldsymbol{w}, r) \in \mathbf{V}_1 \times \mathrm{Q}_1$ and $(\boldsymbol{w}_h, r_h) \in \mathbf{V}_1^{h,k_1} \times \mathrm{Q}_1^{h,k_1}$, suppose that $\theta \le \frac{1}{M}$. Then, the following estimate holds:*

$$\|(\boldsymbol{\zeta} - \boldsymbol{\zeta}_h, \varphi - \varphi_h)\|_{\mathbf{V}_2\times\mathrm{Q}_2} \le C_2 \left\{ \|R_{F_2}\|_{\mathbf{V}_2'} + \|R_{G_2}\|_{Q_2'} + \overline{C}_3 \|(\boldsymbol{w} - \boldsymbol{w}_h, r - r_h)\|_{\mathbf{V}_1\times\mathrm{Q}_1} \right\}.$$

Proof. The proof proceeds in the same way as for Lemma 4.8. □

We finalise with an upper bound for the total error $\overline{\mathrm{e}}_h$ in terms of the residuals defined above.

Theorem 4.10. *Assume that $1 \le \lambda$, $0 < \mu$, $\theta \le \frac{1}{M}$. Furthermore, suppose that $C_1\sqrt{M}L_\ell + C_2\overline{C}_3 < \frac{1}{2}$. Then, the following estimate holds:*

$$\overline{\mathrm{e}}_h \le \max\{C_1, C_2\} \left\{ \|R_{F_1}\|_{\mathbf{V}_1'} + \|R_{G_1^{\varphi_h}}\|_{Q_1'} + \|R_{F_2}\|_{\mathbf{V}_2'} + \|R_{G_2}\|_{Q_2'} \right\}.$$

Proof. The triangle inequality and Lemmas 4.8-4.9 with $\vartheta = \varphi$, $\vartheta_h = \varphi_h$, $(\boldsymbol{w}, r) = (\boldsymbol{u}, p)$, and $(\boldsymbol{w}_h, r_h) = (\boldsymbol{u}_h, p_h)$ show that

$$\begin{aligned}
\overline{\mathrm{e}}_h &= \|(\boldsymbol{u}-\boldsymbol{u}_h, p-p_h, \boldsymbol{\zeta}-\boldsymbol{\zeta}_h, \varphi-\varphi_h)\|_{\mathbf{V}_1\times \mathrm{Q}_1\times \mathbf{V}_2\times \mathrm{Q}_2} \\
&\le \|(\boldsymbol{u}-\boldsymbol{u}_h, p-p_h)\|_{\mathbf{V}_1\times \mathrm{Q}_1} + \|(\boldsymbol{\zeta}-\boldsymbol{\zeta}_h, \varphi-\varphi_h)\|_{\mathbf{V}_2\times \mathrm{Q}_2} \\
&\le C_1(\|R_{F_1}\|_{\mathbf{V}_1'} + \|R_{G_1^{\varphi_h}}\|_{Q_1'}) + C_2(\|R_{F_2}\|_{\mathbf{V}_2'} + \|R_{G_2}\|_{Q_2'}) \\
&\quad + C_1\sqrt{M}L_\ell\|\varphi-\varphi_h\|_{\mathrm{Q}_2} + C_2\overline{C}_3\|(\boldsymbol{u}-\boldsymbol{u}_h, p-p_h)\|_{\mathbf{V}_1\times \mathrm{Q}_1}.
\end{aligned}$$

Under the small data assumption $C_1\sqrt{M}L_\ell + C_2\overline{C}_3 < \frac{1}{2}$, the last two terms on the right-hand side can be absorbed into the left-hand side, yielding the desired estimate. □

Next, we aim to estimate locally the residual operators from Theorem 4.10 in terms of (4.3). First, the residuals of the elasticity problem given in Lemma 4.8 satisfy the following result.

Lemma 4.11. *The following bound holds:*

$$\|R_{F_1}\|^2_{\mathbf{V}_1'} + \|R_{G_1^{\varphi_h}}\|^2_{Q_1'} \lesssim \sum_{E\in\mathcal{E}^h} \Theta^2_{1,E}.$$

Proof. Let $\boldsymbol{v} \in \mathbf{V}_1$ and $\boldsymbol{v}_h = \mathbf{I}_1^{Q,k_1}\boldsymbol{v}$ satisfy Lemma 3.2. Then, the residual $R_{F_1}(\cdot)$ can be rewritten as

$$\begin{aligned}
R_{F_1}(\boldsymbol{v}) &= \sum_{E\in\mathcal{T}^h}\Big(\Big[F_1^E - F_1^{h,E}\Big](\boldsymbol{v}) + \Big[a_1^{h,E} - a_1^E\Big](\boldsymbol{u}_h, \boldsymbol{v}_h) + F_1^{h,E}(\boldsymbol{v}-\boldsymbol{v}_h) - a_1^E(\boldsymbol{u}_h, \boldsymbol{v}-\boldsymbol{v}_h) - b_1^E(\boldsymbol{v}-\boldsymbol{v}_h, p_h)\Big) \\
&=: \sum_{E\in\mathcal{T}^h}\Big(\mathrm{T}_1^{1,E} + \mathrm{T}_1^{2,E} + \mathrm{T}_1^{3,E} + \mathrm{T}_1^{4,E} + \mathrm{T}_1^{5,E}\Big). \qquad (4.4)
\end{aligned}$$

Lemma 4.1, the continuity of the interpolation operator,and Lemma 4.2 imply that

$$\Big|\sum_{E\in\mathcal{T}^h}\mathrm{T}_1^{1,E}\Big| \lesssim \sum_{E\in\mathcal{T}^h}\frac{1}{\sqrt{2\mu}}\eta_{1,E}\|\boldsymbol{v}\|_{\mathbf{V}_1(E)}, \qquad \Big|\sum_{E\in\mathcal{T}^h}\mathrm{T}_1^{2,E}\Big| \lesssim \sum_{E\in\mathcal{T}^h} S_{1,E}\|\boldsymbol{v}\|_{\mathbf{V}_1(E)}. \qquad (4.5)$$

To address $\mathrm{T}_1^{3,E} + \mathrm{T}_1^{4,E} + \mathrm{T}_1^{5,E}$ we shall use the following integration by parts formulae

$$\int_E \boldsymbol{\varepsilon}(\boldsymbol{\Pi}_1^{\boldsymbol{\varepsilon},k_1}\boldsymbol{u}_h) : \boldsymbol{\varepsilon}(\boldsymbol{v}-\boldsymbol{v}_h) = -\int_E \mathbf{div}(\boldsymbol{\varepsilon}(\boldsymbol{\Pi}_1^{\boldsymbol{\varepsilon},k_1}\boldsymbol{u}_h))\cdot(\boldsymbol{v}-\boldsymbol{v}_h) + \int_{\partial E}\boldsymbol{\varepsilon}(\boldsymbol{\Pi}_1^{\boldsymbol{\varepsilon},k_1}\boldsymbol{u}_h)\boldsymbol{n}\cdot(\boldsymbol{v}-\boldsymbol{v}_h), \qquad (4.6a)$$

$$\int_E \mathrm{div}(\boldsymbol{v}-\boldsymbol{v}_h)p_h = -\int_E \nabla p_h\cdot(\boldsymbol{v}-\boldsymbol{v}_h) + \int_{\partial E}(p_h\mathbb{I})\boldsymbol{n}\cdot(\boldsymbol{v}-\boldsymbol{v}_h). \qquad (4.6b)$$

The identities (4.6a)-(4.6b), Lemma 3.2, and a Cauchy–Schwarz inequality lead to

$$\begin{aligned}
\Big|\sum_{E\in\mathcal{T}^h}\mathrm{T}_1^{3,E} + \mathrm{T}_1^{4,E} + \mathrm{T}_1^{5,E}\Big| &= \Big|-\sum_{e\in\mathcal{E}_{\mathrm{N}}^h}\int_e(2\mu\boldsymbol{\varepsilon}(\boldsymbol{\Pi}_1^{\boldsymbol{\varepsilon},k_1}\boldsymbol{u}_h) - p_h\mathbb{I})\boldsymbol{n}\cdot(\boldsymbol{v}-\boldsymbol{v}_h) - \sum_{E\in\mathcal{T}^h} a_1^E(\boldsymbol{u}_h - \boldsymbol{\Pi}_1^{\boldsymbol{\varepsilon},k_1}\boldsymbol{u}_h, \boldsymbol{v}-\boldsymbol{v}_h) \\
&\quad - \sum_{e\in\mathcal{E}_\Omega^h}\int_e(2\mu\boldsymbol{\varepsilon}(\boldsymbol{\Pi}_1^{\boldsymbol{\varepsilon},k_1}\boldsymbol{u}_h) - p_h\mathbb{I})\boldsymbol{n}\cdot(\boldsymbol{v}-\boldsymbol{v}_h) + \sum_{E\in\mathcal{T}^h}\int_E(\boldsymbol{\Pi}_1^{0,k_1-2}\boldsymbol{f} + 2\mu\,\mathbf{div}(\boldsymbol{\varepsilon}(\boldsymbol{\Pi}_1^{\boldsymbol{\varepsilon},k_1}\boldsymbol{u}_h)) - \nabla p_h)\cdot(\boldsymbol{v}-\boldsymbol{v}_h)\Big| \\
&\lesssim \sum_{E\in\mathcal{T}^h}\Big(\frac{1}{\sqrt{2\mu}}\Xi_{1,E} + S_{1,E}\Big)\|\boldsymbol{v}\|_{\mathbf{V}_1(E)}. \qquad (4.7)
\end{aligned}$$

Finally, the residual $R^E_{G_1^{\varphi_h}}(\cdot)$ is handled using a Cauchy–Schwarz inequality as follows

$$\Big|R_{G_1^{\varphi_h}}(q)\Big| \lesssim \sum_{E\in\mathcal{T}^h}\sqrt{2\mu}\Lambda_{1,E}\|q\|_{\mathrm{Q}_1(E)}. \qquad (4.8)$$

Summing the estimates (4.5), (4.7), (4.8), taking the supremum for all $\boldsymbol{v} \in \mathbf{V}_1$ and all $q \in \mathrm{Q}_1$, and applying the Cauchy–Schwarz inequality conclude the proof. □

Remark 2. *It is possible to construct a Fortin interpolation for Stokes-like spaces. Thus, from the commutative property applied to* (4.6b)*, one can eliminate p from the estimator $\Xi_{1,E}$. However, the momentum balance* (2.1a) *also drops from the estimator, leading to convergence issues as the right-hand side $\boldsymbol{f}$ is not recovered. An alternative is proposed in [36], where linear momentum conservation is ensured in a pressure-free formulation.*

Now, we will concentrate on the residuals for the reaction-diffusion problem defined in Lemma 4.9.

Lemma 4.12. *Assume that $\Omega \subset \mathbb{R}^2$ is a connected domain and that Γ_{N} is contained in the boundary of a convex part of Ω, that is, there exists a convex domain B such that $\overline{\Omega} \subseteq B$ and $\Gamma_{\mathrm{N}} \subseteq \partial B$. Assume further that $\varphi_{\mathrm{D}} \in \mathrm{H}^r(\Gamma_{\mathrm{D}})$ for $r > 3/2$. Then, the following bound holds:*

$$\|R_{F_2}\|^2_{\mathbf{V}_2'} + \|R_{G_2}\|^2_{Q_2'} \lesssim \sum_{E\in\mathcal{T}^h} \Theta^2_{2,E}.$$

Proof. Let $\boldsymbol{\xi} \in \mathbf{V}_2$. We construct $\boldsymbol{\xi}_h \in \mathbf{V}_2^{h,k_2}$ combining the continuous Helmholtz decomposition (see [19, Lemma 5.1]) and the interpolators $\mathbf{I}_2^{F,k_2}, \mathrm{I}_3^{Q,k_2+1}$. Indeed, there exist $\boldsymbol{z} \in \mathbf{H}^1(\Omega)$ and $\chi \in \mathrm{H}^1_{\mathrm{N}}(\Omega)$ such that

$$\boldsymbol{\xi} = \boldsymbol{z} + \mathbf{rot}\,\chi \text{ in } \Omega, \text{ with } \frac{1}{\sqrt{M}}\left(\|\boldsymbol{z}\|_{1,\Omega} + \|\chi\|_{1,\Omega}\right) \lesssim \|\boldsymbol{\xi}\|_{\mathbf{V}_2}. \tag{4.9}$$

Therefore, we set $\boldsymbol{\xi}_h := \boldsymbol{z}_h + \mathbf{rot}\,\chi_h$, where $\boldsymbol{z}_h = \mathbf{I}_2^{F,k_2}\boldsymbol{z}$ and $\chi_h = \mathrm{I}_3^{Q,k_2+1}\chi$. Note that Lemma 3.2 and Lemma 4.5 turn the bound in (4.9) into

$$\begin{aligned}\frac{1}{\sqrt{M}}\sum_{E\in\mathcal{T}^h}\|\boldsymbol{\xi}_h\|_{0,E} &\le \frac{1}{\sqrt{M}}\sum_{E\in\mathcal{T}^h}\left(\|\boldsymbol{z}-\boldsymbol{z}_h\|_{0,E} + \|\boldsymbol{z}\|_{0,E} + |\chi-\chi_h|_{1,E} + |\chi|_{1,E}\right)\\ &\lesssim \frac{1}{\sqrt{M}}\sum_{E\in\mathcal{T}^h}\left(\|\boldsymbol{z}\|_{1,E} + \|\chi\|_{1,E}\right) \lesssim \|\boldsymbol{\xi}\|_{\mathbf{V}_2}.\end{aligned} \tag{4.10}$$

We can assert that

$$\boldsymbol{\xi} - \boldsymbol{\xi}_h = \boldsymbol{z} - \boldsymbol{z}_h + \mathbf{rot}(\chi-\chi_h) \text{ in } \Omega, \quad \text{with} \quad \frac{1}{\sqrt{M}}\sum_{E\in\mathcal{T}^h}\|\boldsymbol{\xi}-\boldsymbol{\xi}_h\|_{0,E} \lesssim \|\boldsymbol{\xi}\|_{\mathbf{V}_2}. \tag{4.11}$$

Next, given $E \in \mathcal{T}^h$, we rewrite the residual of $R_{F_2}(\cdot)$ as

$$\begin{aligned}R_{F_2}(\boldsymbol{\xi}) &= \sum_{E\in\mathcal{T}^h}\left(\left[a_2^{\overline{\boldsymbol{u}}_h,p_h,h,E} - a_2^{\overline{\boldsymbol{u}}_h,p_h,E}\right](\boldsymbol{\zeta}_h,\boldsymbol{\xi}_h) + F_2^E(\boldsymbol{\xi}-\boldsymbol{\xi}_h) - a_2^{\overline{\boldsymbol{u}}_h,p_h,E}(\boldsymbol{\zeta}_h,\boldsymbol{\xi}-\boldsymbol{\xi}_h) - b_2^E(\boldsymbol{\xi}-\boldsymbol{\xi}_h,\varphi_h)\right)\\ &=: \sum_{E\in\mathcal{T}^h}\left(\mathrm{T}_2^{1,E} + \mathrm{T}_2^{2,E} + \mathrm{T}_2^{3,E} + \mathrm{T}_2^{4,E}\right).\end{aligned}$$

For $\mathrm{T}_2^{1,E}$, Lemma 4.3 and (4.10) imply that

$$\left|\sum_{E\in\mathcal{T}^h}\mathrm{T}_2^{1,E}\right| \lesssim \sum_{E\in\mathcal{T}^h}\left(\sqrt{M}\eta_{2,E} + S_{2,E}\right)\|\boldsymbol{\xi}\|_{\mathbf{V}_2(E)}. \tag{4.12}$$

For $\mathrm{T}_2^{2,E}$, substituting (4.11) and applying [24, Lemma 3.5] for $\chi - \chi_h \in \mathrm{H}^1_{\mathrm{N}}(\Omega)$ and a suitable extension of the data $\varphi_{\mathrm{D}} \in \mathrm{H}^1(\Omega)$ such that $\varphi_{\mathrm{D}} = 0$ on Γ_{N} (see [28, Lemma 2.2]), we obtain

$$\begin{aligned}\sum_{E\in\mathcal{T}^h}\mathrm{T}_2^{2,E} &= \sum_{E\in\mathcal{T}^h}\langle(\boldsymbol{z}-\boldsymbol{z}_h)\cdot\boldsymbol{n}_e,\varphi_{\mathrm{D}}\rangle_{\partial E\cap\Gamma_{\mathrm{D}}} + \sum_{E\in\mathcal{T}^h}\langle\mathbf{rot}(\chi-\chi_h)\cdot\boldsymbol{n}_e,\varphi_{\mathrm{D}}\rangle_{\partial E\cap\Gamma_{\mathrm{D}}}\\ &= \sum_{E\in\mathcal{T}^h}\langle(\boldsymbol{z}-\boldsymbol{z}_h)\cdot\boldsymbol{n}_e,\varphi_{\mathrm{D}}\rangle_{\partial E\cap\Gamma_{\mathrm{D}}} - \sum_{E\in\mathcal{T}^h}\langle\chi-\chi_h,\nabla\varphi_{\mathrm{D}}\cdot\boldsymbol{t}_e\rangle_{\partial E\cap\Gamma_{\mathrm{D}}}.\end{aligned}$$

For $\mathrm{T}_2^{3,E}$, the addition and subtraction of the terms $\boldsymbol{\Pi}_2^{0,k_2}(\mathbb{M}^{-1}(\boldsymbol{\varepsilon}(\overline{\boldsymbol{u}}_h),p_h)\boldsymbol{\Pi}_2^{0,k_2}\boldsymbol{\zeta}_h)$ and $\mathbb{M}^{-1}(\boldsymbol{\varepsilon}(\overline{\boldsymbol{u}}_h),p_h)\boldsymbol{\Pi}_2^{0,k_2}\boldsymbol{\zeta}_h$, and for $\mathrm{T}_2^{4,E}$ an application of integration by parts lead to

$$\begin{aligned}\sum_{E\in\mathcal{T}^h}\mathrm{T}_2^{3,E} &= \sum_{E\in\mathcal{T}^h}\left(\int_E\boldsymbol{\Pi}_2^{0,k_2}(\mathbb{M}^{-1}(\boldsymbol{\varepsilon}(\overline{\boldsymbol{u}}_h),p_h)\boldsymbol{\Pi}_2^{0,k_2}\boldsymbol{\zeta}_h)\cdot(\boldsymbol{\xi}-\boldsymbol{\xi}_h) + \int_E\mathbb{M}^{-1}(\boldsymbol{\varepsilon}(\overline{\boldsymbol{u}}_h),p_h)(\boldsymbol{\zeta}_h-\boldsymbol{\Pi}_2^{0,k_2}\boldsymbol{\zeta}_h)\cdot(\boldsymbol{\xi}-\boldsymbol{\xi}_h)\right.\\ &\quad\left.+\int_E\left[\mathbb{M}^{-1}(\boldsymbol{\varepsilon}(\overline{\boldsymbol{u}}_h),p_h)\boldsymbol{\Pi}_2^{0,k_2}\boldsymbol{\zeta}_h - \boldsymbol{\Pi}_2^{0,k_2}(\mathbb{M}^{-1}(\boldsymbol{\varepsilon}(\overline{\boldsymbol{u}}_h),p_h)\boldsymbol{\Pi}_2^{0,k_2}\boldsymbol{\zeta}_h)\right]\cdot(\boldsymbol{\xi}-\boldsymbol{\xi}_h)\right),\\ \sum_{E\in\mathcal{T}^h}\mathrm{T}_2^{4,E} &= -\sum_{E\in\mathcal{T}^h}\int_E\varphi_h\,\mathrm{div}(\boldsymbol{\xi}-\boldsymbol{\xi}_h) = \sum_{E\in\mathcal{T}^h}\int_E\nabla\varphi_h\cdot(\boldsymbol{\xi}-\boldsymbol{\xi}_h) - \sum_{e\in\mathcal{E}^h}\int_e\varphi_h(\boldsymbol{\xi}-\boldsymbol{\xi}_h)\cdot\boldsymbol{n}_e.\end{aligned}$$

Thus, integration by parts, the Cauchy–Schwarz inequality, Lemma 4.5, Lemma 3.2, and (3.3b) imply that

$$\begin{aligned}
\left|\sum_{E\in\mathcal{T}^h} \mathrm{T}_2^{2,E} + \mathrm{T}_2^{3,E} + \mathrm{T}_2^{4,E}\right| &= \Bigg|\sum_{e\in\mathcal{E}_{\mathrm{D}}^h} \langle(\boldsymbol{z}-\boldsymbol{z}_h)\cdot\boldsymbol{n}_e, \varphi_{\mathrm{D}}-\varphi_h\rangle_e - \sum_{e\in\mathcal{E}_{\mathrm{D}}^h}\langle\chi-\chi_h, \nabla\varphi_{\mathrm{D}}\cdot\boldsymbol{t}_e\rangle_e \\
&+ \sum_{e\in\mathcal{E}^h}\langle\chi-\chi_h, \boldsymbol{\Pi}_2^{0,k_2}(\mathbb{M}^{-1}(\boldsymbol{\varepsilon}(\overline{\boldsymbol{u}}_h),p_h)\boldsymbol{\Pi}_2^{0,k_2}\boldsymbol{\zeta}_h)\cdot\boldsymbol{t}_e\rangle_e \\
&- \sum_{E\in\mathcal{T}^h}\int_E \left[\boldsymbol{\Pi}_2^{0,k_2}(\mathbb{M}^{-1}(\boldsymbol{\varepsilon}(\overline{\boldsymbol{u}}_h),p_h)\boldsymbol{\Pi}_2^{0,k_2}\boldsymbol{\zeta}_h)-\nabla\varphi_h\right]\cdot(\boldsymbol{z}-\boldsymbol{z}_h) \\
&- \sum_{E\in\mathcal{T}^h}\int_E \operatorname{rot}\left(\boldsymbol{\Pi}_2^{0,k_2}(\mathbb{M}^{-1}(\boldsymbol{\varepsilon}(\overline{\boldsymbol{u}}_h),p_h)\boldsymbol{\Pi}_2^{0,k_2}\boldsymbol{\zeta}_h)\right)(\chi-\chi_h) \\
&- \sum_{E\in\mathcal{T}^h}\int_E \mathbb{M}^{-1}(\boldsymbol{\varepsilon}(\overline{\boldsymbol{u}}_h),p_h)(\boldsymbol{\zeta}_h-\boldsymbol{\Pi}_2^{0,k_2}\boldsymbol{\zeta}_h)\cdot(\boldsymbol{\xi}-\boldsymbol{\xi}_h) \\
&- \sum_{E\in\mathcal{T}^h}\int_E \left[\mathbb{M}^{-1}(\boldsymbol{\varepsilon}(\overline{\boldsymbol{u}}_h),p_h)\boldsymbol{\Pi}_2^{0,k_2}\boldsymbol{\zeta}_h - \boldsymbol{\Pi}_2^{0,k_2}(\mathbb{M}^{-1}(\boldsymbol{\varepsilon}(\overline{\boldsymbol{u}}_h),p_h)\boldsymbol{\Pi}_2^{0,k_2}\boldsymbol{\zeta}_h)\right]\cdot(\boldsymbol{\xi}-\boldsymbol{\xi}_h)\Bigg| \\
&\lesssim \sum_{E\in\mathcal{T}^h}(\sqrt{M}\Xi_{2,E} + S_{2,E} + \sqrt{M}\eta_{2,E})\|\boldsymbol{\xi}\|_{\mathbf{V}_2(E)}.
\end{aligned} \tag{4.13}$$

Finally, concerning the residual $R_{G_2}(\cdot)$, the Cauchy–Schwarz inequality and proper scaling give us that

$$\left|R_{G_2}(\psi)\right| \lesssim \sum_{E\in\mathcal{T}^h}\sqrt{M}\Lambda_{2,E}\|\psi\|_{\mathrm{Q}_2(E)}. \tag{4.14}$$

Adding (4.12), (4.13), and (4.14), taking the supremum for all $\boldsymbol{\xi}\in\mathbf{V}_2$ and all $\psi\in\mathrm{Q}_2$, and applying the Cauchy–Schwarz inequality complete the proof. □

To finalise, the following reliability of the total residual global estimator Θ is a direct consequence of Lemmas 4.11-4.12.

Theorem 4.13. *Under the assumption of Theorem 4.10 and Lemma 4.12, the following bound holds*

$$\bar{\mathrm{e}}_h \lesssim \max\{C_1, C_2\}\,\Theta.$$

4.4. **Efficiency**

This section aims to show the efficiency of the global residual and mixed estimators Ξ and Λ up to data oscillation η, the stabilisation estimator S and higher-order terms (HOTs). In what follows, we use the properties of bubble functions, the Lipschitz continuity of the nonlinear terms from Section 2, and the strong mixed formulation in (2.1). The main result is then a consequence of Lemmas 4.14-4.15.

Lemma 4.14. *The following bound holds*

$$\sum_{E\in\mathcal{T}^h}\left(\frac{1}{2\mu}\Xi_{1,E}^2 + 2\mu\Lambda_{1,E}^2\right) \lesssim \max\{1, 2\mu M\}\sum_{E\in\mathcal{T}^h}\left(\bar{\mathrm{e}}_h^2 + \frac{1}{2\mu}\eta_{1,E}^2 + S_{1,E}^2\right).$$

Proof. Let $E\in\mathcal{T}^h$, $\mathbf{q}_E := \boldsymbol{\Pi}_1^{0,k_1-2}\boldsymbol{f} + 2\mu\,\mathbf{div}(\boldsymbol{\varepsilon}(\boldsymbol{\Pi}_1^{\boldsymbol{\varepsilon},k_1}\boldsymbol{u}_h)) - \nabla p_h \in \boldsymbol{\mathcal{P}}_{k_1-2}(E)$, and $\overline{\boldsymbol{v}}_E := \Psi_E\mathbf{q}_E$ where Ψ_E is an element bubble function from Lemma 4.6. Note that (2.3a) leads to $R_{F_1}(\boldsymbol{v}) = a_1(\boldsymbol{u}-\boldsymbol{u}_h,\boldsymbol{v}) + b_1(\boldsymbol{v},p-p_h)$ for all $\boldsymbol{v}\in\mathbf{V}_1$. Then, we set $\boldsymbol{v}=\overline{\boldsymbol{v}}_E$ and $\boldsymbol{v}_h=\mathbf{0}$ in (4.4). Thus, given that $\overline{\boldsymbol{v}}_E$ vanishes on ∂E and outside E, we can apply integration by parts to arrive at

$$\|\mathbf{q}_E\|_{0,E}^2 \lesssim \left|\int_E \mathbf{q}_E\cdot\overline{\boldsymbol{v}}_E\right| = \left|a_1^E(\boldsymbol{u}-\boldsymbol{u}_h,\overline{\boldsymbol{v}}_E) + b_1^E(\overline{\boldsymbol{v}}_E,p-p_h) - \left[F_1^E - F_1^{h,E}\right](\overline{\boldsymbol{v}}_E) + a_1^E(\boldsymbol{u}_h - \boldsymbol{\Pi}_1^{\boldsymbol{\varepsilon},k_1}\boldsymbol{u}_h,\overline{\boldsymbol{v}}_E)\right|.$$

Next, the continuity of $a_1(\cdot,\cdot)$ and $b_1(\cdot,\cdot)$ together with the Cauchy–Schwarz inequality and (3.3a) lead to

$$\|\mathbf{q}_E\|_{0,E}^2 \lesssim (\|\boldsymbol{u}-\boldsymbol{u}_h\|_{\mathbf{V}_1(E)} + \|p-p_h\|_{\mathrm{Q}_1(E)} + S_{1,E})\|\overline{\boldsymbol{v}}_E\|_{\mathbf{V}_1(E)} + \|\boldsymbol{f}-\boldsymbol{\Pi}_1^{0,k_1-2}\boldsymbol{f}\|_{0,E}\|\overline{\boldsymbol{v}}_E\|_{0,E}.$$

From the inequality $\|\boldsymbol{\varepsilon}(\cdot)\|_{0,E}\le|\cdot|_{1,E}$ and Lemma 4.6 we obtain

$$\|\mathbf{q}_E\|_{0,E}^2 \lesssim \frac{\sqrt{2\mu}}{h_E}(\|\boldsymbol{u}-\boldsymbol{u}_h\|_{\mathbf{V}_1(E)} + \|p-p_h\|_{\mathrm{Q}_1(E)} + S_{1,E})\|\mathbf{q}_E\|_{0,E} + \|\boldsymbol{f}-\boldsymbol{\Pi}_1^{0,k_1-2}\boldsymbol{f}\|_{0,E}\|\mathbf{q}_E\|_{0,E},$$

and consequently, we have

$$\frac{1}{2\mu}h_E^2\|\mathbf{q}_E\|_{0,E}^2 \lesssim \left(\|\boldsymbol{u}-\boldsymbol{u}_h\|_{\mathbf{V}_1(E)}^2 + \|p-p_h\|_{\mathrm{Q}_1(E)}^2 + S_{1,E}^2 + \frac{1}{2\mu}\eta_{1,E}^2\right). \tag{4.15}$$

Now, we define the edge polynomial $\mathbf{q}_e = [\![(2\mu\varepsilon(\boldsymbol{\Pi}_1^{\boldsymbol{\varepsilon},k_1}\boldsymbol{u}_h) - p_h\mathbb{I})\boldsymbol{n}_e]\!] \in \boldsymbol{\mathcal{P}}_{k_1-1}(e)$ and the edge bubble function $\overline{\boldsymbol{v}}_e = \Psi_e\mathbf{q}_e$ as in Lemma 4.7. Note that, this polynomial can be extended to $\mathcal{T}_e^h$ by the techniques used in [42, Remark 3.1]. Choosing $\boldsymbol{v} = \overline{\boldsymbol{v}}_e$ and $\boldsymbol{v}_h = \mathbf{0}$ in (4.4), we readily see that $\|\mathbf{q}_e\|_{0,e}^2 \lesssim \left|\int_e \mathbf{q}_e\cdot\overline{\boldsymbol{v}}_e\right|$, and

$$\left|\int_e \mathbf{q}_e\cdot\overline{\boldsymbol{v}}_e\right| \le \sum_{E\in\mathcal{T}_e^h}\left|\int_E \mathbf{q}_E\cdot\overline{\boldsymbol{v}}_e + \left[F_1^E - F_1^{h,E}\right](\overline{\boldsymbol{v}}_e) - a_1^E(\boldsymbol{u}_h - \boldsymbol{\Pi}_1^{\boldsymbol{\varepsilon},k_1}\boldsymbol{u}_h,\overline{v}_e) - a_1^E(\boldsymbol{u}-\boldsymbol{u}_h,\overline{\boldsymbol{v}}_e) - b_1^E(\overline{\boldsymbol{v}}_e, p-p_h)\right|.$$

Similarly, note that

$$\|\mathbf{q}_e\|_{0,e}^2 \lesssim \sum_{E\in\mathcal{T}_e^h}\left(\|\boldsymbol{u}-\boldsymbol{u}_h\|_{\mathbf{V}_1(E)} + \|p-p_h\|_{\mathrm{Q}_1(E)} + S_{1,E}\right)\|\overline{\boldsymbol{v}}_e\|_{\mathbf{V}_1(E)} + \left(\|\boldsymbol{f}-\boldsymbol{\Pi}_1^{0,k_1-2}\boldsymbol{f}\|_{0,E} + \|\mathbf{q}_E\|_{0,E}\right)\|\overline{\boldsymbol{v}}_e\|_{0,E},$$

which together with Lemma 4.7 and the fact that $h_e \le h_E$, imply that

$$\sqrt{h_e}\|\mathbf{q}_e\|_{0,e} \lesssim \sum_{E\in\mathcal{T}_e^h}\left[\sqrt{2\mu}(\|\boldsymbol{u}-\boldsymbol{u}_h\|_{\mathbf{V}_1(E)} + \|p-p_h\|_{\mathrm{Q}_1(E)} + S_{1,E}) + h_E(\|\boldsymbol{f}-\boldsymbol{\Pi}_1^{0,k_1-2}\boldsymbol{f}\|_{0,E} + \|\mathbf{q}_E\|_{0,E})\right].$$

Therefore,

$$\frac{1}{2\mu}h_e\|\mathbf{q}_e\|_{0,e}^2 \lesssim \sum_{E\in\mathcal{T}_e^h}\left[\|\boldsymbol{u}-\boldsymbol{u}_h\|_{\mathbf{V}_1(E)}^2 + \|p-p_h\|_{\mathrm{Q}_1(E)}^2 + S_{1,E}^2 \quad + \frac{1}{2\mu}\eta_{1,E}^2 + \frac{1}{2\mu}h_E^2\|\mathbf{q}_E\|_{0,E}\right]. \tag{4.16}$$

Finally, from (2.1b), the Lipschitz continuity of $\ell(\cdot)$, the inequality $\|\mathrm{div}(\cdot)\|_{0,E} \le |\cdot|_{1,E}$, Körn's inequality, and given that $\frac{1}{\lambda} \le 1$, we easily see that

$$\begin{aligned}\sqrt{2\mu}\Lambda_{1,E} &= \sqrt{2\mu}\|\frac{1}{\lambda}(\ell(\varphi)-\ell(\varphi_h)) + \mathrm{div}(\boldsymbol{u}-\boldsymbol{u}_h) + \frac{1}{\lambda}(p-p_h)\|_{0,E}\\ &\lesssim \max\left\{\sqrt{2\mu M}, 1\right\}(\|\varphi-\varphi_h\|_{\mathrm{Q}_2(E)} + \|\boldsymbol{u}-\boldsymbol{u}_h\|_{\mathbf{V}_1(E)} + \|p-p_h\|_{\mathrm{Q}_1(E)}).\end{aligned} \tag{4.17}$$

Summing the bounds in (4.15)-(4.17) for all E, and (4.16) for all $e\subset\partial E$ concludes the proof. □

Lemma 4.15. *The following bound holds*

$$\sum_{E\in\mathcal{T}^h} M\Xi_{2,E}^2 + M\Lambda_{2,E}^2 \lesssim \max\left\{M^2, M\overline{C}_3\right\}\sum_{E\in\mathcal{T}^h}(\bar{\mathrm{e}}_h^2 + M\eta_{2,E}^2 + S_{2,E}^2 + S_{1,E}^2 + \mathrm{HOTs}),$$

with the high-order terms given by

$$\begin{aligned}\mathrm{HOTs} := {}& h_E^2\left[\|\boldsymbol{u}-\boldsymbol{u}_h\|_{\mathbf{V}_1(E)}^2 + \|p-p_h\|_{\mathrm{Q}_1(E)}^2 + S_{1,E}^2 + S_{2,E}^2 + \eta_{2,E}^2 + \|\boldsymbol{\zeta}-\boldsymbol{\zeta}_h\|_{\mathbb{M},E}^2\right]\\ &+ \sum_{e\in\mathcal{E}_{\mathrm{D}}^h(E)} h_e\|\nabla\varphi_{\mathrm{D}}\cdot\boldsymbol{t}_e - \Pi_{2,e}^{0,k_2}(\nabla\varphi_{\mathrm{D}}\cdot\boldsymbol{t}_e)\|_{0,e}^2.\end{aligned}$$

Proof. We start by defining $\mathbf{q}_E = \boldsymbol{\Pi}_2^{0,k_2}(\mathbb{M}^{-1}(\boldsymbol{\varepsilon}(\overline{\boldsymbol{u}}_h), p_h)\boldsymbol{\Pi}_2^{0,k_2}\boldsymbol{\zeta}_h) - \nabla\varphi_h \in \boldsymbol{\mathcal{P}}_{k_2}(E)$, and $\overline{\boldsymbol{\xi}}_E = \Psi_E\mathbf{q}_E$ with an element bubble function Ψ_E from Lemma 4.6. The first inequality in (4.1) and the definition of diffusive-flux in (2.1c) lead to

$$\begin{aligned}\|\mathbf{q}_E\|_{0,E}^2 \lesssim \left|\int_E \overline{\boldsymbol{\xi}}_E\cdot\mathbf{q}_E\right| &= \left|\int_E \overline{\boldsymbol{\xi}}_E\cdot\left(\nabla(\varphi-\varphi_h) - \mathbb{M}^{-1}(\boldsymbol{\varepsilon}(\boldsymbol{u}),p)\boldsymbol{\zeta} + \boldsymbol{\Pi}_2^{0,k_2}(\mathbb{M}^{-1}(\boldsymbol{\varepsilon}(\overline{\boldsymbol{u}}_h),p_h)\boldsymbol{\Pi}_2^{0,k_2}\boldsymbol{\zeta}_h)\right)\right|\\ &= \left|\int_E \mathrm{div}\,\overline{\boldsymbol{\xi}}_E(\varphi-\varphi_h) + \overline{\boldsymbol{\xi}}_E\cdot\left(\mathbb{M}^{-1}(\boldsymbol{\varepsilon}(\boldsymbol{u}),p)\boldsymbol{\zeta} - \boldsymbol{\Pi}_2^{0,k_2}(\mathbb{M}^{-1}(\boldsymbol{\varepsilon}(\overline{\boldsymbol{u}}_h),p_h)\boldsymbol{\Pi}_2^{0,k_2}\boldsymbol{\zeta}_h)\right)\right|\end{aligned}$$

with an integration by parts and $\Psi_E \in \mathrm{H}_0^1(E)$ in the last step. The Cauchy–Schwarz inequality, the inequality $\|\mathrm{div}(\bullet)\|_{0,E} \le \|\nabla(\bullet)\|_{0,E}$, and Lemma 4.6 show that

$$\|\mathbf{q}_E\|_{0,E}^2 \lesssim \sqrt{M}\Big(h_E^{-1}\|\varphi-\varphi_h\|_{\mathrm{Q}_2(E)}\|\mathbf{q}_E\|_{0,E} + \|\mathbb{M}^{-1}(\boldsymbol{\varepsilon}(\boldsymbol{u}),p)\boldsymbol{\zeta} - \boldsymbol{\Pi}_2^{0,k_2}(\mathbb{M}^{-1}(\boldsymbol{\varepsilon}(\overline{\boldsymbol{u}}_h),p_h)\boldsymbol{\Pi}_2^{0,k_2}\boldsymbol{\zeta}_h)\|_{0,E}\|\mathbf{q}_E\|_{0,E}\Big).$$

Lemma 4.4 implies that

$$Mh_E^2\|\mathbf{q}_E\|_{0,E}^2 \lesssim M^2(\|\varphi-\varphi_h\|_{\mathrm{Q}_2(E)}^2 + \mathrm{HOTs}). \tag{4.18}$$

Similarly, let $q_E = \mathrm{rot}(\boldsymbol{\Pi}_2^{0,k_2}(\mathbb{M}^{-1}(\boldsymbol{\varepsilon}(\overline{\boldsymbol{u}}_h),p_h)\boldsymbol{\Pi}_2^{0,k_2}\boldsymbol{\zeta}_h)) \in \mathcal{P}_{k_2-1}(E)$, and $\overline{\xi}_E = \Psi_E q_E$. Lemma 4.7, the observation that $\mathrm{rot}(\mathbb{M}^{-1}(\boldsymbol{\varepsilon}(\boldsymbol{u}),p)\boldsymbol{\zeta}) = \mathrm{rot}(\nabla\varphi) = 0$, and an integration by parts imply that

$$\begin{aligned}\|q_E\|_{0,E}^2 \lesssim \left|\int_E \overline{\xi}_E q_E\right| &= \left|\int_E \mathbf{rot}(\overline{\xi}_E)\cdot\Big(\boldsymbol{\Pi}_2^{0,k_2}(\mathbb{M}^{-1}(\boldsymbol{\varepsilon}(\overline{\boldsymbol{u}}_h),p_h)\boldsymbol{\Pi}_2^{0,k_2}\boldsymbol{\zeta}_h) - \mathbb{M}^{-1}(\boldsymbol{\varepsilon}(\boldsymbol{u}),p)\boldsymbol{\zeta}\Big)\right|\\ &\lesssim \|\boldsymbol{\Pi}_2^{0,k_2}(\mathbb{M}^{-1}(\boldsymbol{\varepsilon}(\overline{\boldsymbol{u}}_h),p_h)\boldsymbol{\Pi}_2^{0,k_2}\boldsymbol{\zeta}_h) - \mathbb{M}^{-1}(\boldsymbol{\varepsilon}(\boldsymbol{u}),p)\boldsymbol{\zeta}\|_{0,E}|\overline{\xi}_E|_{1,E}.\end{aligned}$$

This and Lemma 4.4 result in

$$Mh_E^2\|q_E\|_{0,E}^2 \lesssim M\max\{M,\overline{C}_3\}\left(\|\boldsymbol{u}-\boldsymbol{u}_h\|_{\mathbf{V}_1(E)}^2 + \|p-p_h\|_{\mathrm{Q}_1(E)}^2 + M\eta_{2,E}^2 + \|\boldsymbol{\zeta}-\boldsymbol{\zeta}_h\|_{\mathbb{M},E}^2 + \sum_{i=1}^2 S_{i,E}^2\right).$$

Now, for $e \in \mathcal{E}^h(E)$, we define $q_e = [\![\boldsymbol{\Pi}_2^{0,k_2}(\mathbb{M}^{-1}(\boldsymbol{\varepsilon}(\overline{\boldsymbol{u}}_h),p_h)\boldsymbol{\Pi}_2^{0,k_2}\boldsymbol{\zeta}_h)\cdot\boldsymbol{t}_e]\!] \in \mathcal{P}_{k_2}(e)$, and $\overline{\xi}_e = \Psi_e q_e$, with a given edge bubble function Ψ_e. Notice that $[\![\mathbb{M}^{-1}(\boldsymbol{\varepsilon}(\boldsymbol{u}),p)\boldsymbol{\zeta}\cdot\boldsymbol{t}_e]\!] = 0$ for all e. Then, from Lemma 4.7 and integration by parts, we readily see that

$$\begin{aligned}\|q_e\|_{0,e}^2 \lesssim \left|\int_e \overline{\xi}_e q_e\right| &= \Bigg|\sum_{E\in\mathcal{T}_e^h}\int_E \mathbf{rot}(\overline{\xi}_e)\cdot\Big(\boldsymbol{\Pi}_2^{0,k_2}(\mathbb{M}^{-1}(\boldsymbol{\varepsilon}(\overline{\boldsymbol{u}}_h),p_h)\boldsymbol{\Pi}_2^{0,k_2}\boldsymbol{\zeta}_h) - \mathbb{M}^{-1}(\boldsymbol{\varepsilon}(\boldsymbol{u}),p)\boldsymbol{\zeta})\Big)\\ &\quad + \sum_{E\in\mathcal{T}_e^h}\int_E \overline{\xi}_e\,\mathrm{rot}(\boldsymbol{\Pi}_2^{0,k_2}(\mathbb{M}^{-1}(\boldsymbol{\varepsilon}(\overline{\boldsymbol{u}}_h),p_h)\boldsymbol{\Pi}_2^{0,k_2}\boldsymbol{\zeta}_h)\Bigg|\\ &\lesssim \sum_{E\in\mathcal{T}_e^h}\|\boldsymbol{\Pi}_2^{0,k_2}(\mathbb{M}^{-1}(\boldsymbol{\varepsilon}(\overline{\boldsymbol{u}}_h),p_h)\boldsymbol{\Pi}_2^{0,k_2}\boldsymbol{\zeta}_h) - \mathbb{M}^{-1}(\boldsymbol{\varepsilon}(\boldsymbol{u}),p)\boldsymbol{\zeta}\|_{0,E}|\overline{\xi}_e|_{1,E}\\ &\quad + \sum_{E\in\mathcal{T}_e^h}\|\mathrm{rot}(\boldsymbol{\Pi}_2^{0,k_2}(\mathbb{M}^{-1}(\boldsymbol{\varepsilon}(\overline{\boldsymbol{u}}_h),p_h)\boldsymbol{\Pi}_2^{0,k_2}\boldsymbol{\zeta}_h)\|_{0,E}\|\overline{\xi}_e\|_{0,E}.\end{aligned}$$

Hence, Lemma 4.4 implies that

$$\begin{aligned}Mh_e\|q_e\|_{0,e} \lesssim M\max\{M,\overline{C}_3\}\Bigg(&\|\boldsymbol{u}-\boldsymbol{u}_h\|_{\mathbf{V}_1(E)}^2 + \|p-p_h\|_{\mathrm{Q}_1(E)}^2 + M\eta_{2,E}^2 + \|\boldsymbol{\zeta}-\boldsymbol{\zeta}_h\|_{\mathbb{M},E}^2\\ &+ \sum_{i=1}^2 S_{i,E}^2 + Mh_E^2\|q_E\|_{0,E}^2\Bigg).\end{aligned} \tag{4.19}$$

The trace inequality yields $\|\varphi_{\mathrm{D}}-\varphi_h\|_{0,e}^2 = \|\varphi-\varphi_h\|_{0,e}^2 \lesssim h_e^{-1}\|\varphi-\varphi_h\|_{0,E}^2 + h_e|\varphi-\varphi_h|_{1,e}^2$, and consequently

$$\begin{aligned}\|\varphi_{\mathrm{D}}-\varphi_h\|_{0,e}^2 &\lesssim h_e^{-1}\|\varphi-\varphi_h\|_{0,e}^2 + h_E\|\boldsymbol{\Pi}_2^{0,k_2}(\mathbb{M}^{-1}(\boldsymbol{\varepsilon}(\overline{\boldsymbol{u}}_h),p_h)\boldsymbol{\Pi}_2^{0,k_2}\boldsymbol{\zeta}_h) - \nabla\varphi_h\|_{0,E}^2\\ &\quad + h_E\|\mathbb{M}^{-1}(\boldsymbol{\varepsilon}(\boldsymbol{u}),p)\boldsymbol{\zeta} - \boldsymbol{\Pi}_2^{0,k_2}(\mathbb{M}^{-1}(\boldsymbol{\varepsilon}(\overline{\boldsymbol{u}}_h),p_h)\boldsymbol{\Pi}_2^{0,k_2}\boldsymbol{\zeta}_h)\|_{0,E}^2,\end{aligned}$$

where we have used $\mathbb{M}^{-1}(\boldsymbol{\varepsilon}(\boldsymbol{u}),p)\boldsymbol{\zeta} = \nabla\varphi$ from (2.1c), added and subtracted $\boldsymbol{\Pi}_2^{0,k_2}(\mathbb{M}^{-1}(\boldsymbol{\varepsilon}(\overline{\boldsymbol{u}}_h),p_h)\boldsymbol{\Pi}_2^{0,k_2}\boldsymbol{\zeta}_h)$, and applied the triangle inequality. This, and a scaling argument together with the inclusion of HOTs and the definition of $\mathbf{q}_E$ lead to the following bound

$$Mh_e\|\varphi_{\mathrm{D}}-\varphi_h\|_{0,e}^2 \lesssim M^2(\|\varphi-\varphi_h\|_{\mathrm{Q}_2(E)}^2 + Mh_E^2\|\mathbf{q}_E\|_{0,E}^2 + \mathrm{HOTs}).$$

In addition, we define $q_e^* = \Pi_{2,e}^{0,k_2}(\nabla\varphi_{\mathrm{D}}\cdot\boldsymbol{t}_e) - \boldsymbol{\Pi}_2^{0,k_2}(\mathbb{M}^{-1}(\boldsymbol{\varepsilon}(\overline{\boldsymbol{u}}_h),p_h)\boldsymbol{\Pi}_2^{0,k_2}\boldsymbol{\zeta}_h)\cdot\boldsymbol{t}_e \in \mathcal{P}_{k_2}(e)$, where $\Pi_{2,e}^{0,k_2}$ is defined as the polynomial projection on the edge e, and $\overline{\xi}_e^* = \Psi_e q_e^*$. Lemma 4.7, $\nabla\varphi\cdot\boldsymbol{t}_e = \nabla\varphi_{\mathrm{D}}\cdot\boldsymbol{t}_e$ on Γ_{D}, (2.1c), and an integration by parts imply that $\|q_e^*\|_{0,e}^2 \lesssim \left|\int_e \overline{\xi}_e^* q_e^*\right|$. Furthermore,

$$\left|\int_e \overline{\xi}_e^* q_e^*\right| = \left|\sum_{E\in\mathcal{T}_e^h}\int_E \mathbf{rot}(\overline{\xi}_e^*)\cdot(\boldsymbol{\Pi}_2^{0,k_2}(\mathbb{M}^{-1}(\boldsymbol{\varepsilon}(\overline{\boldsymbol{u}}_h),p_h)\boldsymbol{\Pi}_2^{0,k_2}\boldsymbol{\zeta}_h) - \mathbb{M}^{-1}(\boldsymbol{\varepsilon}(\boldsymbol{u}),p)\boldsymbol{\zeta})\right.$$

$$+\sum_{E\in\mathcal{T}_e^h}\int_E \overline{\xi}_e^* \operatorname{rot}(\mathbf{\Pi}_2^{0,k_2}(\mathbb{M}^{-1}(\boldsymbol{\varepsilon}(\overline{\boldsymbol{u}}_h),p_h)\mathbf{\Pi}_2^{0,k_2}\boldsymbol{\zeta}_h)) + \sum_{e\in\mathcal{E}_{\mathrm{D}}^h(E)}\int_e \overline{\xi}_e^*\left(\nabla\varphi_{\mathrm{D}}\cdot\boldsymbol{t}_e - \Pi_{2,e}^{0,k_2}(\nabla\varphi_{\mathrm{D}}\cdot\boldsymbol{t}_e)\right)\Bigg|$$
$$\lesssim \|\mathbf{\Pi}_2^{0,k_2}(\mathbb{M}^{-1}(\boldsymbol{\varepsilon}(\overline{\boldsymbol{u}}_h),p_h)\mathbf{\Pi}_2^{0,k_2}\boldsymbol{\zeta}_h) - \mathbb{M}^{-1}(\boldsymbol{\varepsilon}(\boldsymbol{u}),p)\boldsymbol{\zeta}\|_{0,E}|\overline{\xi}_e^*|_{1,E}$$
$$+\|\operatorname{rot}(\mathbf{\Pi}_2^{0,k_2}(\mathbb{M}^{-1}(\boldsymbol{\varepsilon}(\overline{\boldsymbol{u}}_h),p_h)\mathbf{\Pi}_2^{0,k_2}\boldsymbol{\zeta}_h))\|_{0,E}\|\overline{\xi}_e^*\|_{0,E} + \|\nabla\varphi_{\mathrm{D}}\cdot\boldsymbol{t}_e - \Pi_{2,e}^{0,k_2}(\nabla\varphi_{\mathrm{D}}\cdot\boldsymbol{t}_e)\|_{0,e}\|\overline{\xi}_e^*\|_{0,e},$$

which results in the following bound

$$Mh_e\|q_e\|_{0,e}^2 \lesssim M\max\left\{M,\overline{C}_3\right\}\Big(\|\boldsymbol{u}-\boldsymbol{u}_h\|_{\mathbf{V}_1(E)}^2 + \|p-p_h\|_{\mathrm{Q}_1(E)}^2 + M\eta_{2,E}^2 + \|\boldsymbol{\zeta}-\boldsymbol{\zeta}_h\|_{\mathbb{M},E}^2 + \sum_{i=1}^2 S_{i,E}^2 + Mh_E^2\|q_E\|_{0,E}^2 + \mathrm{HOTs}\Big). \tag{4.20}$$

Finally, equation (2.1d) shows that

$$\sqrt{M}\Lambda_{2,E} = \sqrt{M}\|\operatorname{div}(\boldsymbol{\zeta}-\boldsymbol{\zeta}_h) + \theta(\varphi-\varphi_h)\|_{0,E} \lesssim M\left(\|\boldsymbol{\zeta}-\boldsymbol{\zeta}_h\|_{\mathbf{V}_2(E)} + \|\varphi-\varphi_h\|_{\mathrm{Q}_2(E)}\right). \tag{4.21}$$

Summing for all $e\in\partial E$ (4.19)-(4.20) and for all $E\in\mathcal{T}^h$ (4.18)-(4.21) concludes the proof. □

The efficiency of the residual and mixed estimators (up to data oscillation and stabilisation) is summarised below, and we recall that it is a direct consequence of Lemmas 4.14-4.15.

Theorem 4.16. *Under the small data assumption of Theorems 2.1 and 3.3, the following bound holds*

$$\Xi^2 + \Lambda^2 \lesssim \overline{\mathrm{e}}_h^2 + \eta^2 + S^2 + \mathrm{HOTs}.$$

Proof. Notice that by putting together Lemmas 4.14-4.15 we arrive at

$$\Xi^2 + \Lambda^2 \lesssim \max\left\{2\mu M, M^2, M\overline{C}_3\right\}(\overline{\mathrm{e}}_h^2 + \eta^2 + S^2 + \mathrm{HOTs}).$$

On the other hand, the small data assumption (3.4a) implies that

$$\max\left\{\frac{1}{2\mu},2\mu\right\}M^4 < \frac{1}{C_*^2}, \text{ with } C_* = \overline{C}_1\overline{C}_2^2L_\ell L_{\mathbb{M}}\left(\|\varphi_{\mathrm{D}}\|_{\frac{1}{2},\Gamma_{\mathrm{D}}} + \|g\|_{0,\Omega}\right).$$

This observation together with the assumption $1\le M$ (cf. (2.2)) and the fact that $1\le\max\left\{\frac{1}{2\mu},2\mu\right\}$, lead to

$$\max\left\{2\mu M, M^2, M\overline{C}_3\right\} = \max\left\{2\mu M, M^2, \max\left\{\frac{1}{2\mu},2\mu\right\}\sqrt{M^3}C^*\right\} \le \max\{1,C^*\}\max\left\{\frac{1}{2\mu},2\mu\right\}M^4 < \overline{C},$$

with $C^* = L_{\mathbb{M}}\overline{C}_2\left(\|\varphi_{\mathrm{D}}\|_{\frac{1}{2},\Gamma_{\mathrm{D}}} + \|g\|_{0,\Omega}\right)$ and $\overline{C} = \max\left\{\frac{1}{C_*^2},\frac{C^*}{C_*^2}\right\}$. Recall that both the constants C_* and C^* do not depend on physical parameters. □

Remark 3. *The high-order terms (*HOTs*) collect contributions that are asymptotically negligible, in the sense that for some $h_*>0$ such that $h_E<h_*$ these terms decay faster than the actual error, stabilisation terms, and data oscillation due to the presence of an additional factor of h_E. In particular, they consist of a partial error contribution $h_E^2\left[\|\boldsymbol{u}-\boldsymbol{u}_h\|_{\mathbf{V}_1(E)}^2 + \|p-p_h\|_{\mathrm{Q}_1(E)}^2 + \|\boldsymbol{\zeta}-\boldsymbol{\zeta}_h\|_{\mathbb{M},E}^2\right]$, and the stabilisation and data oscillation contributions $h_E^2\left[S_{1,E}^2 + S_{2,E}^2 + \eta_{2,E}^2\right]$. On the other hand, the polynomial approximation error of the Dirichlet datum associated with the diffusion problem, namely*

$$\sum_{e\in\mathcal{E}_D^h(E)} h_e\|\nabla\varphi_{\mathrm{D}}\cdot\boldsymbol{t}_e - \Pi_{2,e}^{0,k_2}(\nabla\varphi_{\mathrm{D}}\cdot\boldsymbol{t}_e)\|_{0,e}^2,$$

exhibits a convergence rate higher that h_e depending on the regularity assumption on φ_{D} (cf. Section 4.2).

5. 3D virtual element formulation

In this section, we extend the discretisation to the 3D case following [6, 9]. We introduce two novel quasi-interpolators for $\mathbf{H}^1$ functions in Stokes-like and edge VE spaces, and an extended Helmholtz decomposition for 3D mixed VEM. Although we only sketch the proof of reliability to avoid repeating arguments from the two-dimensional case, we present a detailed proof of the interpolation estimates, as these constitute essential tools and may be of independent interest.

5.1. Considerations for 3D discretisation

Let $\mathcal{T}^h$ be a decomposition of Ω into polyhedral elements P with diameter h_P and let $\mathcal{F}^h$ be the set of faces f with diameter h_f. Natural extensions of the mesh assumptions from Section 3 are given as follows:

(M1) each polyhedral element P is star-shaped with respect to a ball of radius $\geq \rho h_P$,
(M2) every face f of P is star-shaped with respect to a disk of radius $\geq \rho h_P$,
(M3) every edge e of P has length $\geq \rho h_P$.

Note that the polynomial decompositions discussed in Section 3 also follow in the 3D case for $\boldsymbol{\mathcal{P}}_k(P)$ with the spaces $\boldsymbol{\mathcal{G}}_k^{\oplus}(P) := \boldsymbol{x} \wedge (\mathcal{P}_{k-1}(P))^3$, $\boldsymbol{\mathcal{R}}_k(P) := \mathbf{curl}(\mathcal{P}_{k+1}(P))$, and $\boldsymbol{\mathcal{R}}_k^{\oplus}(P) := \boldsymbol{x}\mathcal{P}_{k-1}(P)$, where $\boldsymbol{x} := (x_1, x_2, x_3)^{\mathtt{t}}$, and $\wedge$ the usual external product.

Following Section 4, the set of faces is divided as $\mathcal{F}^h = \mathcal{F}_\Omega^h \cup \mathcal{F}_D^h \cup \mathcal{F}_N^h$, where $\mathcal{F}_\Omega^h = \{f \in \mathcal{F}^h : f \subset \Omega\}$, $\mathcal{F}_D^h = \{f \in \mathcal{F}^h : f \subset \Gamma_D\}$ and $\mathcal{F}_N^h = \{f \in \mathcal{F}^h : f \subset \Gamma_N\}$. Furthermore, the set of faces of P is denoted by $\mathcal{F}^h(P)$, the set of faces of P which are not in the boundary $\partial\Omega$ is denoted by $\mathcal{F}_\Omega^h(P)$, and the ones that lie on the Dirichlet (resp. Neumann) portion of the boundary are denoted by $\mathcal{F}_D^h(P)$ (resp. $\mathcal{F}_N^h(P)$). Also, the set of elements P that share f as a common face is denoted by $\mathcal{T}_f^h$ and the set of faces f of P that share a common edge e is denoted by $\mathcal{F}_e^h(P)$. The normal and tangential jump operators are defined as usual by $[\![\boldsymbol{u} \cdot \boldsymbol{n}_P^f]\!] := (\boldsymbol{u}|_P - \boldsymbol{u}|_{P'})|_f \cdot \boldsymbol{n}_P^f$ and $[\![\boldsymbol{\zeta} \times \boldsymbol{n}_P^f]\!] := (\boldsymbol{\zeta}|_P - \boldsymbol{\zeta}|_{P'})|_f \times \boldsymbol{n}_P^f$, where P and P' are elements in $\mathcal{T}^h$ with a common face f, also $\boldsymbol{n}_P^f$ and $\boldsymbol{t}_P^{f,1}, \boldsymbol{t}_P^{f,2}$ are the outward normal and tangential vectors of P with respect to the plane defined by f. In addition, for a smooth enough vector-valued function $\boldsymbol{u}$ on P we define the tangential component with respect to f as $\boldsymbol{u}_f := \boldsymbol{u} - (\boldsymbol{u} \cdot \boldsymbol{n}_P^f)\boldsymbol{n}_P^f$. We also set $\boldsymbol{u}_t|_f := \boldsymbol{u}_f$.

We recall that the same definitions from Section 3.2 hold for the 3D case taking into account that the set of rigid body motions for a polyhedral P is given by

$$\mathbf{RBM}(P) = \left\{ \begin{pmatrix} \frac{1}{h_P} \\ 0 \\ 0 \end{pmatrix}, \begin{pmatrix} 0 \\ \frac{1}{h_P} \\ 0 \end{pmatrix}, \begin{pmatrix} 0 \\ 0 \\ \frac{1}{h_P} \end{pmatrix}, \begin{pmatrix} \frac{x_{2,P}-x_2}{h_P} \\ \frac{x_1-x_{1,P}}{h_P} \\ 0 \end{pmatrix}, \begin{pmatrix} 0 \\ \frac{x_{3,P}-x_3}{h_P} \\ \frac{x_2-x_{2,P}}{h_P} \end{pmatrix}, \begin{pmatrix} \frac{x_3-x_{3,P}}{h_P} \\ 0 \\ \frac{x_{1,P}-x_1}{h_P} \end{pmatrix} \right\}.$$

We shall use the notation $\boldsymbol{\Pi}_1^{\boldsymbol{\varepsilon},k_1,P}, \Pi_1^{\boldsymbol{\varepsilon},k_1,P}, \boldsymbol{\Pi}_j^{0,k_j,P}, \Pi_j^{0,k_j,P}$ (resp. $\boldsymbol{\Pi}_1^{\boldsymbol{\varepsilon},k_1,f}$, $\Pi_1^{\boldsymbol{\varepsilon},k_1,f}$, $\boldsymbol{\Pi}_j^{0,k_j,f}$, $\Pi_j^{0,k_j,f}$) for vector and scalar valued polyhedral (resp. face) projections. We refer to [9, Proposition 5.1] and [6, Theorem 3.2] for the computability of the 3D projections in Stokes and H(div) − H(**curl**) spaces, respectively. Furthermore, Lemma 3.1 can be extended to the 3D case by classical techniques for polynomial projections and a scaling argument.

5.2. Discrete spaces

Given $k_1 \geq 2$, we first define a local VE space [9] as

$$\begin{aligned} \mathbf{V}_1^{h,k_1}(P) := \{\boldsymbol{v} \in \mathbf{H}^1(P) \colon \boldsymbol{v}|_{\partial P} \in \widetilde{\boldsymbol{\mathcal{B}}}_1^{h,k_1}(\partial P),\ \operatorname{div} \boldsymbol{v} \in \mathcal{P}_{k_1-1}(P), \\ -2\mu\, \mathbf{div}\, \boldsymbol{\varepsilon}(\boldsymbol{v}) - \nabla s \in \boldsymbol{\mathcal{G}}_{k_1}^{\oplus}(P), \text{ for some } s \in \mathrm{L}_0^2(P)\}, \end{aligned}$$

where the boundary space of VE functions along the boundary ∂P of P, is defined as follows

$$\widetilde{\boldsymbol{\mathcal{B}}}_1^{h,k_1}(\partial P) := \{v \in C^0(\partial P) \colon \boldsymbol{v}|_f \in \widetilde{\mathcal{B}}_1^{h,k_1}(f),\ \forall f \subset \partial P\},$$

and for each face $f \in \partial P$, the enhanced VE space $\widetilde{\boldsymbol{\mathcal{B}}}_1^{h,k_1}(f)$ locally solves the Poisson equation with Dirichlet boundary conditions, and it is defined by (here Δ_f denotes the tangential Laplacian on f)

$$\begin{aligned} \widetilde{\boldsymbol{\mathcal{B}}}_1^{h,k_1}(f) := \{\boldsymbol{v} \in \mathrm{H}^1(f) \colon \boldsymbol{v}|_{\partial f} \in C^0(\partial f),\ \boldsymbol{v}|_e \in \mathcal{P}_{k_1}(e), \forall e \subset \partial f,\ \Delta_f \boldsymbol{v} \in \mathcal{P}_{k_1+1}(f), \\ \int_f (\boldsymbol{v} - \Pi_1^{\boldsymbol{\varepsilon},k_1,f} \boldsymbol{v}) m_{k_1+1} = 0,\ \forall m_{k+1} \in \mathcal{M}_{k_1+1}(f) \setminus \mathcal{M}_{k_1-2}(f)\}. \end{aligned}$$

Notice that the enhanced property on faces is needed in 3D to compute exactly the L^2-orthogonal projection $\Pi_1^{0,k_1+1,f}$ (see [1, Remark 5] for further details). Moreover, $\boldsymbol{\mathcal{P}}_{k_1}(P) \subseteq \mathbf{V}_1^{h,k_1}(P)$. The global discrete spaces are defined by

$$\mathbf{V}_1^{h,k_1} := \{\boldsymbol{v} \in \mathbf{V}_1 : \boldsymbol{v}|_P \in \mathbf{V}_1^{h,k_1}(P), \forall P \in \mathcal{T}^h\}, \quad \mathrm{Q}_1^{h,k_1} := \{q \in \mathrm{Q}_1 \colon q|_P \in \mathcal{P}_{k_1-1}(P), \forall P \in \mathcal{T}^h\}.$$

The DoFs for $\boldsymbol{v}_h \in \mathbf{V}_1^{h,k_1}(P)$ and $q_h \in \mathrm{Q}_1^{h,k_1}(P)$ are as follows

- The values of $\boldsymbol{v}_h$ at the vertices of P,
- The values of $\boldsymbol{v}_h$ at the $k_1 - 1$ internal quadrature points on each edge of P,

- $\displaystyle\fint_f (\boldsymbol{v}_h \cdot \boldsymbol{n}_P^f) m_{k_1-2}, \quad \forall m_{k_1-2} \in \mathcal{M}_{k_1-2}(f),$
- $\displaystyle\fint_f (\boldsymbol{v}_h)_t \cdot \mathbf{m}_{k_1-2}, \quad \forall \mathbf{m}_{k_1-2} \in \boldsymbol{\mathcal{M}}_{k_1-2}(f),$
- $\displaystyle\int_P \boldsymbol{v}_h \cdot \mathbf{m}_{k_1-2}^{\oplus}, \quad \forall \mathbf{m}_{k_1-2}^{\oplus} \in \boldsymbol{\mathcal{M}}_{k_1-2}^{\oplus}(P),$
- $\displaystyle\int_P (\operatorname{div} \boldsymbol{v}_h) m_{k_1-1}, \quad \forall m_{k_1-1} \in \mathcal{M}_{k_1-1}(P) \setminus \left\{ \frac{1}{h_P} \right\},$
- $\displaystyle\int_P q_h m_{k_1-1}, \quad \forall m_{k_1-1} \in \mathcal{M}_{k_1-1}(P).$

The construction of the $\mathbf{H}(\operatorname{div}, \Omega)$ conforming 3D VE space naturally follows its 2D counterpart [6]. The definition differs from the 2D version by setting $k_2 \geq 1$ to ensure continuity of the normal components across faces. The discrete VE space locally solves a $\nabla(\operatorname{div})$-**curl** problem as follows

$$\begin{aligned}\mathbf{V}_2^{h,k_2}(P) := \{\boldsymbol{\xi} \in \mathbf{H}(\operatorname{div}, P) \cap \mathbf{H}(\mathbf{curl}, P) \colon \boldsymbol{\xi} \cdot \boldsymbol{n}_P^f|_f \in \mathcal{P}_{k_2}(f),\, \forall f \in \partial P,\\ \nabla(\operatorname{div} \boldsymbol{\xi}) \in \boldsymbol{\mathcal{G}}_{k_2-2}(P),\ \mathbf{curl}\, \boldsymbol{\xi} \in \boldsymbol{\mathcal{R}}_{k_2-1}(P)\}.\end{aligned}$$

Observe that $\boldsymbol{\mathcal{P}}_{k_2}(P) \subseteq \mathbf{V}_2^{h,k_2}(P)$. Then, the discrete global spaces are defined by

$$\mathbf{V}_2^{h,k_2} := \{\boldsymbol{\xi} \in \mathbf{V}_2 \colon \boldsymbol{\xi}|_P \in \mathbf{V}_2^{h,k_2}(P),\, \forall P \in \mathcal{T}^h\}, \quad \mathrm{Q}_2^{h,k_2} := \{\psi \in \mathrm{Q}_2 \colon \psi|_P \in \mathcal{P}_{k_2-1}(P),\, \forall P \in \mathcal{T}^h\}.$$

The set of DoFs for $\boldsymbol{\xi}_h \in \mathbf{V}_2^{h,k_2}(P)$ and $\psi_h \in \mathrm{Q}_2^{h,k_2}(P)$ can be taken as

- The values of $\boldsymbol{\xi}_h \cdot \boldsymbol{n}_P^f$ at the $k_2 + 1$ quadrature points on each face of P,
- $\displaystyle\int_P \boldsymbol{\xi}_h \cdot \mathbf{m}_{k_2-2}^{\nabla}, \quad \forall \mathbf{m}_{k_2-2}^{\nabla} \in \boldsymbol{\mathcal{M}}_{k_2-2}^{\nabla}(P),$
- $\displaystyle\int_P \boldsymbol{\xi}_h \cdot \mathbf{m}_{k_2}^{\oplus}, \quad \forall \mathbf{m}_{k_2}^{\oplus} \in \boldsymbol{\mathcal{M}}_{k_2}^{\oplus}(P),$
- $\displaystyle\int_P \psi_h m_{k_2}, \quad \forall m_{k_2} \in \mathcal{M}_{k_2}(P).$

5.3. **Interpolation operators**

Our goal is to define a quasi–interpolator $\mathbf{I}_1^{Q,k_1} : \mathbf{H}^1(P) \to \mathbf{V}_1^{h,k_1}(P)$ and Fortin operator $\mathbf{I}_2^{F,k_2} : \mathbf{H}^1(P) \to \mathbf{V}_2^{h,k_2}(P)$, which are essential in extending the reliability result (see Theorem 4.13) to the 3D case. The Fortin operator $\mathbf{I}_2^{F,k_2}$ defined through the DoFs (similarly to the 2D case) is presented in [11, Section 4.1]. On the other hand, the construction of $\mathbf{I}_1^{Q,k_1}$ is more involved due to the minimal regularity, which is stated next.

Proposition 5.1. *Let $\boldsymbol{v} \in \mathbf{H}^{s_1+1}(\Omega)$, and $0 \leq s_1 \leq k_1$. Under the mesh assumptions, there exists $\mathbf{I}_1^{Q,k_1}\boldsymbol{v} \in \mathbf{V}_1^{h,k_1}$ such that, for all $P \in \mathcal{T}^h$*

$$\|\boldsymbol{v} - \mathbf{I}_1^{Q,k_1}\boldsymbol{v}\|_{0,P} + h_P\|\boldsymbol{\varepsilon}(\boldsymbol{v} - \mathbf{I}_1^{Q,k_1}\boldsymbol{v})\|_{0,P} \lesssim h_P^{s_1+1}|\boldsymbol{v}|_{s_1+1,D(P)},$$

where $D(P)$ denote the union of the polyhedral elements in $\mathcal{T}^h$ intersecting P.

Proof. Step 1 (Existence of interpolation in the space $\mathbf{V}_1^{h,k_1}$). Let $P \in \mathcal{T}^h$, we start considering the super-enhanced version of the enhanced VE space $\widetilde{\boldsymbol{\mathcal{B}}}_1^{h,k_1}(f)$ from [18] which locally solves a Poisson problem with Dirichlet boundary conditions. Let $\mathbf{I}_1^{C,k_1}\boldsymbol{v} \in \mathbf{H}_D^1(\Omega)$ be the Clément-type VE interpolation in $\widetilde{\boldsymbol{\mathcal{B}}}_1^{h,k_1}(f)$ satisfying the following estimate for all $P \in \mathcal{T}^h$ (see [18, Theorem 11])

$$\|\boldsymbol{v} - \mathbf{I}_1^{C,k_1}\boldsymbol{v}\|_{0,P} + h_P\|\boldsymbol{\varepsilon}(\boldsymbol{v} - \mathbf{I}_1^{C,k_1}\boldsymbol{v})\|_{0,P} \lesssim h_P^{s_1+1}|\boldsymbol{v}|_{s_1+1,D(P)}. \tag{5.1}$$

Let $\boldsymbol{v}_\pi = \boldsymbol{\Pi}_1^{\boldsymbol{\varepsilon},k_1}\boldsymbol{v}$ be the polynomial approximation of $\boldsymbol{v}$. The decomposition $\boldsymbol{\mathcal{P}}_{k_1-2}(P) = \boldsymbol{\mathcal{G}}_{k_1-2}(P) \oplus \boldsymbol{\mathcal{G}}_{k_1-2}^{\oplus}(P)$ guarantees the existence of $p_\pi \in \mathcal{P}_{k_1-1}(P)$ and $\boldsymbol{g}_\pi^{\oplus} \in \boldsymbol{\mathcal{G}}_{k_1-2}^{\oplus}(P)$ such that

$$-2\mu\, \mathbf{div}\, \boldsymbol{\varepsilon}(\boldsymbol{v}_\pi) = \nabla p_\pi + \boldsymbol{g}_\pi^{\oplus}. \tag{5.2}$$

For $q_{k_1-1}|_P = \Pi_1^{0,k_1-1}(\operatorname{div} \mathbf{I}_1^{C,k_1}\boldsymbol{v})$, we introduce the following Stokes problem for all $P \in \mathcal{T}^h$ as

$$\begin{cases} -2\mu\, \mathbf{div}(\boldsymbol{\varepsilon}(\widetilde{\boldsymbol{v}}_I)) - \nabla s = \boldsymbol{g}_\pi^\oplus & \text{in } P, \\ \operatorname{div} \widetilde{\boldsymbol{v}}_I = q_{k_1-1} & \text{in } P, \\ \widetilde{\boldsymbol{v}}_I = \mathbf{I}_1^{C,k_1}\boldsymbol{v} & \text{on } \partial P. \end{cases} \tag{5.3}$$

Observe that $\widetilde{\boldsymbol{v}}_I \in \mathbf{V}_1^{h,k_1}(P)$ from the definition of $\mathbf{V}_1^{h,k_1}(P)$. This and $\widetilde{\boldsymbol{v}}_I = \mathbf{I}_1^{C,k_1}\boldsymbol{v} \in \mathbf{V}_1$ on each boundary of P imply that $\widetilde{\boldsymbol{v}}_I \in \mathbf{V}_1^{h,k_1}$. Thus, we define the quasi interpolation operator as $\mathbf{I}_1^{Q,k_1}\boldsymbol{v} := \widetilde{\boldsymbol{v}}_I$.
Step 2 (Error estimate). We start by defining the auxiliary problem

$$\begin{cases} -2\mu\, \mathbf{div}(\boldsymbol{\varepsilon}(\widetilde{\boldsymbol{v}})) - \nabla \widetilde{s} = \boldsymbol{g}_\pi^\oplus & \text{in } P, \\ \operatorname{div} \widetilde{\boldsymbol{v}} = \operatorname{div} \mathbf{I}_1^{C,k_1}\boldsymbol{v} & \text{in } P, \\ \widetilde{\boldsymbol{v}} = \mathbf{I}_1^{C,k_1}\boldsymbol{v} & \text{on } \partial P. \end{cases} \tag{5.4}$$

Then, the combination of (5.2) and (5.4) leads to

$$\begin{cases} -2\mu\, \mathbf{div}(\boldsymbol{\varepsilon}(\boldsymbol{v}_\pi - \widetilde{\boldsymbol{v}})) - \nabla(p_\pi - \widetilde{s}) = \mathbf{0} & \text{in } P, \\ \operatorname{div}(\boldsymbol{v}_\pi - \widetilde{\boldsymbol{v}}) = \operatorname{div}(\boldsymbol{v}_\pi - \mathbf{I}_1^{C,k_1}\boldsymbol{v}) & \text{in } P, \\ \boldsymbol{v}_\pi - \widetilde{\boldsymbol{v}} = \boldsymbol{v}_\pi - \mathbf{I}_1^{C,k_1}\boldsymbol{v} & \text{on } \partial P. \end{cases} \tag{5.5}$$

Since $\boldsymbol{z} - (\boldsymbol{v}_\pi - \widetilde{\boldsymbol{v}}) \in \mathbf{H}_0^1(P)$ for any $\boldsymbol{z} \in \mathbf{H}^1(P)$ with $\operatorname{div} \boldsymbol{z} = \operatorname{div}(\boldsymbol{v}_\pi - \mathbf{I}_1^{C,k_1}\boldsymbol{v})$ in P and $\boldsymbol{z} = \boldsymbol{v}_\pi - \mathbf{I}_1^{C,k_1}\boldsymbol{v}$ on ∂P, an integration by parts twice and (5.5) show

$$2\mu \int_P \boldsymbol{\varepsilon}(\boldsymbol{v}_\pi - \widetilde{\boldsymbol{v}}) : \boldsymbol{\varepsilon}(\boldsymbol{z} - (\boldsymbol{v}_\pi - \widetilde{\boldsymbol{v}})) = \int_P \nabla(p_\pi - \widetilde{s}) \cdot (\boldsymbol{z} - (\boldsymbol{v}_\pi - \widetilde{\boldsymbol{v}})) = -\int_P (p_\pi - \widetilde{s}) \operatorname{div}(\boldsymbol{z} - (\boldsymbol{v}_\pi - \widetilde{\boldsymbol{v}})) = 0.$$

This results in $\|\boldsymbol{\varepsilon}(\boldsymbol{v}_\pi - \widetilde{\boldsymbol{v}})\|_{0,P} \le \|\boldsymbol{\varepsilon}(\boldsymbol{z})\|_{0,P}$ and hence for $\boldsymbol{z} = \boldsymbol{v}_\pi - \mathbf{I}_1^{C,k_1}\boldsymbol{v}$ we have

$$\|\boldsymbol{\varepsilon}(\boldsymbol{v}_\pi - \widetilde{\boldsymbol{v}})\|_{0,P} \le \|\boldsymbol{\varepsilon}(\boldsymbol{v}_\pi - \mathbf{I}_1^{C,k_1}\boldsymbol{v})\|_{0,P} \le \|\boldsymbol{\varepsilon}(\boldsymbol{v} - \boldsymbol{v}_\pi)\|_{0,P} + \|\boldsymbol{\varepsilon}(\boldsymbol{v} - \mathbf{I}_1^{C,k_1}\boldsymbol{v})\|_{0,P} \lesssim h_P^{s_1} |\boldsymbol{v}|_{s_1+1,D(P)}, \tag{5.6}$$

where the triangle inequality, $\|\boldsymbol{\varepsilon}(\cdot)\|_{0,P} \le |\cdot|_{1,P}$, Lemma 3.1 and (5.1) were applied. Next, to estimate $\widetilde{\boldsymbol{v}} - \widetilde{\boldsymbol{v}}_I$ we consider the auxiliary problem arising from subtracting (5.4) and (5.3)

$$\begin{cases} -2\mu\, \mathbf{div}(\boldsymbol{\varepsilon}(\widetilde{\boldsymbol{v}} - \widetilde{\boldsymbol{v}}_I)) - \nabla(\widetilde{s} - s) = \mathbf{0} & \text{in } P, \\ \operatorname{div}(\widetilde{\boldsymbol{v}} - \widetilde{\boldsymbol{v}}_I) = \operatorname{div}(\mathbf{I}_1^{C,k_1}\boldsymbol{v}) - q_{k-1} & \text{in } P, \\ \widetilde{\boldsymbol{v}} - \widetilde{\boldsymbol{v}}_I = \mathbf{0} & \text{on } \partial P. \end{cases}$$

Given a star-shaped polyhedral domain P with respect to a ball B, the mesh assumptions lead to $|P||B|^{-1} \le \rho^{-3}$ in 3D (see e.g. [23]). This and [25, Theorem 3.2] imply that there exists a universal positive constant depending only on the mesh regularity parameter ρ and the dimension d (but independent of P) such that

$$\|\boldsymbol{\varepsilon}(\widetilde{\boldsymbol{v}} - \widetilde{\boldsymbol{v}}_I)\|_{0,P} \le |\widetilde{\boldsymbol{v}} - \widetilde{\boldsymbol{v}}_I|_{1,P} \lesssim \|\operatorname{div}(\mathbf{I}_1^{C,k_1}\boldsymbol{v}) - \Pi_1^{0,k_1-1} \operatorname{div}(\mathbf{I}_1^{C,k_1}\boldsymbol{v})\|_{0,P}. \tag{5.7}$$

Note that the triangle inequality, (5.1), and the estimates for Π_1^{0,k_1-1} allow us to assert that

$$\|\operatorname{div}(\mathbf{I}_1^{C,k_1}\boldsymbol{v}) - \Pi_1^{0,k_1-1} \operatorname{div} \boldsymbol{v}\|_{0,P} \lesssim \|\operatorname{div}(\boldsymbol{v} - \mathbf{I}_1^{C,k_1}\boldsymbol{v})\|_{0,P} + \|\operatorname{div} \boldsymbol{v} - \Pi_1^{0,k_1-1} \operatorname{div} \boldsymbol{v}\|_{0,P} \lesssim h^{s_1} |\boldsymbol{v}|_{s_1+1,D(P)}. \tag{5.8}$$

The triangle inequality in (5.7) followed by the L^2-stability of Π_1^{0,k_1-1} leads to

$$\begin{aligned} \|\boldsymbol{\varepsilon}(\widetilde{\boldsymbol{v}} - \widetilde{\boldsymbol{v}}_I)\|_{0,P} &\le \|\operatorname{div}(\mathbf{I}_1^{C,k_1}\boldsymbol{v}) - \Pi_1^{0,k_1-1} \operatorname{div} \boldsymbol{v}\|_{0,P} + \|\Pi_1^{0,k_1-1} \left(\operatorname{div}(\boldsymbol{v}) - \operatorname{div}(\mathbf{I}_1^{C,k_1}\boldsymbol{v})\right)\|_{0,P} \\ &\lesssim \|\operatorname{div}(\mathbf{I}_1^{C,k_1}\boldsymbol{v}) - \Pi_1^{0,k_1-1} \operatorname{div} \boldsymbol{v}\|_{0,P} + \|\operatorname{div}(\boldsymbol{v}) - \operatorname{div}(\mathbf{I}_1^{C,k_1}\boldsymbol{v})\|_{0,P} \\ &\lesssim h^{s_1} |\boldsymbol{v}|_{s_1+1,D(P)}, \end{aligned} \tag{5.9}$$

with the estimates (5.8) and (5.1) in the last step. Hence, the triangle inequality

$$\|\boldsymbol{\varepsilon}(\boldsymbol{v} - \widetilde{\boldsymbol{v}}_I)\|_{0,P} \le \|\boldsymbol{\varepsilon}(\boldsymbol{v} - \boldsymbol{v}_\pi)\|_{0,P} + \|\boldsymbol{\varepsilon}(\boldsymbol{v}_\pi - \widetilde{\boldsymbol{v}})\|_{0,P} + \|\boldsymbol{\varepsilon}(\widetilde{\boldsymbol{v}} - \widetilde{\boldsymbol{v}}_I)\|_{0,P},$$

together with standard polynomial approximation estimates, (5.6), and (5.9) prove the result.

Step 3 (*$\mathbf{L}^2$-error estimate*). The triangle inequality leads to

$$\begin{aligned}\|\boldsymbol{v}-\mathbf{I}_1^{Q,k_1}\boldsymbol{v}\|_{0,P} &\le \|\boldsymbol{v}-\mathbf{I}_1^{C,k_1}\boldsymbol{v}\|_{0,P}+\|\mathbf{I}_1^{C,k_1}\boldsymbol{v}-\mathbf{I}_1^{Q,k_1}\boldsymbol{v}\|_{0,P}\\ &\le \|\boldsymbol{v}-\mathbf{I}_1^{C,k_1}\boldsymbol{v}\|_{0,P}+h_P\|\boldsymbol{\varepsilon}(\mathbf{I}_1^{C,k_1}\boldsymbol{v}-\mathbf{I}_1^{Q,k_1}\boldsymbol{v})\|_{0,P},\end{aligned} \tag{5.10}$$

with the Poincaré inequality (since $\mathbf{I}_1^{C,k_1}\boldsymbol{v}$ and $\mathbf{I}_1^{Q,k_1}\boldsymbol{v}$ coincide on ∂P) in the last step. Using the triangle inequality, the estimate in (5.1), and the H^1 estimate (5.9) of the quasi-interpolator $\mathbf{I}_1^{Q,k_1}$ for the second term in (5.10), we conclude the proof. □

Remark 4. *We recall that the scaled interpolation estimates for $\mathbf{I}_1^{Q,k_1}$ and $\mathbf{I}_2^{F,k_2}$ follow exactly as Lemma 3.2 by adapting Proposition 5.1 and [11, Theorem 4.2] with the correct scaling factor.*

Remark 5. *The well-posedness of problem* (3.2a)-(3.2b) *in 3D is discussed in [9, Section 5.1], whereas the commutative property of $\mathbf{I}_2^{F,k_2}$ (which implies the discrete inf-sup condition) ensures the unique solvability of the 3D reaction-diffusion equation* (3.2c)-(3.2d)*. The well-posedness of the discrete fully-coupled problem* (3.2) *in 3D follows using a Banach fixed-point argument with small data assumption (see [35, Section 4]), while a priori error estimates are provided in [46].*

5.4. A posteriori error analysis in 3D

In this subsection, we formulate the 3D estimator and provide the required ingredients for the extension of Section 4 to the three-dimensional case. First we invoke a 3D Helmholtz decomposition [30, Lemma 3.9] as an extension of the 2D version used in Lemma 4.12.

Lemma 5.2. *Assume that $\Omega \subset \mathbb{R}^3$ is a connected domain and that Γ_N is contained in the boundary of a convex part of Ω, that is, there exists a convex domain B such that $\overline{\Omega} \subseteq B$ and $\Gamma_N \subseteq \partial B$ (see Figure 5.1). Then, for each $\boldsymbol{\xi} \in \mathbf{H}_N(\mathrm{div},\Omega)$, there exist $\boldsymbol{z} \in \mathbf{H}^1(\Omega)$ and $\boldsymbol{\chi} \in \mathbf{H}^1_N(\Omega)$ such that*

$$\boldsymbol{\xi} = \boldsymbol{z} + \mathbf{curl}\,\boldsymbol{\chi} \ \text{in } \Omega \text{ and } \|\boldsymbol{z}\|_{1,\Omega} + \|\boldsymbol{\chi}\|_{1,\Omega} \lesssim \|\boldsymbol{\xi}\|_{\mathrm{div},\Omega}.$$

Next, we introduce the vector space $\mathbf{V}_3 := \mathbf{H}(\mathrm{div},\Omega) \cap \mathbf{H}(\mathbf{curl},\Omega)$ with corresponding local virtual space

$$\mathbf{V}_3^{h,k_2+1}(P) := \{\boldsymbol{\chi} \in \mathbf{V}_3(P) : \boldsymbol{\chi}_t|_{\partial P} \in \mathcal{B}_3^{h,k_2+1}(\partial P), \mathrm{div}\,\boldsymbol{\chi} \in \mathcal{P}_{k_2}(P), \mathbf{curl}(\mathbf{curl}\,\boldsymbol{\chi}) \in \boldsymbol{\mathcal{R}}_{k_2-1}(P)\},$$

with $\mathcal{B}_3^{h,k_2}(\partial P) := \{\boldsymbol{\chi} \in (\mathcal{B}_3)_t : \boldsymbol{\chi}_f \in \mathbf{V}_2^{h,k_2}(f), \forall f \in \partial P\}$. Here, $(\mathcal{B}_3)_t$ is defined as the tangential component of the elements in $\mathcal{B}_3(\partial P)$ given for $f \in \partial P$ by

$$\mathcal{B}_3(\partial P) := \{\boldsymbol{\chi} \in \mathbf{L}^2(\partial P) : \boldsymbol{\chi}|_f \in \mathbf{H}(\mathrm{div},f) \cap \mathbf{H}(\mathrm{rot},f), \forall f \in \mathcal{F}^h, \boldsymbol{\chi}_{f_1}\cdot \boldsymbol{t}_e = \boldsymbol{\chi}_{f_2}\cdot \boldsymbol{t}_e, \forall f_1,f_2 \in \mathcal{F}_e^h,\, e \subset \partial f\}.$$

The VE space $\mathbf{V}_2^{h,k_2}(f)$ refers to the 2D edge space (see [6, Section 4]) which is a rotation by $\pi/2$ of the standard VE space for mixed problems given in Section 3. Finally, the global space $\mathbf{V}_3^{h,k_2+1}$ is given as follows

$$\mathbf{V}_3^{h,k_2+1} := \{\boldsymbol{\chi}_h \in \mathbf{V}_3 : \boldsymbol{\chi}_h|_P \in \mathbf{V}_3^{h,k_2+1}(P), \forall P \in \mathcal{T}^h\}.$$

For further details about DoFs and unisolvence we refer to [6, Section 6]. A key relation between $\mathbf{V}_2^{h,k_2}$ and $\mathbf{V}_3^{h,k_2+1}$ needed for the Helmholtz decomposition is given next and we refer to [6, Theorem 8.2] for a proof.

Lemma 5.3. *For $k_2 \ge 1$ and $\boldsymbol{\chi}_h \in \mathbf{V}_3^{h,k_2+1}$, we have that $\mathbf{curl}\,\boldsymbol{\chi}_h \in \mathbf{V}_2^{h,k_2}$.*

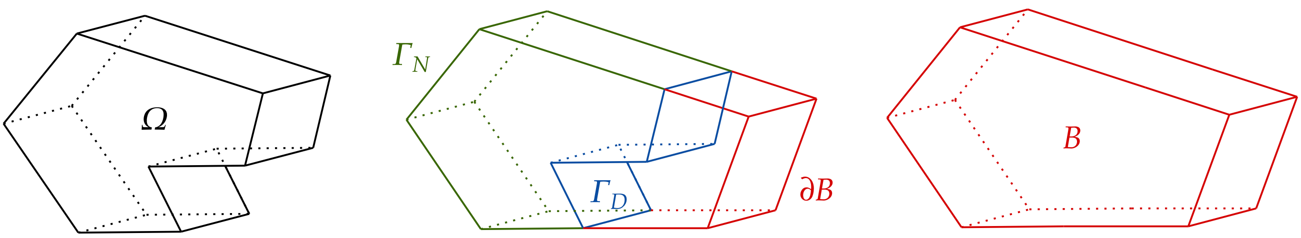

FIGURE 5.1. Extension of Ω (left) to a convex domain B (right), with mixed boundary conditions on Γ_N and Γ_D (centre).

Following the approach outlined in Section 4, we introduce a novel quasi-interpolation operator for the 3D VE edge space, specifically applied to $\mathbf{H}^1(\Omega)$ functions.

Proposition 5.4. *Let $\boldsymbol{\chi} \in \mathbf{H}^{s_2+1}(\Omega)$, and $0 \le s_2 \le k_2$. Under the mesh assumptions, there exists $\mathbf{I}_3^{Q,k_2+1}\boldsymbol{\chi} \in \mathbf{V}_3^{h,k_2+1}$ such that*

$$\|\boldsymbol{\chi} - \mathbf{I}_3^{Q,k_2+1}\boldsymbol{\chi}\|_{0,P} + h_P|\boldsymbol{\chi} - \mathbf{I}_3^{Q,k_2+1}\boldsymbol{\chi}|_{1,P} \lesssim h_P^{s_2+1}|\boldsymbol{\chi}|_{s_2+1,D(P)}.$$

Proof. Step 1 (Existence of interpolation in the 3D edge VE space). First, let $\mathbf{I}_3^{C,k_2+1}\boldsymbol{\chi} \in \mathbf{H}_N^1(\Omega)$ be the 3D Clément-type interpolation in the Nédélec FE space defined on a sub-triangulation allowed by the mesh assumptions (See [26, Theorem 5.2]), satisfying the following estimate

$$\|\boldsymbol{\chi} - \mathbf{I}_3^{C,k_2+1}\boldsymbol{\chi}\|_{0,P} + h_P|\boldsymbol{\chi} - \mathbf{I}_3^{C,k_2+1}\boldsymbol{\chi}|_{1,P} \lesssim h_P^{s_2+1}|\boldsymbol{\chi}|_{s_2+1,D(P)}. \tag{5.11}$$

For each polyhedron $P \in \mathcal{T}^h$, let $\boldsymbol{\chi}_\pi = \mathbf{\Pi}_2^{0,k_2+1}\boldsymbol{\chi}$ be the polynomial approximation of $\boldsymbol{\chi}$. Then, we consider

$$\begin{cases} \mathbf{curl}(\mathbf{curl}(\mathbf{I}_3^{Q,k_2+1}\boldsymbol{\chi})) = \mathbf{curl}(\mathbf{curl}\,\boldsymbol{\chi}_\pi) & \text{in } P,\\ \operatorname{div}(\mathbf{I}_3^{Q,k_2+1}\boldsymbol{\chi}) = \operatorname{div}\boldsymbol{\chi}_\pi & \text{in } P,\\ (\mathbf{I}_3^{Q,k_2+1}\boldsymbol{\chi})_t = (\mathbf{I}_3^{C,k_2+1}\boldsymbol{\chi})_t & \text{on } \partial P. \end{cases} \tag{5.12}$$

Note that the definition of the Nédélec space implies that $[\![(\mathbf{I}_3^{C,k_2+1}\boldsymbol{\chi})_f \cdot \boldsymbol{t}_e]\!] = 0$ for all $e \in \partial f$, and $f \in \partial P$. Therefore, the unique solvability of (5.12) (see [6, Section 6.2]) for all P implies that $\mathbf{I}_3^{Q,k_2+1}\boldsymbol{\chi} \in \mathbf{V}_3^{h,k_2+1}$.
Step 2 (Error estimate). Subtracting $\boldsymbol{\chi}_\pi$ from (5.12) leads to

$$\begin{cases} \mathbf{curl}(\mathbf{curl}(\mathbf{I}_3^{Q,k_2+1}\boldsymbol{\chi} - \boldsymbol{\chi}_\pi)) = \mathbf{0} & \text{in } P,\\ \operatorname{div}(\mathbf{I}_3^{Q,k_2+1}\boldsymbol{\chi} - \boldsymbol{\chi}_\pi) = 0 & \text{in } P,\\ (\mathbf{I}_3^{Q,k_2+1}\boldsymbol{\chi} - \boldsymbol{\chi}_\pi)_t = (\mathbf{I}_3^{C,k_2+1}\boldsymbol{\chi} - \boldsymbol{\chi}_\pi)_t & \text{on } \partial P. \end{cases} \tag{5.13}$$

We invoke the analysis of [6, Section 6.2] to show that the unique solution of (5.13) has the decomposition $\mathbf{I}_3^{Q,k_2+1}\boldsymbol{\chi} - \boldsymbol{\chi}_\pi = \tilde{\boldsymbol{\psi}} + \nabla\tilde{\varphi}$, where $\tilde{\boldsymbol{\psi}} \in \mathbf{H}^1(P)$ and $\tilde{\varphi} \in \mathrm{H}_0^1(P)$ are the respective unique solutions of

$$\begin{cases} \Delta\tilde{\varphi} = 0 & \text{in } P,\\ \tilde{\varphi} = 0 & \text{on } \partial P, \end{cases} \qquad \begin{cases} \mathbf{curl}\,\tilde{\boldsymbol{\psi}} = \boldsymbol{h} & \text{in } P,\\ \operatorname{div}\tilde{\boldsymbol{\psi}} = 0 & \text{in } P,\\ \tilde{\boldsymbol{\psi}}_t = (\mathbf{I}_3^{C,k_2+1}\boldsymbol{\chi} - \boldsymbol{\chi}_\pi)_t & \text{on } \partial P. \end{cases} \tag{5.14}$$

The above data $\boldsymbol{h} \in \mathbf{H}^1(P)$ is the solution of the following problem

$$\begin{cases} \mathbf{curl}\,\boldsymbol{h} = \mathbf{0} & \text{in } P,\\ \operatorname{div}\boldsymbol{h} = 0 & \text{in } P,\\ \boldsymbol{h}\cdot\boldsymbol{n} = \operatorname{rot}(\mathbf{I}_3^{C,k_2+1}\boldsymbol{\chi} - \boldsymbol{\chi}_\pi)_t & \text{on } \partial P. \end{cases} \tag{5.15}$$

Notice from (5.14) that $\tilde{\varphi} = 0$. Thus, the well-posedness of Maxwell-type equations from [48, Theorem 2.3], and the trace inequality imply that

$$|\mathbf{I}_3^{Q,k_2+1}\boldsymbol{\chi} - \boldsymbol{\chi}_\pi|_{1,P} \lesssim \|\mathbf{curl}\,\tilde{\boldsymbol{\psi}}\|_{0,P} + \|(\mathbf{I}_3^{C,k_2+1}\boldsymbol{\chi} - \boldsymbol{\chi}_\pi)_t\|_{\frac{1}{2},\partial P} \lesssim \|\boldsymbol{h}\|_{0,P} + |\mathbf{I}_3^{C,k_2+1}\boldsymbol{\chi} - \boldsymbol{\chi}_\pi|_{1,P}. \tag{5.16}$$

Next, we follow a local version of [54] to estimate $\|\boldsymbol{h}\|_{0,P}$. For this, we recall the Helmholtz decomposition $\mathbf{L}^2(P) = \mathbf{H}(\mathbf{curl}_{\mathbf{0}}, P) \oplus \mathbf{H}_{\partial P}(\operatorname{div}_0, P)$ (see [34]) where $\mathbf{H}(\mathbf{curl}_{\mathbf{0}}, P)$, $\mathbf{H}_{\partial P}(\operatorname{div}_0, P)$ correspond to **curl**-free and div-free (with zero boundary condition) functions, respectively. Thus, there exist $\boldsymbol{h}_1 \in \mathbf{H}(\mathbf{curl}\times\mathbf{0}, P)$ and $\boldsymbol{h}_2 \in \mathbf{H}_{\partial P}(\operatorname{div}\cdot\mathbf{0}, P)$ such that $\boldsymbol{h} = \boldsymbol{h}_1 + \boldsymbol{h}_2$. Moreover, $\boldsymbol{h}_1 = \nabla q$ for some $q \in \mathrm{H}^1(P)$ with $\int_P q = 0$, and $\boldsymbol{h}_2 = \mathbf{curl}(\boldsymbol{\phi})$ for some $\boldsymbol{\phi} \in \mathbf{H}_{\partial P}(\mathbf{curl}, P) \cap \mathbf{H}(\operatorname{div}_0, P)$, with

$$\|\boldsymbol{h}\|_{0,P}^2 = \|\nabla q\|_{0,P}^2 + \|\mathbf{curl}(\boldsymbol{\phi})\|_{0,P}^2. \tag{5.17}$$

An integration by parts and (5.15) imply that

$$\begin{aligned} \|\boldsymbol{h}\|_{0,P}^2 = \left|\int_P \boldsymbol{h}\cdot(\nabla q + \mathbf{curl}(\boldsymbol{\phi}))\right| &= \left|-\int_P \operatorname{div}(\boldsymbol{h})q + \int_{\partial P}(\boldsymbol{h}\cdot\boldsymbol{n})q + \int_P \mathbf{curl}(\boldsymbol{h})\cdot\boldsymbol{\phi} + \int_{\partial P}\boldsymbol{h}\cdot(\boldsymbol{\phi}\times\boldsymbol{n})\right| \\ &= \left|\int_{\partial P}\operatorname{rot}(\mathbf{I}_3^{C,k_2+1}\boldsymbol{\chi} - \boldsymbol{\chi}_\pi)_t q\right|. \end{aligned}$$

This, the trace inequality together with (5.17) and the Poincaré inequality lead to

$$\|\boldsymbol{h}\|_{0,P}^2 = \left|\int_{\partial P}\operatorname{rot}(\mathbf{I}_3^{C,k_2+1}\boldsymbol{\chi} - \boldsymbol{\chi}_\pi)_t q\right| \lesssim h_P^{-\frac{1}{2}}\|\mathbf{curl}(\mathbf{I}_3^{C,k_2+1}\boldsymbol{\chi} - \boldsymbol{\chi}_\pi)\|_{0,P}(h_P^{-\frac{1}{2}}\|q\|_{0,P} + h_P^{\frac{1}{2}}\|\nabla q\|_{0,P})$$

$$\lesssim h_P^{-\frac{1}{2}}\|\mathbf{curl}(\mathbf{I}_3^{C,k_2+1}\boldsymbol{\chi}-\boldsymbol{\chi}_\pi)\|_{0,P}(h_P^{\frac{1}{2}}\|\nabla q\|_{0,P})$$
$$\lesssim \|\mathbf{curl}(\mathbf{I}_3^{C,k_2+1}\boldsymbol{\chi}-\boldsymbol{\chi}_\pi)\|_{0,P}\|\boldsymbol{h}\|_{0,P}. \tag{5.18}$$

The triangle inequality, the inequality $\|\mathbf{curl}(\cdot)\|_{0,P}\lesssim|\cdot|_{1,P}$, (5.18), and (5.16) lead to

$$|\boldsymbol{\chi}-\mathbf{I}_3^{Q,k_2+1}\boldsymbol{\chi}|_{1,P}\le|\boldsymbol{\chi}-\boldsymbol{\chi}_\pi|_{1,P}+|\mathbf{I}_3^{Q,k_2+1}\boldsymbol{\chi}-\boldsymbol{\chi}_\pi|_{1,P}\lesssim|\boldsymbol{\chi}-\boldsymbol{\chi}_\pi|_{1,P}+|\boldsymbol{\chi}-\mathbf{I}_3^{C,k_2+1}\boldsymbol{\chi}|_{1,P}. \tag{5.19}$$

Finally, Lemma 3.1 and (5.11) imply the $\mathbf{H}^1$-error estimate.
Step 3 ($\mathbf{L}^2$-error estimate) Since $(\mathbf{I}_3^{Q,k_2+1}\boldsymbol{\chi})_t-(\mathbf{I}_3^{C,k_2+1}\boldsymbol{\chi})_t=0$, a Poincaré inequality can be applied to the polynomial $\mathbf{I}_3^{Q,k_2+1}\boldsymbol{\chi}-\mathbf{I}_3^{C,k_2+1}\boldsymbol{\chi}$, which together with the triangle inequality lead to

$$\|\boldsymbol{\chi}-\mathbf{I}_3^{Q,k_2+1}\boldsymbol{\chi}\|_{0,P}\le\|\boldsymbol{\chi}-\mathbf{I}_3^{C,k_2+1}\boldsymbol{\chi}\|_{0,P}+h_P|\mathbf{I}_3^{C,k_2+1}\boldsymbol{\chi}-\mathbf{I}_3^{Q,k_2+1}\boldsymbol{\chi}|_{1,P}.$$

The proof follows by applying again the triangle inequality, (5.19), (5.11), and Lemma 3.1. □

Finally, we focus on the extension of the reliability and efficiency of the estimators for the 3D case. Notice that the presence of the **curl** operator motivates the redefinition of the reaction-diffusion estimator as follows

$$\begin{aligned}\Xi_{2,P}^2 &:= \sum_{f\in\mathcal{F}_{\mathrm{D}}^h(P)} h_f\|\varphi_{\mathrm{D}}-\varphi_h\|_{0,f}^2+\sum_{f\in\mathcal{F}_{\mathrm{D}}^h(P)} h_f\|(\nabla\varphi_{\mathrm{D}}-\boldsymbol{\Pi}_2^{0,k_2}(\mathbb{M}^{-1}(\boldsymbol{\varepsilon}(\overline{\boldsymbol{u}}_h),p_h)\boldsymbol{\Pi}_2^{0,k_2}\boldsymbol{\zeta}_h))\times\boldsymbol{n}\|_{0,f}^2\\
&+\sum_{f\in\mathcal{F}_\Omega^h(P)} h_f\|[\![\boldsymbol{\Pi}_2^{0,k_2}(\mathbb{M}^{-1}(\boldsymbol{\varepsilon}(\overline{\boldsymbol{u}}_h),p_h)\boldsymbol{\Pi}_2^{0,k_2}\boldsymbol{\zeta}_h)\times\boldsymbol{n}_f]\!]\|_{0,f}^2\\
&+h_P^2\|\boldsymbol{\Pi}_2^{0,k_2}(\mathbb{M}^{-1}(\boldsymbol{\varepsilon}(\overline{\boldsymbol{u}}_h),p_h)\boldsymbol{\Pi}_2^{0,k_2}\boldsymbol{\zeta}_h)-\nabla\varphi_h\|_{0,P}^2+h_P^2\|\mathbf{curl}(\boldsymbol{\Pi}_2^{0,k_2}(\mathbb{M}^{-1}(\boldsymbol{\varepsilon}(\overline{\boldsymbol{u}}_h),p_h)\boldsymbol{\Pi}_2^{0,k_2}\boldsymbol{\zeta}_h))\|_{0,P}^2.\end{aligned}$$

On the other hand, $\Theta_{1,P}$ and the remaining terms of $\Theta_{2,P}$ are defined analogously to (4.3) replacing edges e and polygons E with faces f and polyhedrons P, respectively.

Following the techniques from Section 4 and the definition of the quasi-interpolator $\mathbf{I}_1^{Q,k_1}$ in Lemma 5.1, we readily see that Lemma 4.11 holds in the 3D case. In turn, Lemma 4.14 is a consequence of bubble functions in polyhedra and faces (see [18, Lemmas 8,9]).

Next, we recall integration by parts formulae involving $\mathbf{curl}(\boldsymbol{\chi}-\boldsymbol{\chi}_h)$, with $\boldsymbol{\chi}\in\mathbf{H}_N^1(\Omega)$ and $\boldsymbol{\chi}_h:=\mathbf{I}_3^{Q,k_2+1}(\boldsymbol{\chi})\in\mathbf{V}_3^{h,k_2+1}$ [34, Equation 2.17, Theorem 2.11]:

$$\sum_{f\in\mathcal{F}_D^h}\langle\mathbf{curl}(\boldsymbol{\chi}-\boldsymbol{\chi}_h),\varphi_{\mathrm{D}}\rangle_f=-\sum_{f\in\mathcal{F}_D^h}\langle\boldsymbol{\chi}-\boldsymbol{\chi}_h,\nabla\varphi_{\mathrm{D}}\times\boldsymbol{n}_f\rangle_f, \tag{5.20a}$$

$$\begin{aligned}\int_P\boldsymbol{\Pi}_2^{0,k_2}(\mathbb{M}^{-1}(\boldsymbol{\varepsilon}(\overline{\boldsymbol{u}}_h),p_h)\boldsymbol{\Pi}_2^{0,k_2}\boldsymbol{\zeta}_h)\cdot\mathbf{curl}(\boldsymbol{\chi}-\boldsymbol{\chi}_h)&=\int_P\mathbf{curl}\left(\boldsymbol{\Pi}_2^{0,k_2}(\mathbb{M}^{-1}(\boldsymbol{\varepsilon}(\overline{\boldsymbol{u}}_h),p_h)\boldsymbol{\Pi}_2^{0,k_2}\boldsymbol{\zeta}_h)\right)\cdot(\boldsymbol{\chi}-\boldsymbol{\chi}_h)\\
&+\sum_{f\in\mathcal{F}^h(P)}\langle\boldsymbol{\chi}-\boldsymbol{\chi}_h,\boldsymbol{\Pi}_2^{0,k_2}(\mathbb{M}^{-1}(\boldsymbol{\varepsilon}(\overline{\boldsymbol{u}}_h),p_h)\boldsymbol{\Pi}_2^{0,k_2}\boldsymbol{\zeta}_h)\times\boldsymbol{n}_f\rangle_f.\end{aligned} \tag{5.20b}$$

Note that this observation together with Lemmas 5.2-5.4 are the necessary tools to extend Lemma 4.12 to the 3D case. Finally, since $\mathbf{curl}(\nabla\varphi)=\mathbf{0}$, Lemma 4.15 can be extended again using bubble function techniques and the integration by parts presented in (5.20). Therefore, all the required ingredients to extend Theorem 4.13 and Theorem 4.16 are provided.

6. Numerical tests

In this section, we present numerical results illustrating the properties of the robust estimator from Section 4 and show the optimal behaviour of the associated adaptive algorithm under different polygonal convex meshes and polynomial orders. We also use L-shaped and Australia-shaped domains to illustrate the capability of capturing singularities in non-convex domains. Finally, we show some 3D tests.

The error will be computed as usual in the VEM framework using the local polynomial approximation of the solution as follows

$$\overline{\mathrm{e}}_*^2=\|(\boldsymbol{u}-\boldsymbol{\Pi}_1^{\boldsymbol{\varepsilon},k_1}\boldsymbol{u}_h,p-p_h)\|_{\mathbf{V}_1^{h,k_1}\times\mathrm{Q}_1^{h,k_1}}^2+\|(\boldsymbol{\zeta}-\boldsymbol{\Pi}_2^{0,k_2}\boldsymbol{\zeta}_h,\varphi-\varphi_h)\|_{\mathbf{V}_2^{h,k_2}\times\mathrm{Q}_2^{h,k_2}}^2.$$

The numerical implementation has been done with the library `VEM++` [21]. We separately implemented the elasticity and reaction-diffusion equations for arbitrary orders k_1 and k_2, respectively. Then, the nonlinear coupled problem (3.2) is solved with an optimised Picard iteration, following the same structure as in the fixed-point analysis from [35], with a tolerance of 10^{-6}. In this optimised version, the blocks corresponding to the

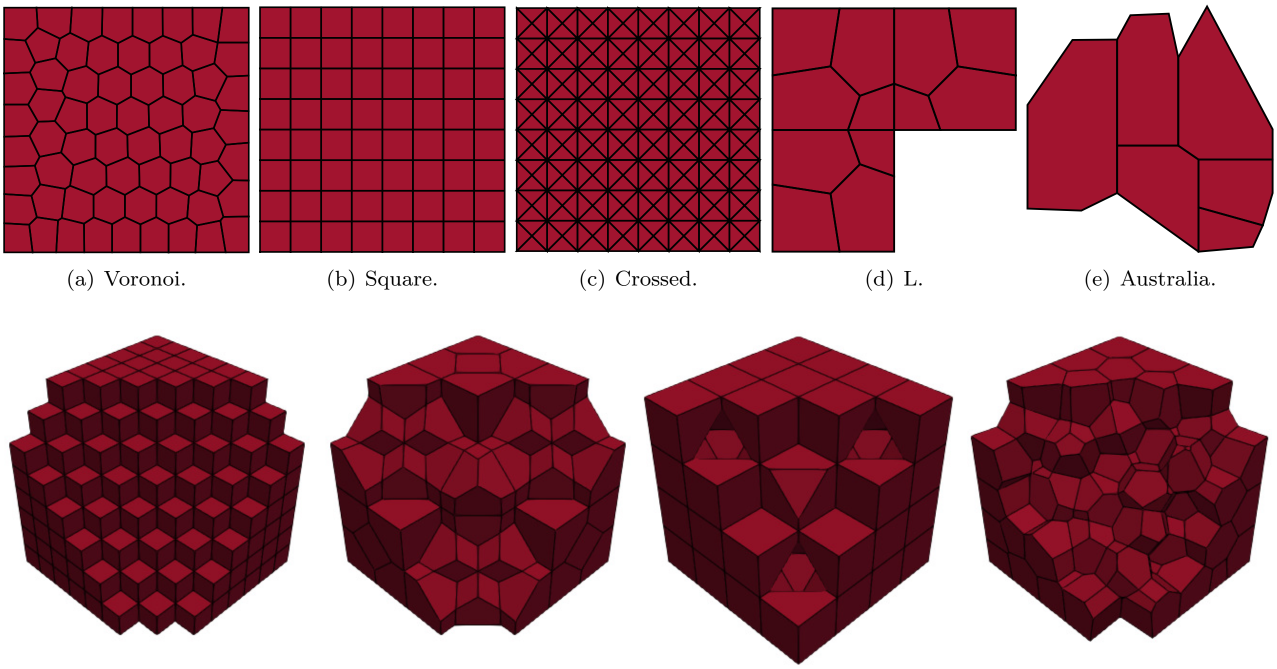

(a) Voronoi. (b) Square. (c) Crossed. (d) L. (e) Australia.

(f) Cube. (g) Nove. (h) Octa. (i) Voro.

FIGURE 6.1. An illustration of the distinct meshes used in the examples.

coupling terms ($G_1^{\varphi_h}(\cdot)$ and $a_2^{\overline{\boldsymbol{u}}_h,p,h}(\cdot,\cdot)$) are the only ones that are reconstructed on each fixed point iteration. We recall that the elasticity and reaction-diffusion equations have sufficiently smooth forcing and source terms that will be manufactured according to the given exact solutions. The non-homogeneous boundary conditions require a slight modification of the right-hand side functionals as well as the estimator boundary term $\Xi_{1,E}$ regarding Γ_{N}. The experimental order of convergence $r(\cdot)$ applied to either error $\overline{\mathrm{e}}_*$ or estimator Θ and the effectivity index (following Theorem 4.13) of the refinement $1 \leq j$ are computed from the formulae

$$r(\cdot)^{j+1} = -d\frac{\log\left(\frac{(\cdot)^{j+1}}{(\cdot)^{j}}\right)}{\log\left(\frac{\mathrm{DOF}_*^{j+1}}{\mathrm{DOF}_*^{j}}\right)} \quad \text{and} \quad \mathrm{eff}^j = \frac{\Theta^j}{\overline{\mathrm{e}}_*^j},$$

with DOF_* indicating the total number of DoFs. To facilitate a direct visual comparison with the theoretical results, the reference lines for the theoretical convergence rates in all convergence plots are labeled as $\mathrm{DOF}_*^{\text{order}}$. Here, order indicates the expected convergence rate provided in Theorem 3.4. Note that the standard DOF exponent $(-\text{order}/d)$ has been pre-multiplied by $-d$. In turn, the stabilisation term $S_1^E(\boldsymbol{u}_h, \boldsymbol{v}_h)$ follows the "diagonal recipe" introduced in [8] (weighted by 2μ) and $S_2^{\overline{\boldsymbol{u}}_h,p_h,E}(\boldsymbol{\zeta}_h, \boldsymbol{\xi}_h)$ have into account the nonlinearity $\mathbb{M}^{-1}(\boldsymbol{\varepsilon}(\overline{\boldsymbol{u}}_h), p_h)$ as in [35]. In the following experiments, we set $M \geq \max_{(x,y)\in\Omega} \quad \|\mathbb{M}(\boldsymbol{\varepsilon}(\boldsymbol{u}), p)\|_F$, where the Frobenius norm $\|\mathbb{M}(\boldsymbol{\varepsilon}(\boldsymbol{u}), p)\|_F$ is computed by the `fmincom` MATLAB optimisation subroutine.

The adaptive algorithm follows the usual strategy: SOLVE → ESTIMATE → MARK → REFINE. The first three steps are performed inside `VEM++`, exploiting the efficiency capabilities of C++. For the REFINE step, we use the Matlab-based method from [53], which connects edge midpoints to the polygon barycentre (in 2D). In turn, the adaptive refinement used in this paper relies on the library `p4est` [17] executed through the module GridapP4est of the Julia package `Gridap` [4]. The `VEM++` code is executed through Matlab/Julia (2D/3D, respectively), generating a list of elements to refine, which is then processed by the refinement routine. These refinement routines restrict the mesh elements to convex polygons in 2D and cubes (with hanging nodes/faces) in 3D. However, we recall that this procedure is independent of the SOLVE, ESTIMATE, and MARK stages. Therefore, the implementation can be extended to general star-shaped polygons with more general refinement routines. For the MARK procedure we follow a Dörfler/Bulk strategy, marking the subset of mesh elements $\mathcal{K} \subseteq \mathcal{T}^h$ with the largest estimated errors such that for $\delta = \frac{1}{2} \in [0,1]$, we have $\delta \sum_{E\in\mathcal{T}^h} \Theta_E^2 \leq \sum_{E\in\mathcal{K}} \Theta_E^2$.

6.1. Example 1: Robust behaviour of the estimator under uniform refinement

We consider the meshes in Fig 6.1 for the unit square domain $\Omega = (0,1)^2$ with Dirichlet part $\Gamma_{\mathrm{D}} = \{(x,y) \in \partial\Omega\colon x = 0 \text{ or } y = 0\}$, and Neumann part $\Gamma_{\mathrm{N}} = \partial\Omega \setminus \Gamma_{\mathrm{D}}$. We explore different polynomial degrees for the elasticity and reaction-diffusion equations given by $k_1 = 2, 3, 4$ and $k_2 = 1, 2, 3$. Smooth manufactured solutions

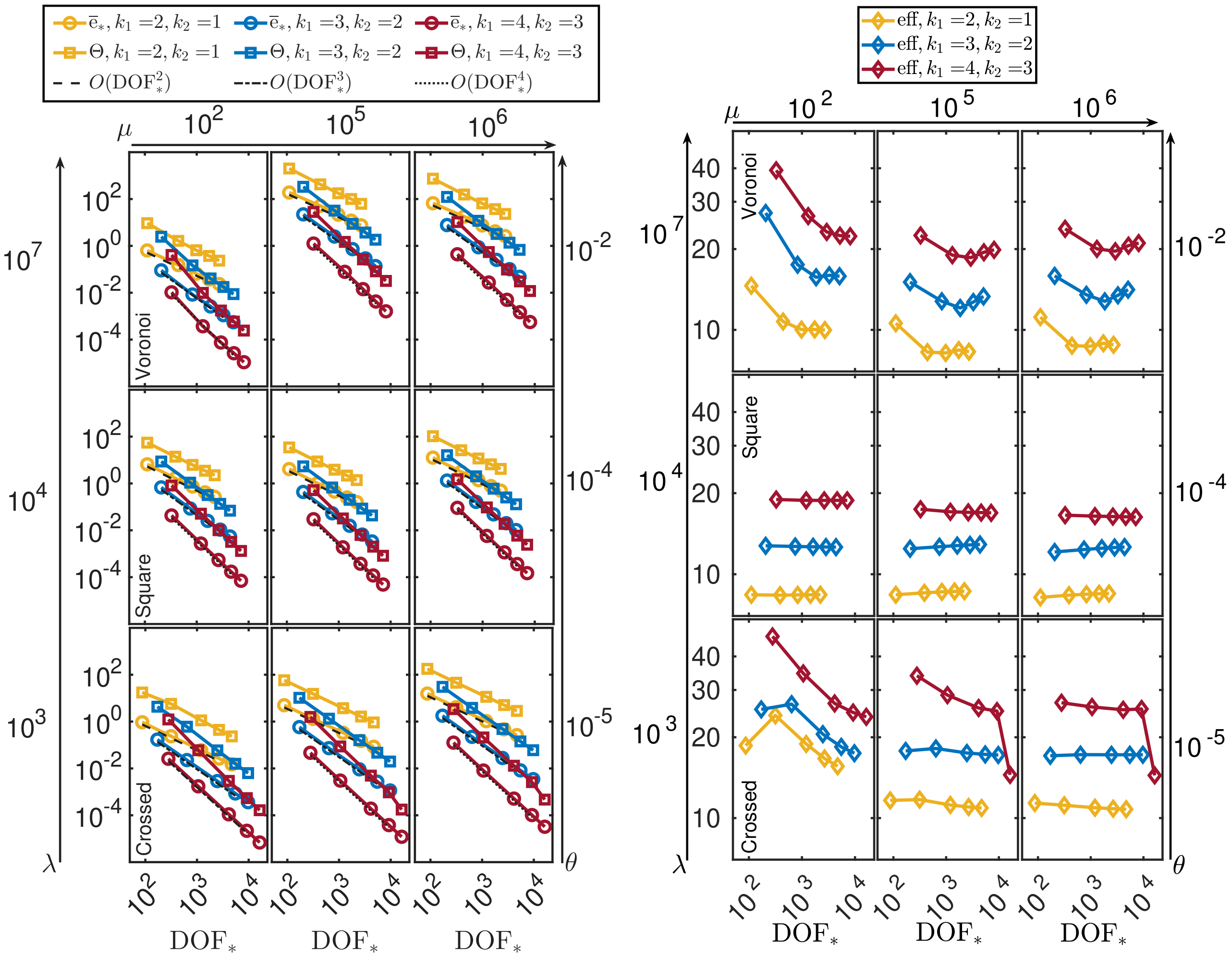

FIGURE 6.2. Example 1. Behaviour of the error $\bar{\mathrm{e}}_*$, estimator Θ (left), and effectivity index eff (right) under uniform refinement across various meshes, polynomial orders, and parameter selections.

and nonlinearities are set as

$$\boldsymbol{u}(x,y) = 5^{-1}\left(x^2 + x\cos(x)\sin(y), y^2 + x\cos(y)\sin(x)\right)^{\mathrm{t}}, \quad \ell(\varphi) = \varphi,$$
$$\varphi(x,y) = \cos(\pi y) + \sin(\pi x) + x^2 + y^2, \quad \mathbb{M}(\boldsymbol{\varepsilon}(\boldsymbol{u}), p) = 10^{-1}\exp\left[-10^{-8}\,\mathrm{tr}(2\mu\boldsymbol{\varepsilon}(\boldsymbol{u}) - p\mathbb{I})\right]\mathbb{I}.$$

As usual, the exact displacement $\boldsymbol{u}$ and concentration φ are used to compute exact Herrmann pressure p and total flux $\boldsymbol{\zeta}$, as well as appropriate forcing term, source, and non-homogeneous traction, displacement, and flux boundary data. Finally, we use the parameter value $M = 12$.

The results in Figure 6.2 demonstrate robust optimal convergence rates predicted by Theorem 3.4 for $\bar{\mathrm{e}}_*$ and Θ under uniform refinement for a variation in the involved parameters μ, λ, θ. In addition, Figure 6.2 shows the effectivity index for the different experiments, here we can observe that it oscillates around a fixed number for each case, confirming the reliability of the estimator given by Theorem 4.13.

6.2. **Example 2: Non-smooth solution on non-convex domains**

In this case, we set an initial polygonal discretisation for the L-shaped domain $\Omega = (-1,1)^2 \setminus [0,1) \times [0,-1)$ with boundary conditions defined on $\Gamma_{\mathrm{N}} = \{(x,y) \in \partial\Omega : x = -1,\ y = 1\}$ and $\Gamma_{\mathrm{D}} = \partial\Omega \setminus \Gamma_N$ (see Figure 1(d)). In contrast, the Australia-shaped domain is set to fit inside the unit square where each element in the initial discretisation represents the in-land states (See Figure 1(e)), the further east edge coincides with $x = 0$ where Γ_{N} is defined, whereas $\Gamma_{\mathrm{D}} = \partial\Omega \setminus \Gamma_N$.

The non-smooth manufactured solutions and the non-linear terms are set as follows

$$\boldsymbol{u}(x,y) = \left(\frac{(x-1.0)(y-1.0)}{(x-x_*)^2 + (y-y_*)^2}, \frac{(x+1.0)(y+1.0)}{(x-x_*)^2 + (y-y_*)^2}\right)^{\mathrm{t}}, \quad \ell(\varphi) = 2 + \frac{\varphi^2}{1+\varphi^2},$$
$$\varphi(x,y) = \frac{(x-1.0)(x+1.0)(y-1.0)(y+1.0)}{(x-x_*)^2 + (y-y_*)^2}, \quad \mathbb{M}(\boldsymbol{\varepsilon}(\boldsymbol{u}), p) = \left(1 + \frac{10^{-5}}{\mathrm{tr}(2\mu\boldsymbol{\varepsilon}(\boldsymbol{u}) - p\mathbb{I})}\right)\mathbb{I},$$

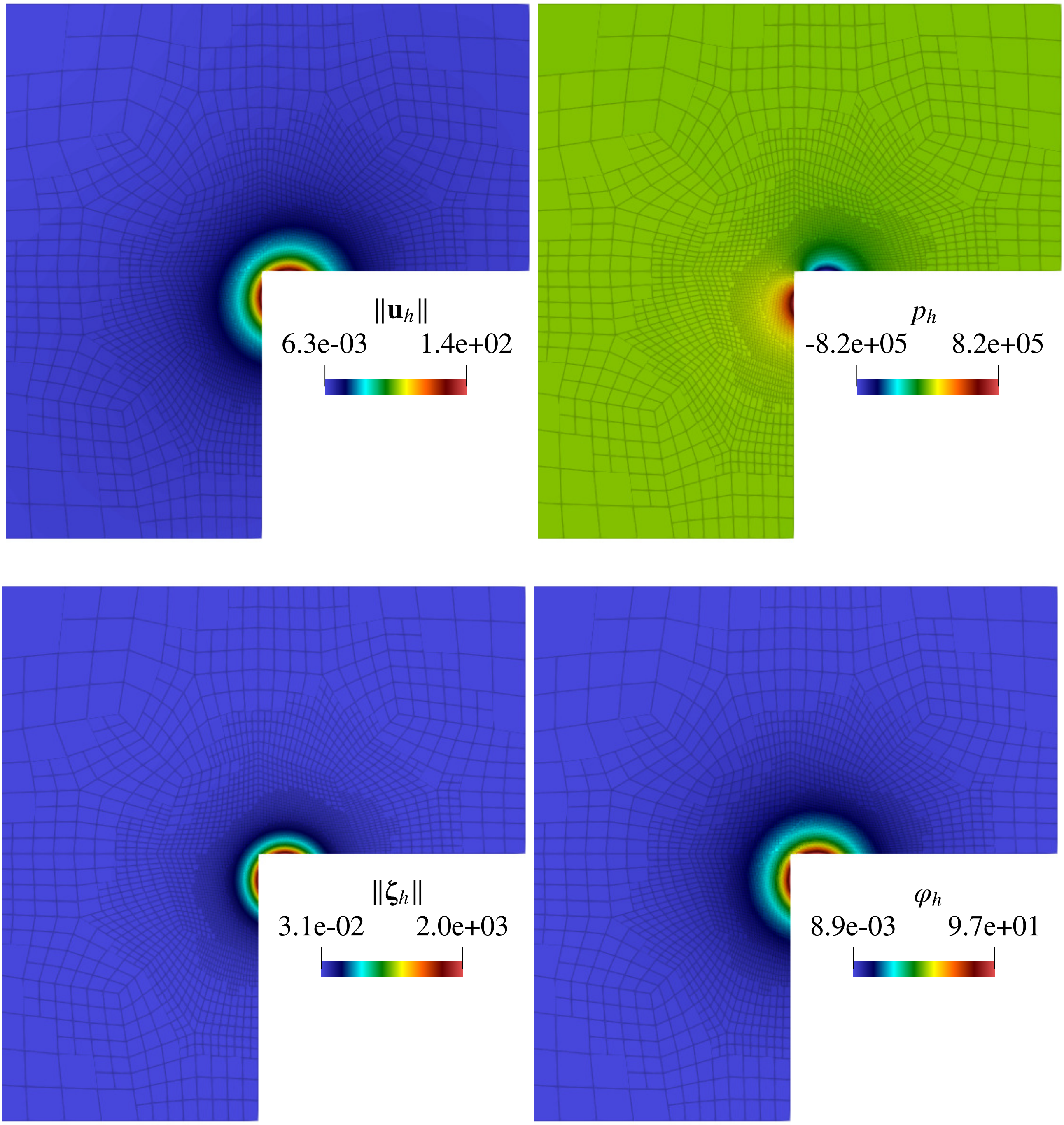

FIGURE 6.3. Example 2. Snapshots of the interest variables on the L-shape mesh are shown for polynomial degrees $k_1 = 2$ and $k_2 = 1$ after 19 refinement steps.

with parameter values $\mu = 1.4286 \times 10^3$, $\lambda = 357.1429$, $\theta = 10^{-3}$, and $M = 2$. Displacement and concentration admit a singularity depending on the selection of the point $(x_*, y_*)^{\mathtt{t}}$. For the L-shaped domain we set $(x_*, y_*)^{\mathtt{t}} = (10^{-1}, -10^{-1})^{\mathtt{t}}$, expecting high gradients close to the reentrant corner. In contrast, the Australian-shaped domain expects high gradients near the location of Melbourne, i.e., $(x_*, y_*)^{\mathtt{t}} = (8.5 \times 10^{-1}, -10^{-1})^{\mathtt{t}}$.

Note that high values of the total error $\overline{\mathrm{e}}_*$ are expected in this simulation because the manufactured solutions attain large magnitudes near the singularity. This effect is further amplified by the parameter-dependent norms used to measure the total error. Alternatives, such as computing relative errors (with respect to the energy of the problem), can be used to mitigate this observation.

Figure 6.4 shows the behaviour of $\overline{\mathrm{e}}_h$, Θ, and eff under uniform and adaptive refinement for different polynomial degrees. As expected, the error decreases faster (optimally) under the adaptive procedure, and the effectivity index remains bounded, confirming the robustness of the estimator. Moreover, Figure 6.5 illustrates the behaviour of the different contributions of the error estimator for the lowest-order polynomial order ($k = 2$), we observe that all the contributions of the estimator (including the stabilisation estimator) decay with the optimal rate of $O(\mathrm{DOF}_*^2)$ under the adaptive procedure. In particular, the global data oscillation term η is the dominant

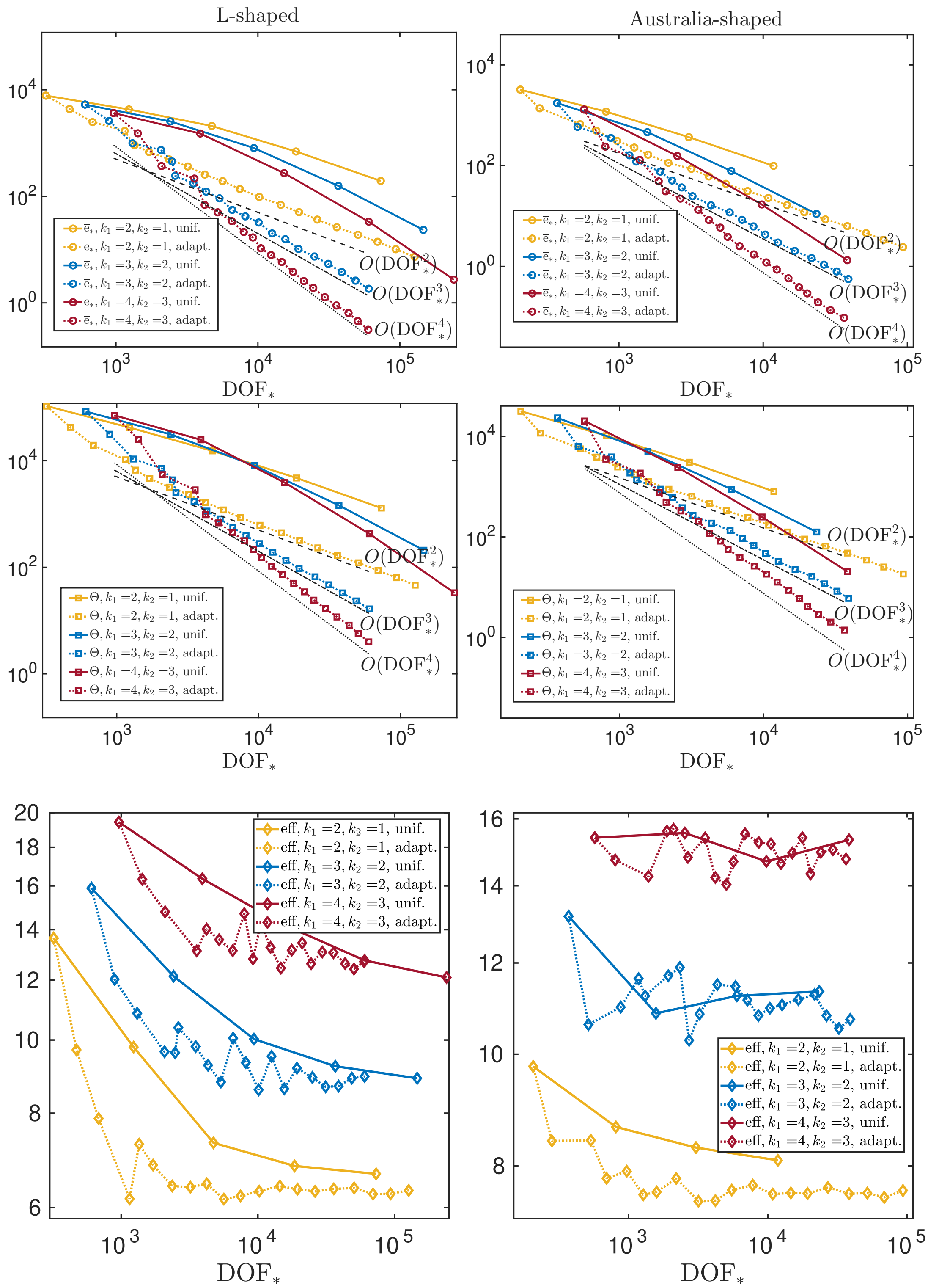

FIGURE 6.4. Example 2. Behaviour of $\overline{e}_*$ (top row), Θ (middle row), and eff (bottom row) under uniform and adaptive refinement on L-shape (left column) and Australia-shape (right column) domains for a variety polynomial orders.

contribution and dictates the overall behaviour of the estimator, while keeping the effectivity index bounded. The experiment suggests that, from a practical standpoint, the stabilisation term may be neglected whenever it is not a dominant contribution to the estimator. Finally, Figures 6.3 and 6.6 display approximate solutions after 19 adaptive mesh refinement steps according to Θ. Most of the refinement occurs around the singularities, demonstrating how the method identifies regions where accuracy deteriorates.

6.3. **Example 3: Behaviour of estimator under uniform refinement in 3D**

We consider the meshes in Figure 6.1 for the unit cube domain $\Omega = (0,1)^3$ with Dirichlet part $\Gamma_{\mathrm{D}} = \{(x,y,z) \in \partial\Omega\colon x = 0 \text{ or } y = 0 \text{ or } z = 0\}$, and Neumann part $\Gamma_{\mathrm{N}} = \partial\Omega \setminus \Gamma_{\mathrm{D}}$. We set the polynomial degrees to $k_1 = 2$

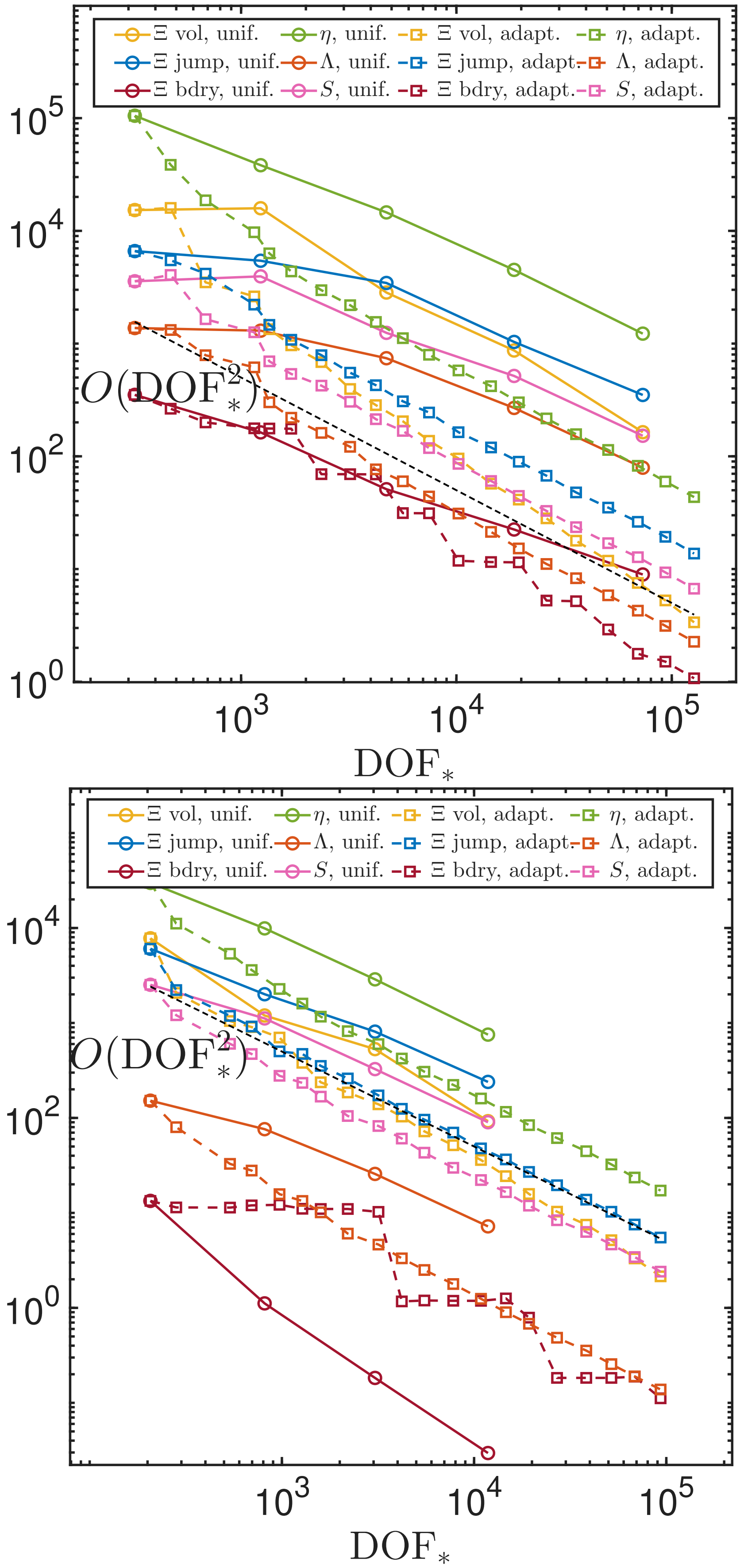

FIGURE 6.5. Example 2. Behaviour of the volume, jump and boundary contributions of the global residual Ξ, the global data oscillation η, the global mixed Λ, and global stabilisation S estimators under uniform and adaptive refinement on L-shaped (top row) and Australia-shaped (bottom row) domains for a lowest-order polynomial order $k_1 = 2$ and $k_2 = 1$.

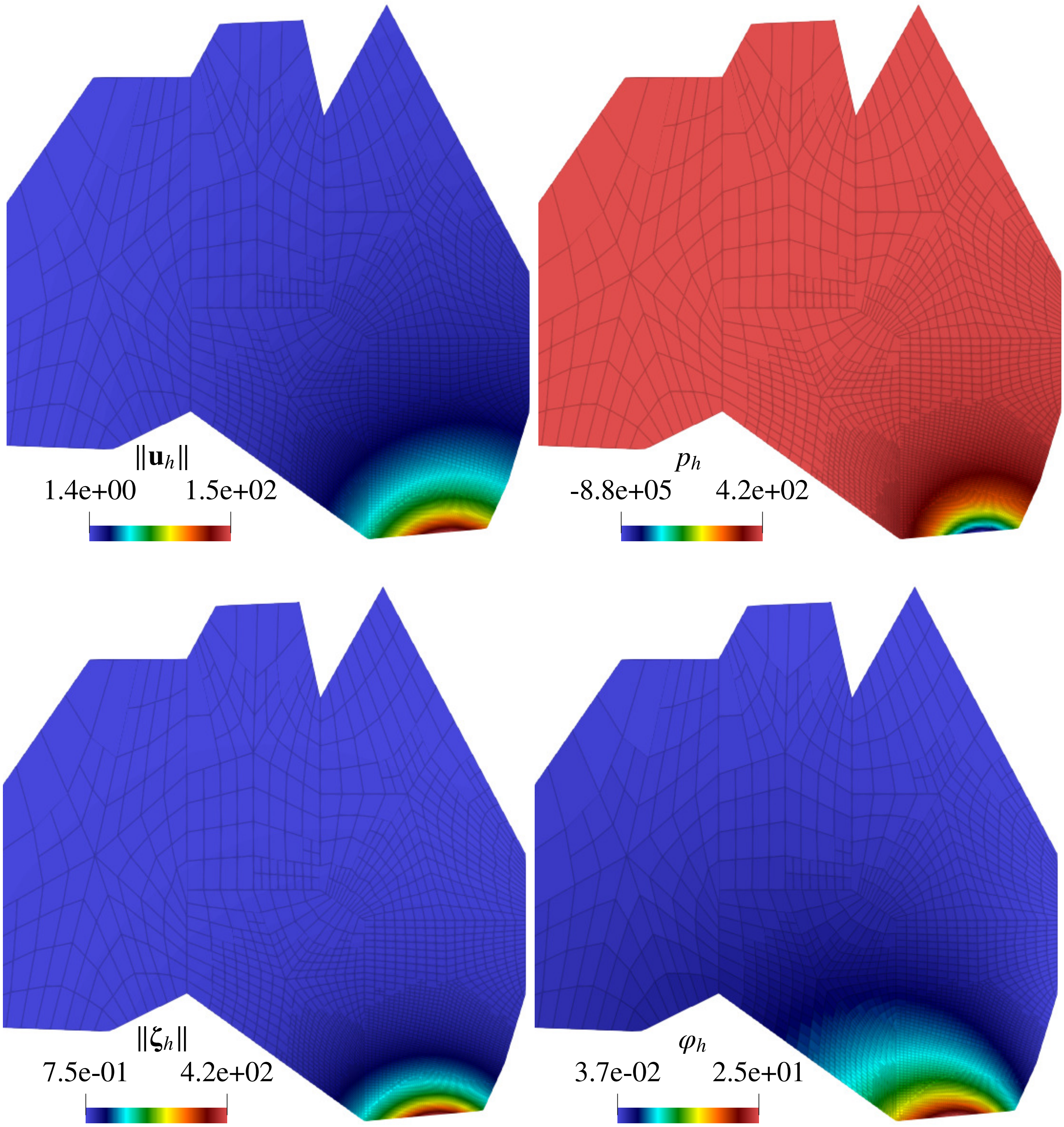

FIGURE 6.6. Example 2. Snapshots of the interest variables on the Australia-shaped mesh are shown for polynomial degrees $k_1 = 2$ and $k_2 = 1$ after 19 refinement steps.

and $k_2 = 2$ for the discrete spaces defined in Section 5.2, noting that the implementation presented in this paper supports arbitrary polynomial degrees. For this example, we fix the adimensional parameters as $\mu = 10^2$, $\lambda = 10^3$, $\theta = 10^{-3}$, and $M = 20$. On the other hand, the manufactured solutions and non-linear terms are given as follows

$$\boldsymbol{u}(x,y,z) = 5^{-1}\left(x^2 + x\cos(x)\sin(y), y^2 + x\cos(y)\sin(x), z^2 + x\cos(x)\cos(y)\right)^{\mathtt{t}},$$
$$\varphi(x,y,z) = \cos(\pi y) + \sin(\pi x) + x^2 + y^2 + z^2,$$
$$\ell(\varphi) = \varphi + \varphi^2, \quad \mathbb{M}(\boldsymbol{\varepsilon}(\boldsymbol{u}), p) = 10^{-1}\exp\left[-10^{-4}\operatorname{tr}(2\mu\boldsymbol{\varepsilon}(\boldsymbol{u}) - p\mathbb{I})\right]\mathbb{I}.$$

We recall that the right-hand sides and non-homogeneous boundary conditions are introduced in the computations according to these terms.

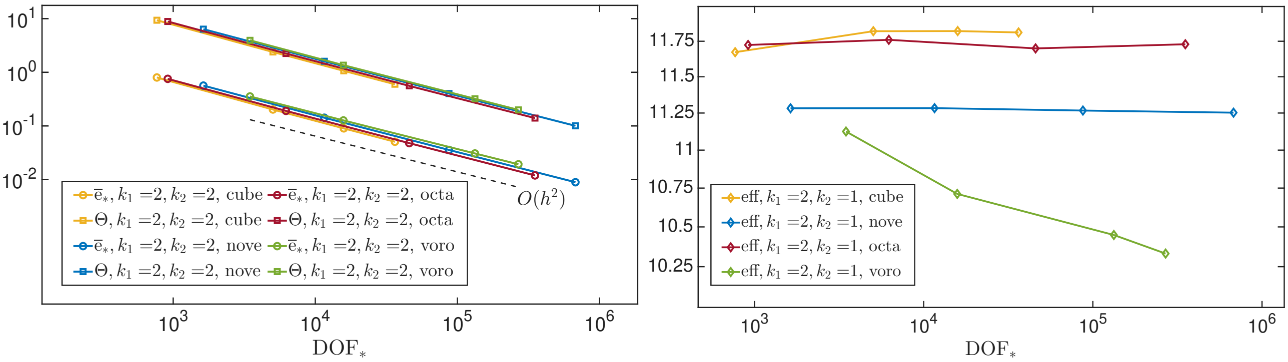

FIGURE 6.7. Example 3. Behaviour of the error $\overline{e}_*$, estimator Θ (left), and effectivity index eff (right) under uniform refinement across various meshes with $k_1 = 2$ and $k_2 = 2$.

The results reported in Figure 6.7 indicate optimal convergence rates for $k_1 = 2$ and $k_2 = 2$, as in [46]. In addition, the effectivity index remains bounded, which confirms the reliability and efficiency of the estimator (see Theorem 4.13 and Theorem 4.16).

6.4. Example 4: Adaptivity in 3D

For this example, we consider the unit cube domain $\Omega = (0, 1)^3$ with Dirichlet part $\Gamma_D = \{(x, y, z) \in \partial\Omega : x = 0 \text{ or } y = 0 \text{ or } z = 0\}$, and Neumann part $\Gamma_N = \partial\Omega \setminus \Gamma_D$. The starting mesh is defined by 4^3 cubes. Here we fix the adimensional parameters as $\mu = 10^2$, $\lambda = 10^3$, $\theta = 10^{-3}$, and $M = 100$.

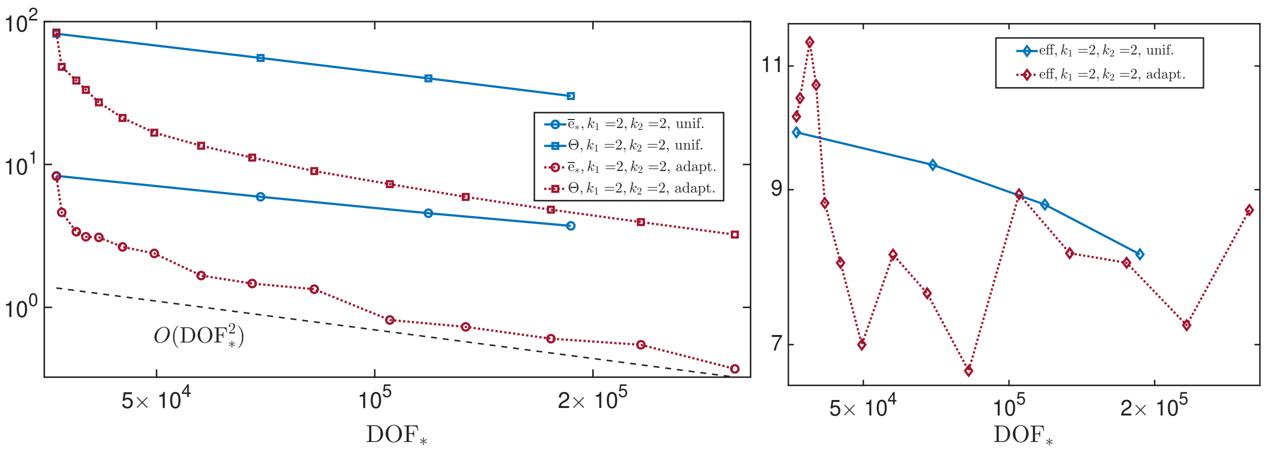

FIGURE 6.8. Example 4. Behaviour of the error $\overline{e}_*$, estimator Θ (left), and effectivity index eff (right) under adaptive and uniform refinement for the lowest-order case.

The non-smooth manufactured solutions and non-linear terms are given as follows

$$\boldsymbol{u}(x, y, z) = 5^{-1}\left(\left((x + 0.1)^2 + (y + 0.1)^2 + (z - 1.1)^2\right)^{-1}, z\cos(x)\sin(y), x\cos(z)\sin(y)\right)^{\mathtt{t}},$$

$$\varphi(x, y, z) = xyz\left((x - 1.1)^2 + (y - 1.1)^2\right)^{-1},$$

$$\ell(\varphi) = 10^{-2}\varphi, \quad \mathbb{M}(\boldsymbol{\varepsilon}(\boldsymbol{u}), p) = 10^{-3}\exp\left[-10^{-4}\operatorname{tr}(2\mu\boldsymbol{\varepsilon}(\boldsymbol{u}) - p\mathbb{I})\right]\mathbb{I}.$$

The first displacement component has a singularity close to the point $(x, y, z)^{\mathtt{t}} = (0, 0, 1)^{\mathtt{t}}$. In addition, the concentration φ has a high gradient close to the line $(x, y, z)^{\mathtt{t}} = (1, 1, 1 - t)^{\mathtt{t}}$ for $t \in \mathbb{R}$. The results reported in Figure 6.8 show optimal convergence as predicted in [46]. Moreover, we observe that the adaptive refinement outperforms the uniform refinement. In addition, the effectivity index remains bounded, confirming the robustness of the estimator proved in Theorems 4.13 and 4.16. Finally, Figure 6.9 shows snapshots of the approximate solutions on a mesh after 15 refinement steps. The method is able to capture the expected solution singularities.

Acknowledgement. We kindly thank A/Prof. Lorenzo Mascotto for his insight on the construction of quasi-interpolators for edge VE spaces in 3D. We also thank Mr. Jordi Manyer for providing the `Gridap` interface for `p4est` (GridapP4est).

REFERENCES

[1] B. Ahmad, A. Alsaedi, F. Brezzi, L. D. Marini, and A. Russo, *Equivalent projectors for virtual element methods*, Comput. Math. Appl., 66 (2013), pp. 376–391.

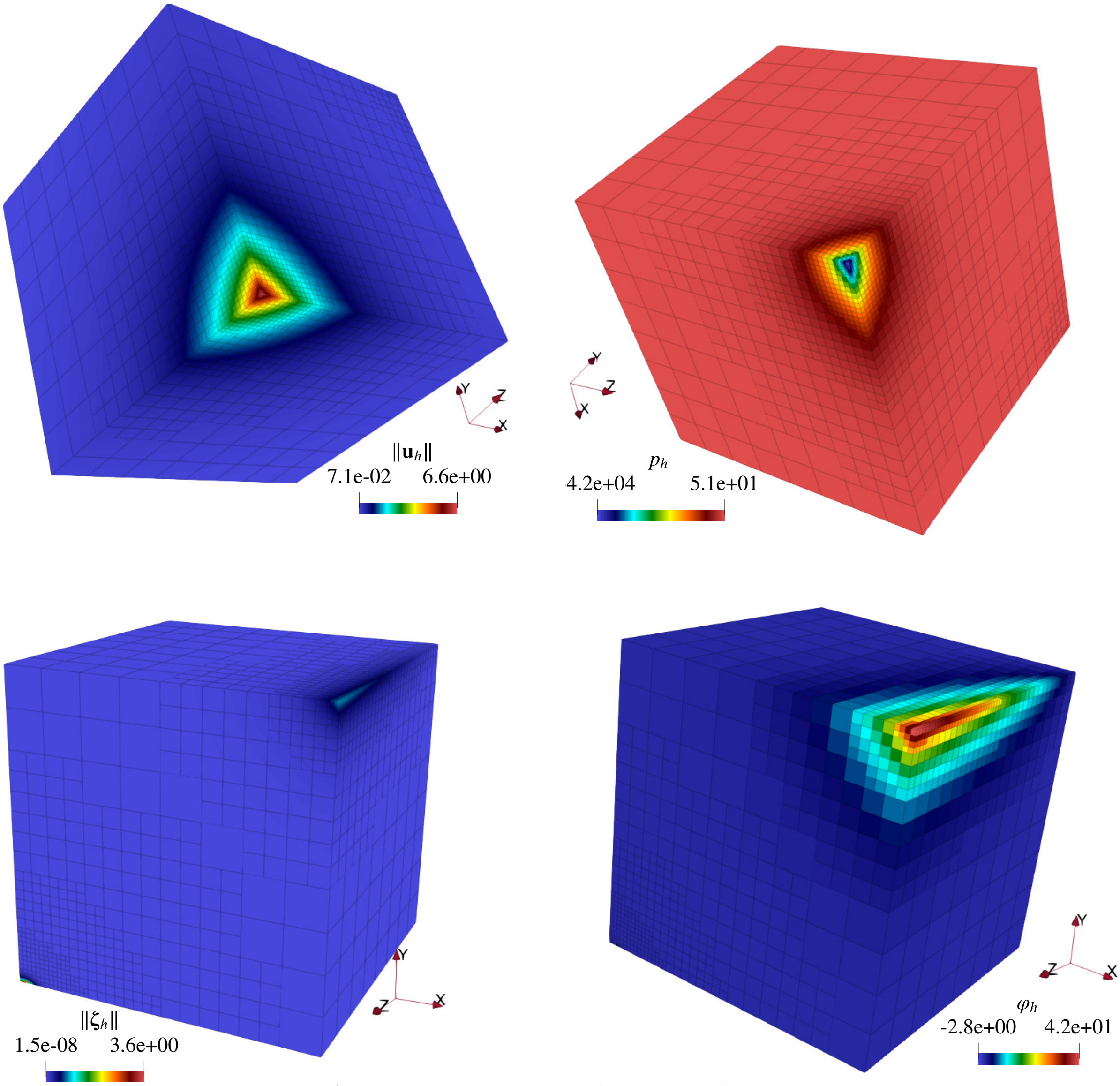

FIGURE 6.9. Example 4. Approximate solutions obtained with polynomial degrees $k_1 = 2$ and $k_2 = 2$ after 14 adaptive refinements.

[2] M. Ainsworth and J. Oden, *A posteriori error estimation in finite element analysis*, Comput. Methods Appl. Mech. Engrg., 142 (1997), pp. 1–88.
[3] P. Antonietti, F. Dassi, and E. Manuzzi, *Machine learning based refinement strategies for polyhedral grids with applications to virtual element and polyhedral discontinuous Galerkin methods*, J. Comput. Phys., 469 (2022), p. 111531.
[4] S. Badia and F. Verdugo, *Gridap: An extensible finite element toolbox in Julia*, J. Open Source Softw., 5 (2020), p. 2520.
[5] L. Beirão da Veiga, F. Brezzi, A. Cangiani, G. Manzini, L. D. Marini, and A. Russo, *Basic principles of virtual element methods*, Math. Models Meth. Appl. Sci., 23 (2013), pp. 199–214.
[6] L. Beirão da Veiga, F. Brezzi, L. D. Marini, and A. Russo, *H(div) and H(curl)-conforming VEM*, Numer. Math., 133 (2016), p. 303–332.
[7] ———, *Mixed virtual element methods for general second order elliptic problems on polygonal meshes*, ESAIM: M2AN, 50 (2016), pp. 727–747.
[8] L. Beirão da Veiga, F. Dassi, and A. Russo, *High-order virtual element method on polyhedral meshes*, Comput. Math. Appl., 74 (2017), pp. 1110–1122.
[9] L. Beirão da Veiga, F. Dassi, and G. Vacca, *The Stokes complex for virtual elements in three dimensions*, Math. Models Meth. Appl. Sci., 30 (2020), pp. 477–512.
[10] L. Beirão da Veiga, C. Lovadina, and G. Vacca, *Divergence free virtual elements for the Stokes problem on polygonal meshes*, ESAIM: M2AN, 51 (2017), pp. 509–535.
[11] L. Beirão da Veiga, L. Mascotto, and J. Meng, *Interpolation and stability estimates for edge and face virtual elements of general order*, Math. Models Meth. Appl. Sci., 32 (2022), pp. 1589–1631.
[12] L. Beirão da Veiga, D. Mora, and G. Vacca, *The Stokes complex for virtual elements with application to Navier–Stokes flows*, J. Sci. Comput., 81 (2019).
[13] W. Boon, M. Kuchta, K.-A. Mardal, and R. Ruiz-Baier, *Robust preconditioners and stability analysis for perturbed saddle-point problems – application to conservative discretizations of Biot's equations utilizing total pressure*, SIAM J. Sci. Comput., 43 (2021), pp. B961–B983.
[14] D. Braess, *Stability of saddle point problems with penalty*, M2AN - Modélisation Mathématique et Analyse Numérique, 30 (1996), pp. 731–742.

[15] S. C. Brenner and L. R. Scott, *Polynomial Approximation Theory in Sobolev Spaces*, Springer, New York, NY, 1994, pp. 91–122.

[16] F. Brezzi, R. S. Falk, and L. Donatella Marini, *Basic principles of mixed virtual element methods*, ESAIM: M2AN, 48 (2014), p. 1227–1240.

[17] C. Burstedde, L. C. Wilcox, and O. Ghattas, *p4est: Scalable algorithms for parallel adaptive mesh refinement on forests of octrees*, SIAM J. Sci. Comput., 33 (2011), pp. 1103–1133.

[18] A. Cangiani, E. H. Georgoulis, T. Pryer, and O. J. Sutton, *A posteriori error estimates for the virtual element method*, Numer. Math., 137 (2017), pp. 857–893.

[19] J. Cascón, R. Nochetto, and K. Siebert, *Design and convergence of AFEM in H(div)*, Math. Models Meth. Appl. Sci., 20 (2007), pp. 1849–1881.

[20] C. Cherubini, S. Filippi, A. Gizzi, and R. Ruiz-Baier, *A note on stress-driven anisotropic diffusion and its role in active deformable media*, J. Theoret. Biol., 430 (2017), pp. 221–228.

[21] F. Dassi, *VEM++, a C++ library to handle and play with the virtual element method*, Numer. Algor., 101 (2026), pp. 1633–1675.

[22] F. Dassi, A. Fumagalli, A. Scotti, and G. Vacca, *Bend 3d mixed virtual element method for Darcy problems*, Comput. Math. Appl., 119 (2022), pp. 1–12.

[23] D. A. Di Pietro and J. Droniou, *The Hybrid High-Order Method for Polytopal Meshes: Design, Analysis, and Applications*, vol. 19 of MS&A, Springer, Switzerland AG, 2020.

[24] C. Domínguez, G. N. Gatica, and S. Meddahi, *A posteriori error analysis of a fully-mixed finite element method for a two-dimensional fluid-solid interaction problem*, J. Comput. Math., 33 (2015), pp. 606–641.

[25] R. Duran, *An elementary proof of the continuity from $L^2_0(\Omega)$ to $H^1_0(\Omega)^n$ of Bogovskii's right inverse of the divergence*, Rev. Unión Mat. Argentina, (2012).

[26] A. Ern and J.-L. Guermond, *Finite element quasi-interpolation and best approximation*, ESAIM: M2AN, 51 (2017), pp. 1367–1385.

[27] ———, *Finite Elements I: Approximation and Interpolation*, Springer, Switzerland AG, Feb 2021.

[28] J. Galvis and M. Sarkis, *Non-matching mortar discretization analysis for the coupling Stokes-Darcy equations*, Elect. Trans. Numer. Anal., 26 (2007), pp. 350–384.

[29] G. Gatica, *A Simple Introduction to the Mixed Finite Element Method. Theory and Applications*, Springer, Cham, Jan 2014.

[30] G. Gatica, M. Álvarez, and R. Ruiz-Baier, *A posteriori error analysis for a viscous flow–transport problem*, ESAIM: M2AN, 50 (2016), pp. 1789–1816.

[31] G. N. Gatica, B. Gómez-Vargas, and R. Ruiz-Baier, *Analysis and mixed-primal finite element discretisations for stress-assisted diffusion problems*, Comput. Methods Appl. Mech. Engrg., 337 (2018), pp. 411–438.

[32] ———, *A posteriori error analysis of mixed finite element methods for stress-assisted diffusion problems*, J. Comput. Appl. Math., 409 (2022), p. 114144.

[33] G. N. Gatica, C. Inzunza, and F. A. Sequeira, *A pseudostress-based mixed-primal finite element method for stress-assisted diffusion problems in Banach spaces*, J. Sci. Comput., 92 (2022), pp. Paper No. 103, 43.

[34] V. Girault and P.-A. Raviart, *Mathematical Foundation of the Stokes Problem*, Springer, Berlin, Heidelberg, 1986, pp. 1–111.

[35] R. Khot, A. E. Rubiano, and R. Ruiz-Baier, *Robust virtual element methods for coupled stress-assisted diffusion problems*, SIAM J. Sci. Comput., 47 (2025), pp. A497–A526.

[36] P. L. Lederer, C. Merdon, and J. Schöberl, *Refined a posteriori error estimation for classical and pressure-robust Stokes finite element methods*, Numer. Math., 142 (2019), pp. 713–748.

[37] M. Lewicka and P. B. Mucha, *A local and global well-posedness results for the general stress-assisted diffusion systems*, J. Elast., 123 (2016), pp. 19–41.

[38] A. Loppini, A. Gizzi, R. Ruiz-Baier, C. Cherubini, F. H. Fenton, and S. Filippi, *Competing mechanisms of stress-assisted diffusivity and stretch-activated currents in cardiac electromechanics*, Front. Physiol., 9 (2018), p. 1714.

[39] H. Malaeke and M. Asghari, *A mathematical formulation for analysis of diffusion-induced stresses in micropolar elastic solids*, Arch. Appl. Mech., 93 (2023), pp. 3093–3111.

[40] J. Meng, L. Beirão da Veiga, and L. Mascotto, *Stability and interpolation properties for Stokes-like virtual element spaces*, J. Sci. Comput., 94 (2023), p. e56.

[41] D. Mora, G. Rivera, and R. Rodriguez, *A virtual element method for the Steklov eigenvalue problem*, Math. Models Meth. Appl. Sci., 25 (2015), pp. 1–25.

[42] ———, *A posteriori error estimates for a virtual element method for the Steklov eigenvalue problem*, Comput. Math. Appl., 74 (2017), pp. 2172–2190.

[43] M. Munar, A. Cangiani, and I. Velásquez, *Residual-based a posteriori error estimation for mixed virtual element methods*, Comput. Math. Appl., 166 (2024), pp. 182–197.

[44] J. D. Murray, *Mathematical Biology II: Spatial Models and Biomedical Applications*, vol. 3, Springer, New York, 2003.

[45] T. P. Prevost, A. Balakrishnan, S. Suresh, and S. Socrate, *Biomechanics of brain tissue*, Acta Biomater., 7 (2011), pp. 83–95.

[46] A. E. Rubiano, *Robust virtual element methods for 3D stress-assisted diffusion problems*, in Proceedings of the 22nd Biennial Computational Techniques and Applications Conference, CTAC-2024, R. R. Baier, B. Lamichhane, Q. T. L. Gia, and J. Bunder, eds., vol. 66 of Proc. ANZIAM, 2025, pp. C45–C60.

[47] D. Shaw, *Diffusion in Semiconductors*, Springer, Boston, MA, 2007, pp. 121–135.

[48] Z. Shen and L. Song, *On Lp estimates in homogenization of elliptic equations of Maxwell's type*, Adv. Math., 252 (2014), pp. 7–21.

[49] M. Taralov, *Simulation of Degradation Processes in Lithium-Ion Batteries*, PhD thesis, Technische Universität Kaiserslautern, 2015.

[50] D. Unger and E. Aifantis, *On the theory of stress-assisted diffusion, II*, Acta Mech., 47 (1983), pp. 117–151.

[51] G. Wang, Y. Wang, and Y. He, *A posteriori error estimates for the virtual element method for the Stokes problem*, J. Sci. Comput., 84 (2020).

[52] R. Wilson and E. Aifantis, *On the theory of stress-assisted diffusion, I*, Acta Mech., 45 (1982), pp. 273–296.

[53] Y. Yu, *Implementation of polygonal mesh refinement in MATLAB*, arXiv preprint, 2101.03456 (2021).

[54] A. Zaghdani and C. Daveau, *Two new discrete inequalities of Poincaré–Friedrichs on discontinuous spaces for Maxwell's equations*, C. R. Math., 342 (2006), pp. 29–32.